arXiv:2502.17403v6 [cs.LG] 7 Aug 2026

Large Language Models are Powerful Electronic Health Record Encoders

Stefan Hegselmann[1,2,3*†], Georg von Arnim[1†], Tillmann Rheude[1], Noel Kronenberg[1], David Sontag[4,5], Gerhard Hindricks[3], Roland Eils[1,6], Benjamin Wild[1]

[1]Berlin Institute of Health at Charité – Universitätsmedizin Berlin, Center of Digital Health, Berlin, Germany.
[2]Berlin Institute of Health at Charité – Universitätsmedizin Berlin, BIH Biomedical Innovation Academy, BIH Charité Digital Clinician Scientist Program, Berlin, Germany.
[3]Deutsches Herzzentrum der Charité – Medical Heart Center of Charité and German Heart Institute Berlin, Berlin, Germany.
[4]Computer Science and Artificial Intelligence Laboratory (CSAIL), Massachusetts Institute of Technology (MIT), Cambridge, MA, USA.
[5]Layer Health, Inc., MA, USA.
[6]Intelligent Medicine Institute, Fudan University, Shanghai, China.

*Corresponding author(s). E-mail(s): stefan.hegselmann@charite.de;
†These authors contributed equally to this work.

Abstract

Electronic Health Records (EHRs) offer considerable potential for clinical prediction, but their complexity and heterogeneity challenge traditional machine learning. Domain-specific Electronic Health Record (EHR) foundation models trained on unlabeled EHR data have shown improved predictive accuracy and generalization. However, their development is constrained by limited data access and site-specific vocabularies. We convert EHR data into plain text by replacing medical codes with natural-language descriptions, enabling general-purpose Large Language Models (LLMs) to produce high-dimensional embeddings for downstream prediction tasks without access to private medical training data. LLM-based embeddings perform on par with a specialized EHR foundation model, CLMBR-T-Base, across 15 clinical tasks from the EHRSHOT benchmark. In an external validation using the UK Biobank, an LLM-based model shows statistically significant improvements for some tasks, which we attribute to higher vocabulary coverage and slightly better generalization. Overall, we reveal

a trade-off between the computational efficiency of specialized EHR models and the portability and data independence of LLM-based embeddings.

Keywords: electronic health records, clinical prediction, machine learning, large language models, foundation models

1 Introduction

Electronic Health Records (EHRs) are now widely used in modern healthcare, providing comprehensive, longitudinal views of a patient's health status [1]. Machine learning methods can leverage this rich data for risk stratification and to support clinical decision-making [2–4]. In recent years, researchers have explored a variety of prediction tasks based on EHRs, including hospital readmission [5, 6], length of hospital stay [6], sepsis onset detection [7, 8], mortality prediction [6, 9], discharge diagnoses [6], and heart failure outcomes [10]. The overarching goal is to harness EHR data using machine learning to improve clinical outcomes and reduce healthcare costs.

However, machine learning on EHR data poses significant challenges due to its inherent complexity. EHR data is characterized by variable-length sequences of patient visits, irregular sampling intervals, missing entries, heterogeneous and noisy information, and a wide range of hierarchical medical concepts [11]. As a result, deep learning models often achieve only modest improvements over traditional methods such as logistic regression or tree-based models for EHR prediction tasks [6, 12, 13]. To address these challenges, recent approaches have employed large-scale foundation models pretrained on unlabeled EHR data using unsupervised learning [14]. Many of these models adopt strategies from natural language processing, such as masked word prediction as in BERT [15] or autoregressive next-word prediction as in GPT [16]. Treating EHR data as sequences of medical codes enables analogous methods such as masked code prediction [12, 17–19] or next-code prediction [13, 20, 21]. However, code-based EHR foundation models face two fundamental obstacles to interoperability and generalization: site-specific coding practices and fixed vocabularies learned during pretraining. For example, CLMBR-T-Base [13] supports only 26,249 unique codes from its training corpus, and when applied to the UK Biobank (UKB) with 50,702 unique medical codes, only 7,969 (16%) could be mapped, leaving 84% of codes unseen by the model. Achieving interoperability would require pretraining on diverse EHR datasets from many institutions, which is difficult due to the sensitivity of healthcare data. This motivates models that operate on natural-language descriptions of clinical codes, which avoid fixed vocabularies and transfer more readily across institutions.

Large Language Models (LLMs) benefit from pretraining on vast general-purpose text corpora and a broad range of natural-language tasks [22, 23]. This extensive pretraining enables strong language comprehension and allows them to capture domain-agnostic patterns that can be adapted for healthcare applications. Consequently, LLMs have demonstrated strong performance in extracting medical concepts [24], summarizing medical texts [25], and predicting medical outcomes [26], even in low-resource settings. Recent work extends LLMs to structured EHR by serializing records

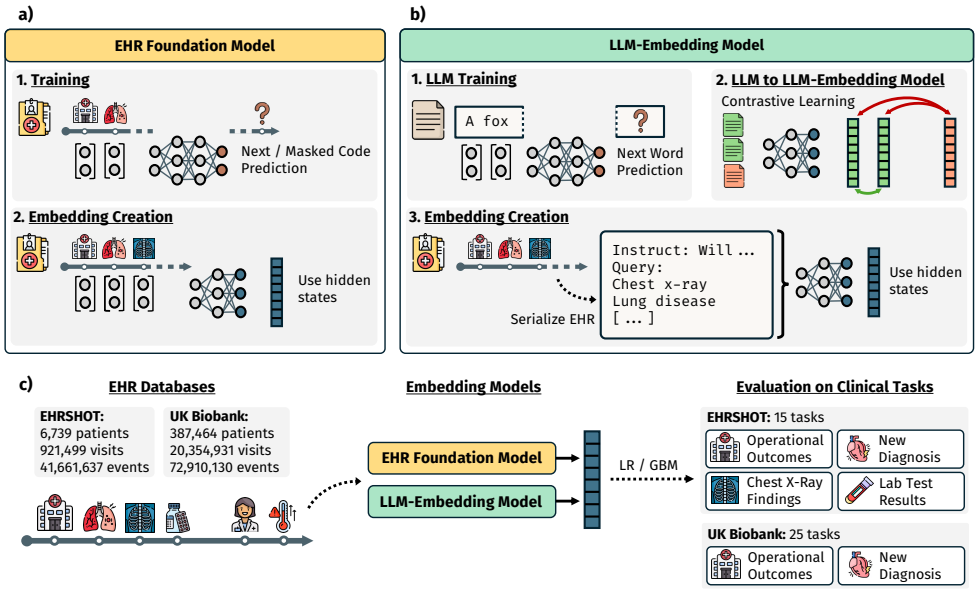

Fig. 1 Study Overview. (a) EHR foundation models are pretrained on unlabeled EHR data. Common unsupervised learning tasks are masked-code or next-code prediction. To obtain a representation for an EHR, we use the hidden states of the pretrained model. (b) Large Language Models (LLMs) are pretrained on vast amounts of text data. To obtain an LLM embedding model, architectural changes are applied, and contrastive learning is used to improve representational performance. To obtain an EHR embedding, the data is first serialized as text and then processed by the LLM embedding model. Again, we use the hidden states for the embedding. (c) We use the EHRSHOT benchmark and the UK Biobank (UKB) cohort for our experiments. Medical events of each patient are converted into numerical embeddings using an EHR foundation model and an LLM embedding model, respectively. A logistic regression (LR) model is trained, validated, and tested for each clinical prediction task. We also test a Gradient Boosted Machine (GBM) prediction model for the count-based baseline. Images from Flaticon.com.

into text and either using model generations for prediction [27–32] or extracting fixed-dimensional embeddings for downstream classifiers [33–36]. While both paradigms can be competitive with common baselines, many prior studies use short context windows and evaluate on private or emergency-department cohorts, limiting longitudinal coverage and external validity [33–35] (Section 4.7). Moreover, most modern LLMs, such as GPT [37] and Qwen [38, 39], use decoder-only transformer architectures trained with left-to-right objectives, which are not optimized for representation learning. To address this limitation, recent work converts decoder-only LLMs into effective LLM embedding models via contrastive learning or related techniques [40–44]. Additionally, these state-of-the-art models offer large context windows, making them well suited for handling long inputs such as serialized EHR data.

In this study, we present a systematic evaluation of modern general-purpose LLM embedding models as encoders of longitudinal EHR data for clinical prediction [45] (Fig. 1). To this end, we convert structured EHR records into a list of plain-text descriptions of medical codes available at prediction time. Using a state-of-the-art LLM embedding model, Qwen3-Embedding-8B (Qwen3-Emb-8B) [39, 44] with a context size

Table 1 Cohort Overview. Summary statistics for EHRSHOT and UK Biobank, including the number of patients, visits, events, and patient characteristics.

Attribute	EHRSHOT	UK Biobank
Num Patients	6,739	387,464
Num Visits	921,499	20,354,931
Num Events	41,661,637	72,910,130
Num Female	3,441	214,565
Num Male	3,298	172,899
Age, mean ± SD	59.3 ± 17.9	56.78 ± 8.11
American Indian	25	0
Asian	1,043	8,659
Black	298	5,715
Pacific Islander	74	0
Unknown	1,563	7,202
White	3,736	365,888
Hispanic	1,038	-
Non-Hispanic	5,701	-

of 8,192 tokens, we generate high-dimensional EHR embeddings that serve as inputs to logistic regression classifiers across 15 clinical tasks from the EHRSHOT benchmark. Rather than proposing a new modeling architecture, we assess the representation capabilities of these models under a standardized and reproducible evaluation protocol. We intentionally use a simple embedding-plus-classifier pipeline to enable fair comparison with prior work and to isolate representation quality from downstream modeling choices. We analyze performance in the few-shot setting to evaluate generalization, apply paired statistical tests to assess task-level differences between the LLM embedding model and competing methods, and conduct extensive ablation studies to identify the factors that drive its effectiveness. Finally, we perform an external validation on the UKB for predicting mortality, hospitalization, and the onset of 23 diseases [46] to assess generalization across datasets and coding systems.

2 Results

2.1 Experimental Setup

Our primary analyses used the EHRSHOT benchmark, which contains EHRs from 6,739 adult patients treated at Stanford Health Care and Lucile Packard Children's Hospital between 1990 and 2023. The dataset includes 921,499 visits and more than 41.6 million clinical events, and defines a standardized evaluation across 15 clinical prediction tasks from 4 task categories, with predefined splits and public code [45]. Table 1 summarizes cohort statistics, and task details are shown in Table 2. Additional information on task definitions and preprocessing is provided in Section 4.1.

For external validation, we used the UKB, a population-based cohort of 502,489 UK participants [47, 48]. This setting allowed us to assess generalization across healthcare systems, particularly because CLMBR-T-Base was trained on data from the same hospital system as EHRSHOT. We followed the EHRSHOT setup as closely as possible and evaluated one-year risk of hospitalization, mortality, and onset of 23 diseases [46] (Section 4.10). The processed UKB subset used in our study comprised 387,464

Table 2 EHRSHOT Prediction Tasks Overview. The EHRSHOT benchmark defines 15 clinical prediction tasks spanning four task groups. The number of examples per task differs based on the prevalence and frequency of clinical events. Canonical splits for training, validation, and testing are defined to ensure reproducible experiments [45].

Attribute	Train Labels (Positive)	Valid Labels (Positive)	Test Labels (Positive)	Total Labels (Positive)
Operational Outcomes				
Long Length of Stay	2,569 (681)	2,231 (534)	2,195 (552)	6,995 (1,767)
30-day Readmission	2,609 (370)	2,207 (281)	2,189 (260)	7,005 (911)
ICU Transfer	2,402 (113)	2,052 (92)	2,037 (85)	6,491 (290)
Anticipating Lab Test Results				
Thrombocytopenia	68,776 (9,774)	54,504 (6,962)	56,338 (7,960)	179,618 (24,696)
Hyperkalemia	76,349 (1,215)	60,168 (886)	63,653 (948)	200,170 (3,049)
Hypoglycemia	122,108 (1,065)	95,488 (858)	100,568 (783)	318,164 (2,706)
Hyponatremia	81,336 (20,181)	64,473 (14,674)	67,028 (16,003)	212,837 (50,858)
Anemia	70,501 (9,544)	56,224 (7,445)	58,155 (7,636)	184,880 (24,625)
Assignment of New Diagnoses				
Hypertension	1,260 (184)	1,250 (177)	1,261 (160)	3,771 (521)
Hyperlipidemia	1,684 (205)	1,441 (189)	1,317 (172)	4,442 (566)
Pancreatic Cancer	2,576 (155)	2,215 (53)	2,220 (56)	7,011 (264)
Celiac	2,623 (62)	2,284 (11)	2,222 (21)	7,129 (94)
Lupus	2,570 (104)	2,226 (33)	2,243 (20)	7,039 (157)
Acute MI	2,534 (175)	2,177 (146)	2,127 (144)	6,838 (465)
Anticipating Chest X-ray Findings				
Chest X-Ray Findings	7,481 (4,771)	9,366 (6,032)	9,428 (6,400)	26,275 (17,203)

patients, approximately 20.4 million visits, and more than 72 million clinical events (Table 1). Table S1 reports tasks and label distributions for the UKB.

To apply LLMs to structured EHR data, we serialized each patient record into plain text with a maximum context length of 8,192 tokens. Our default serialization was a simple newline-separated list of medical code descriptions, including units and values when available, with minimal preprocessing. To remain within the token budget, we retained only the most recent occurrence of each medical code, which performed better than using the first occurrence or adding basic date and time information. An example serialization is shown in Fig. 2, and further details are provided in Section 4.2. For the UKB, we used the same list-based serialization but omitted units and values because they were not available.

We evaluated three instruction-tuned LLM embedding models: Qwen3-Embedding-8B (Qwen3-Emb-8B) [39, 44], GTE-Qwen2-7B-Instruct (Qwen2-Emb-7B) [38, 43], and LLM2Vec-Llama-3.1-8B-Instruct (Llama3.1-LLM2Vec-8B) [40, 49]. We focused primarily on Qwen3-Emb-8B because of its recency and stronger long-context performance. All embedding models received task-specific prompts (Table S3). As an in-domain baseline, we included CLMBR-T-Base, a 141-million-parameter autoregressive foundation model trained on 2.57 million de-identified EHRs from Stanford Medicine [13, 45]. The EHRSHOT validation and test splits were fully separated from CLMBR-T-Base pretraining (Fig. 1 in [45]). We also extended the comparison to

```
Instruct: Given a patient's electronic
healthcare record (EHR) as a newline
separated list, retrieve relevant passages
that answer the query: will the patient stay
in the hospital for more than 7 days

Query:
Body weight (ounces): 1801
Body mass index (BMI) [Ratio]: 18.7
Systolic blood pressure (mmHg): 148
Diastolic blood pressure (mmHg): 80
Body surface area: 1.47
Pulse rate: 121
Electrocardiogram, tracing
Therapeutic activities
Hematocrit [Volume Fraction] of Blood (%): 24
Erythrocytes [#/volume] in Blood
Glucose [Mass/volume] in Serum or Plasma
Creatinine [Mass/volume] in Serum or Plasma
Sodium [Moles/volume] in Serum or Plasma
Inpatient Visit
quetiapine 50 MG Oral Tablet
acetaminophen 325 MG Oral Tablet
bisacodyl 10 MG Rectal Suppository
Chest x-ray
Electrocardiogram report
Body height: 70

[ ... ]

Foley catheter long term use
ABO and Rho(D) typing
Insertion of catheter into peripheral vein
Emergency Room and Inpatient Visit
Hispanic or Latino
FEMALE
Black
Birth
```

Fig. 2 Example EHR Text Serialization with Instruction. The EHR data are serialized into plain text to enable the use of LLM embedding models. The default serialization consists of a newline-separated list of the most recent occurrence of each medical code. No additional preprocessing or filtering is applied. Each code is represented by its text description, with an optional unit (given in brackets), and an optional value. Floating-point values are rounded to two decimal places.

encoder-only biomedical language models using mean pooling and chunk-wise concatenation of 512-token segments, and a simplified variant of the Multiple Embedding Model for EHR (MEME) method [34].

For each embedding model, we computed patient-level embeddings and trained a logistic regression classifier on the training split, with hyperparameters selected on the validation set. Following the EHRSHOT protocol, we used the same logistic-regression head for all embedding-based representations to isolate embedding quality from downstream model complexity and reduce overfitting risk in few-shot settings. As a baseline, we trained a Gradient Boosted Machine (GBM) on count-based representations of medical concepts. The count baselines used ontology expansion from EHRSHOT [45] and were further extended with string values, numeric values, and time binning.

Table 3 Performance for All Examples on EHRSHOT. Mean area under the receiver operating characteristic curve (AUROC) performance and approximate 95% confidence intervals across tasks of selected models for four task groups. The macro-averaged performance across all task groups is given in the right-most column. The LLM embedding model Qwen3-Emb-8B with a context size of 8,192 tokens and a logistic regression (LR) classification head performs on par with the EHR foundation model CLMBR-T-Base. Combining the embeddings of the LLM embedding model and CLMBR-T-Base by concatenation leads to an increase in performance. Additional model variants can be found in Table S4.

Model	Operational Outcomes	Anticipating Lab Test Results	Assignment of New Diagnosis	Anticipating Chest X-ray Findings	Macro Avg. Across Task Groups
Baselines [45]					
CLMBR-T-Base	0.824 .803-.845	0.832 .824-.840	0.707 .667-.746	0.713 .702-.724	0.769 .746-.792
Count-based + GBM	0.824 .804-.844	0.841 .833-.849	0.758 .724-.793	0.686 .674-.699	0.777 .756-.799
LLM Embedding Models					
Qwen3-Emb-8B	0.797 .773-.820	0.842 .835-.850	0.714 .672-.757	0.722 .711-.733	0.769 .744-.794
Qwen3-Emb-4B	0.787 .764-.810	0.824 .816-.831	0.718 .667-.768	0.708 .696-.719	0.759 .730-.787
Qwen3-Emb-0.6B	0.778 .753-.803	0.742 .732-.753	0.684 .631-.737	0.705 .694-.716	0.727 .697-.758
LLM Embedding Model + EHR Foundation Model [45]					
Qwen3-Emb-8B + CLMBR-T-Base	0.821 .800-.842	0.864 .858-.871	0.736 .695-.777	0.731 .721-.742	0.788 .764-.812
Multiple Embedding Model for EHR (MEME) [34] **with Linear Head**					
Qwen3-Emb-8B MEME	0.814 .793-.834	0.845 .837-.852	0.728 .673-.784	0.717 .705-.728	0.776 .746-.806
BioClinicalBERT MEME	0.756 .733-.778	0.699 .686-.713	0.704 .651-.758	0.648 .635-.661	0.702 .671-.732
Encoder Language Models with Chunked Inputs					
BioClinicalBERT	0.738 .712-.763	0.698 .685-.711	0.707 .668-.746	0.679 .666-.691	0.705 .680-.730
MedBERT	0.742 .718-.767	0.694 .683-.706	0.663 .614-.713	0.683 .671-.696	0.696 .667-.725

2.2 General-Purpose LLM Embeddings Rival Domain-Specific EHR Models

Using all available training and validation examples, Qwen3-Emb-8B matched the in-domain EHR foundation model CLMBR-T-Base on EHRSHOT, with an overall macro-area under the receiver operating characteristic curve (AUROC) of 0.769 (0.744–0.794) versus 0.769 (0.746–0.792) (Table 3). Qwen3-Emb-8B performed slightly better in three of four task categories, namely lab prediction, assignment of new diagnoses, and chest X-ray prediction. Task-level statistical testing showed that Qwen3-Emb-8B significantly outperformed CLMBR-T-Base on thrombocytopenia, hyponatremia, and hyperkalemia, whereas CLMBR-T-Base performed significantly better on anemia and hypoglycemia (Table 4 and Table S5). No significant differences were observed for the remaining tasks, indicating that most task-level differences were small within statistical uncertainty. Concatenating Qwen3-Emb-8B and CLMBR-T-Base embeddings improved performance to 0.788 (0.764–0.812), suggesting that the two models capture complementary information (Table 3). Smaller Qwen3 variants performed worse, with 0.759 (0.730–0.787) for Qwen3-Emb-4B and 0.727 (0.697–0.758) for Qwen3-Emb-0.6B.

Table 4 Win–Tie–Loss Summary of Qwen3-Emb-8B Compared to Competing Models. Entries report the number of tasks where Qwen3-Emb-8B significantly outperforms (W), ties with (T), or significantly underperforms (L) the comparator model in the 8-shot, 64-shot, and all-data settings. Higher wins or losses are in bold. Full statistical results are in Table S5, Table S15, and Table S17.

Qwen3-Emb-8B+LR vs.	8-shot	64-shot	All
EHRSHOT			
CLMBR+LR	**4**/10/1	**3**/10/2	**3**/10/2
BioClinicalBERT+LR	**6**/9/0	**7**/8/0	**8**/7/0
Count-based+GBM	**8**/7/0	1/12/**2**	2/10/**3**
UKB			
CLMBR+LR	**2**/23/0	**4**/16/0	**6**/19/0
BioClinicalBERT+LR	**6**/19/0	**2**/18/0	**8**/17/0
Count-based+GBM	**2**/22/1	**1**/19/0	**8**/14/3
UKB; Qwen3-Emb-8B restricted to CLMBR codes			
CLMBR+LR	**5**/18/2	**3**/17/0	**2**/23/0

The GBM-based count baseline with ontology expansion, string and numeric values, and time binning substantially improved over the original EHRSHOT count baseline that used ontology expansion alone [45] (Table S6). Using all data, the count model achieved 0.777 (0.756–0.799), slightly exceeding both Qwen3-Emb-8B and CLMBR-T-Base (Table 3). It significantly outperformed Qwen3-Emb-8B on thrombocytopenia, hyponatremia, and anemia, whereas Qwen3-Emb-8B only outperformed it on hypoglycemia and chest X-ray prediction (Table 4 and Table S5). These results underscore the strength of count-based models when many labeled examples are available and the marginal gains of pretrained representations. We evaluated 14 encoder-based configurations, of which BioClinicalBERT with mean embeddings over 512-token chunks performed best at 0.705 (0.680–0.730) (Table 3 and Table S4). Qwen3-Emb-8B significantly outperformed BioClinicalBERT on eight of 15 tasks, indicating a clear advantage over encoder-only baselines under long-context list-based serialization (Table 4). Using MEME with a logistic-regression head yielded slight gains for Qwen3-Emb-8B but no improvement for BioClinicalBERT (Table 3).

Scaling analyses showed only modest gains with increasing size for Qwen-based and DeBERTa models, whereas larger BERT variants performed worse (Fig. 3). CLMBR-T-Base remained the most parameter-efficient model relative to predictive performance. Runtime analysis on EHRSHOT further emphasized this efficiency difference (Table S12). CLMBR-T-Base required 6:04 minutes to encode all examples of the EHRSHOT benchmark, whereas Qwen3-Emb-8B required 21:48:56 hours and encoder models required 2:21:35 to 7:00:21 hours because of chunking (Section 4.4). Thus, LLM-based methods achieved similar predictive performance at the cost of a substantially larger memory footprint and higher computational cost.

In the UKB, Qwen3-Emb-8B achieved slightly higher overall performance than CLMBR-T-Base, with 0.751 (0.740–0.761) compared to 0.736 (0.726–0.747) (Table 5).

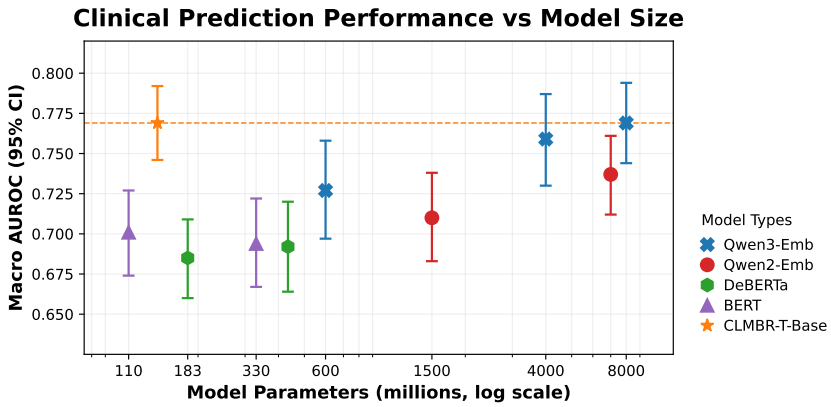

Fig. 3 Scaling Behavior on EHRSHOT. Number of model parameters (x-axis) and macro-averaged area under the receiver operating characteristic curve (AUROC) performance with approximate 95% confidence intervals across all four task groups (y-axis). We include only models with varying sizes. The performance results of Qwen3- and Qwen2-based LLM embedding models suggest scaling behavior with model size. Encoder-only models based on the BERT architecture do not show this trend. The specialized EHR foundation model, CLMBR-T-Base, is the most parameter-efficient model. Full results in Table S4.

Table 5 Performance for All Examples on UKB. Mean area under the receiver operating characteristic curve (AUROC) performance and approximate 95% confidence intervals across tasks for three task groups. The LLM embedding model Qwen3-Emb-8B with a logistic regression (LR) classification head outperforms the EHR foundation model CLMBR-T-Base and the count-based baseline using a Gradient Boosted Machine (GBM) head. The assignment of new diagnoses prediction is based on the mean across all 23 provided diseases. Additional model variants can be found in Table S14.

Model	Mortality prediction	Operational Outcomes (Hospitalization)	Assignment of New Diagnoses	Macro Avg. Across Task Groups
Baselines [45]				
CLMBR-T-Base	0.801 $_{.772\text{-}.830}$	0.689 $_{.685\text{-}.693}$	0.719 $_{.708\text{-}.731}$	0.736 $_{.726\text{-}.747}$
Count-based + GBM	0.780 $_{.749\text{-}.810}$	0.709 $_{.705\text{-}.712}$	0.634 $_{.622\text{-}.646}$	0.708 $_{.697\text{-}.719}$
LLM Embedding Model				
Qwen3-Emb-8B	0.811 $_{.781\text{-}.840}$	0.698 $_{.694\text{-}.702}$	0.743 $_{.731\text{-}.755}$	0.751 $_{.740\text{-}.761}$
Sensitivity Analysis Restricted to CLMBR Codes				
Qwen3-Emb-8B CLMBR	0.806 $_{.775\text{-}.836}$	0.687 $_{.683\text{-}.691}$	0.736 $_{.723\text{-}.749}$	0.743 $_{.732\text{-}.754}$
Encoder Language Models with Chunked Inputs				
BioClinicalBERT	0.778 $_{.746\text{-}.811}$	0.675 $_{.671\text{-}.678}$	0.705 $_{.693\text{-}.717}$	0.719 $_{.708\text{-}.731}$

Statistical testing showed significant improvements on six of 25 tasks and no significant differences otherwise (Table 4). Because only 16% of UKB codes mapped to the CLMBR-T-Base vocabulary, we performed a sensitivity analysis restricting Qwen3-Emb-8B to the same codes (Table 5 and Fig. S13). Under this restriction, performance decreased to 0.743 (0.732–0.754), placing it between full Qwen3-Emb-8B and

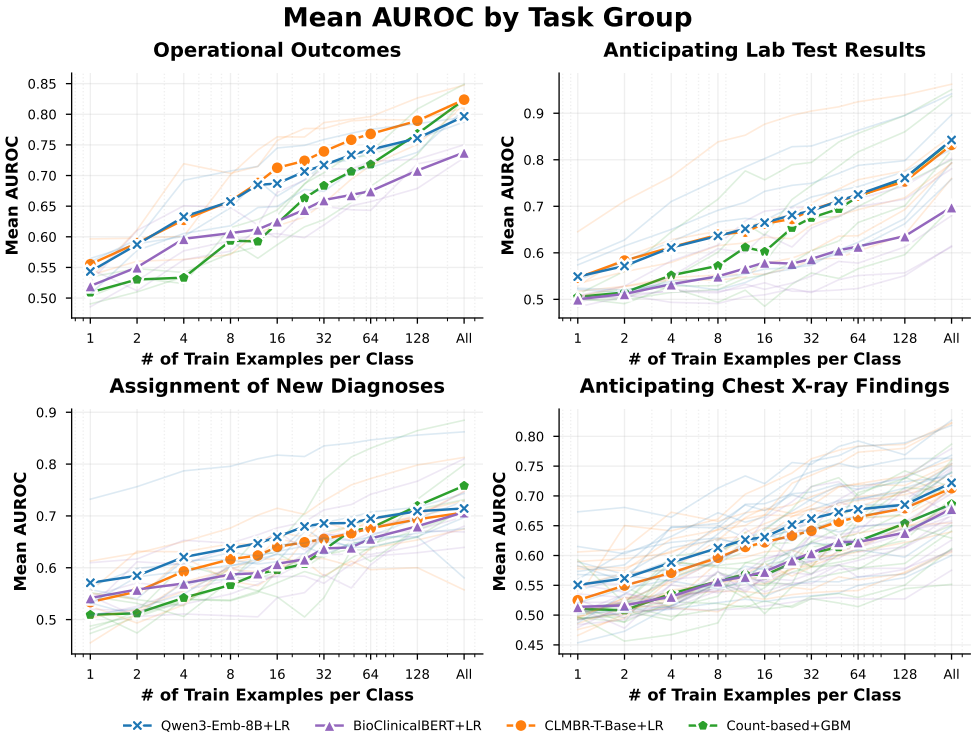

Fig. 4 Few-Shot Performance on EHRSHOT. Mean area under the receiver operating characteristic curve (AUROC) performance across subtasks for four task groups (bold). Blurred lines show averaged AUROC values across five bootstrapped runs using different seeds [45]. The LLM embedding model performs similarly to the EHR foundation model, CLMBR-T-Base, and shows the largest performance gains over the count-based model at intermediate numbers of training examples. The LLM embedding model consistently outperforms the biomedical embedding model BioClinicalBERT.

CLMBR-T-Base. Qwen3-Emb-8B restricted to CLMBR-T-Base-mappable codes significantly outperformed CLMBR-T-Base on two instead of six tasks (Table 4). This indicates that the gains on UKB can be explained by both broader vocabulary coverage and slightly improved generalization. Qwen3-Emb-8B also significantly outperformed BioClinicalBERT on eight UKB tasks (Table 4). The count-based model performed slightly worse overall in the UKB, likely reflecting the difficulty of GBM learning on highly imbalanced tasks (Table S1).

2.3 LLM Embeddings Achieve Strong Performance in Low-Data Regimes

We evaluated performance under limited supervision using the few-shot protocol from EHRSHOT [45], including statistical comparisons for 8-shot and 64-shot settings. Across EHRSHOT task groups, Qwen3-Emb-8B maintained slightly higher performance than CLMBR-T-Base for new diagnoses and chest X-ray tasks across most shot settings (Fig. 4). CLMBR-T-Base showed higher performance only for operational

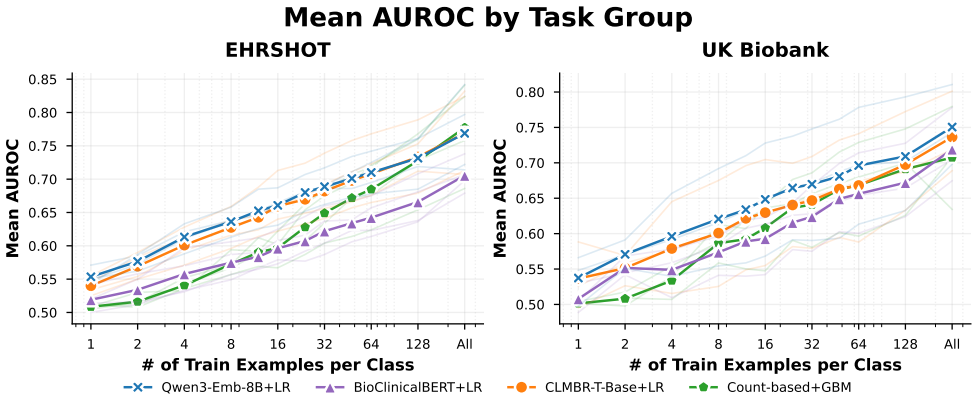

Fig. 5 Few-Shot Performance on EHRSHOT and UKB. Macro-averaged area under the receiver operating characteristic curve (AUROC) performance across all subtasks of EHRSHOT (left) and UK Biobank (right). Blurred lines show averaged AUROC values for the different task groups. On EHRSHOT, the LLM embedding model performs on par with the EHR foundation model, CLMBR-T-Base. On the UK Biobank, the LLM embedding model slightly outperforms the EHR foundation model across all shot sizes.

outcomes, beginning at 16 shots. Statistical testing confirmed that Qwen3-Emb-8B significantly outperformed CLMBR-T-Base on four versus one tasks in the 8-shot setting and on three versus two tasks in the 64-shot setting, while most tasks remained indistinguishable (Table 4). The count baseline performed worse in the smallest-shot settings, but often matched or exceeded Qwen3-Emb-8B and CLMBR-T-Base by 64 or 128 shots, consistent with its strength in higher-data regimes (Fig. 4). These findings indicate that the advantage of LLM embeddings is most apparent with limited labeled data. Qwen3-Emb-8B also consistently outperformed BioClinicalBERT, which was likewise reflected in the task-level statistical testing (Table 4). Additional metrics are reported in the supplement, including area under the precision-recall curve (AUPRC) and Brier score (Fig. S1, Fig. S2) and task-level AUROC, AUPRC, and Brier scores (Fig. S3, Fig. S4, and Fig. S5).

In the UKB, Qwen3-Emb-8B again showed slightly higher average performance than CLMBR-T-Base across shot sizes (Fig. 5). Statistical analysis showed significant improvements over CLMBR-T-Base on two tasks in the 8-shot setting and four tasks in the 64-shot setting, while most tasks showed no significant difference (Table 4). Restricting Qwen3-Emb-8B to CLMBR-T-Base-mappable codes again yielded intermediate performance between full Qwen3-Emb-8B and CLMBR-T-Base (Table 4 and Fig. S13), supporting a mixed contribution of vocabulary coverage and representation quality. Qwen3-Emb-8B also outperformed the count baseline in few-shot UKB settings, although by smaller margins than in EHRSHOT. Only two significant improvements over the count model were observed at 8 shots and one at 64 shots, indicating that most few-shot performance differences were modest in this cohort (Table 4). Qwen3-Emb-8B also remained consistently stronger than BioClinicalBERT across few-shot settings.

Table 6 Performance for All Examples on EHRSHOT for Different Serializations. Mean area under the receiver operating characteristic curve (AUROC) performance and approximate 95% confidence intervals for the list serialization used in this work and three alternatives using the first occurrence of each code and adding timestamps to each code. We also tested a handcrafted Markdown EHR serialization and JSON, XML, and YAML data formats derived from it, showing slightly lower performance than the simple list serialization. Additional serialization results can be found in Table S7.

Model	Operational Outcomes	Anticipating Lab Test Results	Assignment of New Diagnosis	Anticipating Chest X-ray Findings	Macro Avg. Across Task Groups
EHR List Serializations for Qwen3-Emb-8B					
List codes recent (ours)	0.797 .773-.820	0.842 .835-.850	0.714 .672-.757	0.722 .711-.733	0.769 .744-.794
List codes first	0.761 .736-.785	0.715 .701-.728	0.731 .688-.773	0.676 .663-.690	0.721 .694-.747
List codes recent + time	0.795 .772-.818	0.844 .837-.851	0.692 .637-.748	0.727 .716-.738	0.765 .734-.795
List codes first + time	0.746 .720-.772	0.703 .689-.716	0.718 .674-.761	0.645 .629-.660	0.703 .675-.730
EHR Alternative Serialization Formats for Qwen3-Emb-8B					
Markdown	0.773 .749-.797	0.859 .852-.866	0.725 .683-.767	0.694 .681-.707	0.763 .737-.788
JSON	0.773 .749-.796	0.858 .851-.865	0.736 .692-.780	0.690 .677-.704	0.764 .738-.790
XML	0.771 .747-.795	0.862 .855-.868	0.726 .681-.771	0.676 .663-.690	0.759 .732-.785
YAML	0.773 .749-.796	0.863 .856-.870	0.723 .677-.769	0.684 .670-.698	0.761 .734-.787

2.4 Effect of the EHR Serialization on LLM-Based Embedding Performance

To assess the effect of the EHR text serialization, we compared our default list format, which retains the most recent occurrence of each medical code, with variants using the first occurrence or adding date and time information (Table 6). Using first rather than most recent occurrences substantially reduced performance, especially for lab-test prediction and chest X-ray findings, indicating that these tasks depend strongly on recent information. Adding date and time information did not improve performance and instead caused a small decrease for recent-code serializations and a larger decrease for first-code serializations. This suggests that current LLM embedding models do not effectively exploit explicit temporal markers in this simple long-context list format. We also evaluated a handcrafted Markdown serialization designed to emphasize clinically relevant structure (Section 4.3). Overall, Markdown did not improve performance for Qwen3-Emb-8B relative to the simpler list-based serialization (Table 6). For lab-test prediction, however, Markdown with preprocessed laboratory information yielded small AUROC gains of 0.006 to 0.021 for Qwen3-Emb-8B, Qwen2-Emb-7B, and Llama3.1-LLM2Vec-8B (Table S7). These gains are consistent with stronger text cues in the Markdown lab-value representation. Notably, Qwen3-Emb-8B remained clearly stronger than Qwen2-Emb-7B and Llama3.1-LLM2Vec-8B on the default list serialization (Table S4), suggesting that it effectively extracts relevant signals from the raw data without relying strongly on preprocessing. Replacing Markdown with JSON, XML, or YAML led to only minor differences (Table 6). XML showed the largest decrease, likely because of its greater formatting overhead.

We further quantified the contribution of individual serialization components using ablations with Qwen3-Emb-8B (Fig. 6). Replacing task-specific instructions with a generic prompt slightly reduced performance, and removing instructions entirely

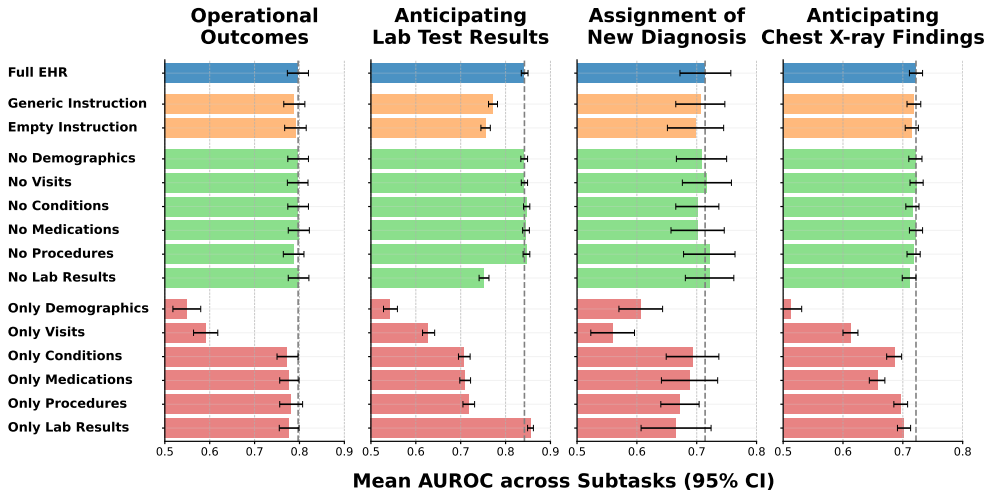

Fig. 6 Effects of EHR Serialization Content on EHRSHOT. Mean area under the receiver operating characteristic curve (AUROC) performance with approximate 95% confidence intervals for Qwen3-Emb-8B. The default list serialization (Full EHR) appears at the top, followed by runs with a generic and an empty instruction (orange). We then evaluate the serialization by removing specific code categories (green) and by retaining only individual categories (red). Category definitions are given in Table S8, and full results are reported in Table S9.

caused a further decrease. The largest drop occurred for lab-test prediction, suggesting that task-aligned instructions help the model focus on relevant spans. Removing individual code categories for demographics, visits, conditions, medications, procedures, and labs had limited impact overall except for lab results, which were critical for lab prediction tasks (Fig. 6). This pattern indicates substantial redundancy across EHR information sources. Using only a single modality showed that demographics and visits alone, accounting for up to 1.5% of all recorded events, were weak predictors. Using only conditions, medications, procedures, or lab results yielded similar overall performance across task groups, with lab results being especially informative for lab-test prediction. However, no single modality matched the full-EHR representation, indicating that the modalities provide complementary information.

2.5 Effect of Context Length and Temporal Scope on Embedding Effectiveness

To assess sensitivity to input length and recency, we performed ablation studies on context size and temporal window using EHRSHOT (Fig. 7). The models differed markedly in their optimal context sizes, with Qwen3-Emb-8B performing best at 4,096 tokens, Qwen2-Emb-7B at 2,048 tokens, and Llama3.1-LLM2Vec-8B at 1,024 to 2,048 tokens. For Qwen2-Emb-7B and Llama3.1-LLM2Vec-8B, performance dropped substantially at 8,192 tokens. These results show that only Qwen3-Emb-8B handled unstructured long-context EHR input robustly for the simple list serialization, indicating that model scale alone is insufficient for strong long-context performance. Temporal-window analyses showed a similar pattern, in part because larger windows

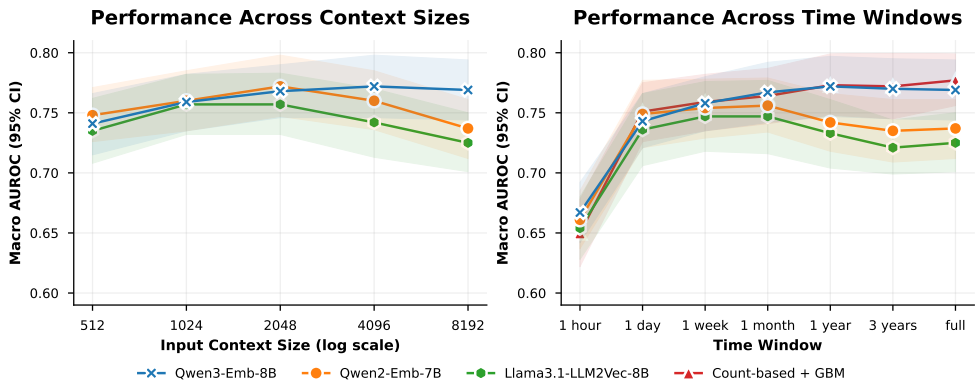

Fig. 7 Performance Across Context Size and Time Windows on EHRSHOT. Macro-averaged area under the receiver operating characteristic curve (AUROC) performance with approximate 95% confidence intervals (y-axis) across all task groups for different LLM embedding models and the count-based baseline, shown for different context sizes (left) and different time windows before prediction time (right). The LLM embedding models for the time-window experiments use a context size of 8,192 tokens. All results are given in Table S10 and Table S11.

also increase effective input length. Qwen3-Emb-8B performed best with a one-year window, whereas Qwen2-Emb-7B and Llama3.1-LLM2Vec-8B performed best with shorter windows of one month and one week, respectively (Fig. 7). Again, Qwen3-Emb-8B was the only LLM embedding model without a pronounced performance drop at longer time horizons. In contrast, the count-based baseline improved with larger time windows, further highlighting its robustness when many training examples are available. A one-hour window caused a large performance drop across all models, indicating insufficient information for prediction in EHRSHOT.

2.6 Fine-Tuned LLM Embedding and LLM Decoder Models

We evaluated decoder-style LLMs that generate text, where token probabilities can be used for classification. We extended the prompt with an additional instruction to produce `Yes` and `No` tokens leveraged for prediction (Table S3). In addition, we fine-tuned both the LLM embedding model and the LLM decoder model using LoRA, and evaluated decoder in-context learning with 2, 4, and 6 examples. The decoder experiments train the instruction-tuned causal language model Qwen3-8B to generate direct `Yes` and `No` predictions for each serialized EHR, while the encoder experiments pair Qwen3-Emb-8B with a supervised classification head (Section 4.6). Both approaches preserve the EHRSHOT task definitions, operate on the same default list-based EHR serialization, and employ the same few-shot sampling strategy across all shot sizes and replicates. Due to model constraints, we restricted the decoder ICL experiments to at most 6 in-context examples and used a maximum input length of 4,096 tokens.

The decoder with in-context examples achieved its best performance at 2-shot, with a macro-AUROC of 0.636 (0.588–0.685), compared with 0.611 (0.563–0.659) in the zero-shot setting (see Fig. 8). This early advantage is consistent with architectural

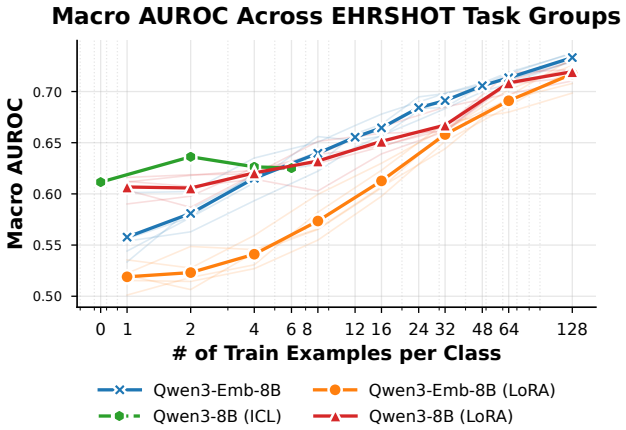

Fig. 8 Few-Shot AUROC Performance of Encoder and Decoder Models on EHRSHOT. Macro-averaged area under the receiver operating characteristic curve (AUROC) across all EHRSHOT subtasks for zero to 128 training examples per class. The frozen Qwen3-Emb-8B encoder baseline (blue) is compared with its Low-Rank Adaptation (LoRA)-tuned variant (orange), decoder in-context learning (ICL) runs at 0, 2, 4, and 6 shots (green), and the LoRA-tuned Qwen3-8B decoder (red). Decoder ICL beyond 6 shots was not computationally feasible.

differences between the two approaches: the decoder can directly exploit pretrained logits for `Yes` and `No` tokens, whereas embedding variants must learn a classification head from limited supervision. Increasing the number of in-context examples beyond 2 did not lead to further gains.

With more supervision, the fine-tuned decoder improved steadily, reaching macro-AUROC values of 0.632 (0.584–0.679) at $k = 8$, 0.708 (0.664–0.752) at $k = 64$, and 0.719 (0.673–0.764) at $k = 128$. The fine-tuned encoder showed a complementary trade-off with slightly lower overall performance, reaching 0.573 (0.524–0.623) at $k = 8$, 0.691 (0.643–0.737) at $k = 64$, and 0.717 (0.669–0.762) at $k = 128$. Although both fine-tuned variants benefited from additional labeled data, neither surpassed the frozen Qwen3-Emb-8B baseline from the main experiments, which reached 0.733 (0.686–0.777) at $k = 128$ (Table S18).

3 Discussion

This study shows that general-purpose LLM embedding models pretrained on large-scale natural-language corpora can serve as effective encoders of longitudinal EHR data for clinical prediction. On the EHRSHOT benchmark, Qwen3-Emb-8B performed on par with the domain-specific EHR foundation model CLMBR-T-Base [13, 45], with most task-level differences not reaching statistical significance. In the external UKB validation, Qwen3-Emb-8B performed modestly better overall and showed significant improvements on a subset of tasks. Our sensitivity analysis, in which Qwen3-Emb-8B was restricted to codes mappable to CLMBR-T-Base, suggests that this advantage reflects both broader vocabulary coverage and slightly better generalization [36]. Together, these findings indicate that LLM embeddings can match strong EHR foundation models on in-domain benchmarks while transferring effectively across settings

with different coding practices. A key practical advantage of Qwen3-Emb-8B is that it operates on a simple list-based EHR serialization with minimal preprocessing. Because it uses natural-language code descriptions rather than a fixed medical vocabulary, it can incorporate arbitrary clinical codes with textual representations, and it does not require institution-specific code mapping. Despite this simple representation, the model captured clinically meaningful structure, including information from laboratory values embedded in raw EHR text. These results extend prior work on encoder-based models for EHR modalities [34] and on LLM-based embeddings at the medical-code level [36]. Overall, LLM embeddings provide a flexible and powerful alternative for EHR representation learning.

Our results also highlight a trade-off between the flexibility of LLM embeddings and the efficiency of specialized EHR foundation models. CLMBR-T-Base encoded the EHRSHOT benchmark in several minutes with substantially lower memory requirements. However, it relies on pretraining on a large private EHR dataset of approximately 1.8 billion clinical events and operates with a fixed vocabulary. In contrast, Qwen3-Emb-8B required more than 20 hours for encoding, but was pretrained on a much larger and more diverse general-text corpus of approximately 36 trillion tokens without requiring access to sensitive clinical data. The limitations of fixed-vocabulary models became apparent in the UKB, where only 16% of codes could be mapped to the CLMBR-T-Base vocabulary, covering only 25% of clinical events and requiring a complex, potentially lossy mapping procedure [50, 51]. By operating directly on natural-language descriptions, LLM embeddings can incorporate all available codes without retraining. This text-based interface may also facilitate future multimodal extensions that integrate structured records with notes, reports, and imaging metadata [52]. Thus, domain-specific EHR models remain substantially more computationally efficient, whereas LLM embeddings offer greater flexibility and portability across datasets.

Our analyses provide insights into why LLM embeddings perform well for EHR data. A simple newline-separated list of medical code descriptions was sufficient for strong performance with Qwen3-Emb-8B, indicating that extensive preprocessing or structured input formats were not required. However, model behavior differed markedly with respect to long-context inputs. Among similarly sized models, only Qwen3-Emb-8B handled list inputs up to 8,192 tokens robustly, whereas the other embedding models degraded at longer lengths and often performed better with shorter or more structured inputs such as Markdown. This suggests that model scale alone does not ensure effective long-context representations of EHRs. Task-specific instructions further improved performance, indicating that instruction-tuned embeddings can better focus on clinically relevant information [40, 43]. Performance was driven largely by recent events, although this is partly confounded by the longer inputs induced by larger time windows, and explicit temporal information did not improve results in our setup. Ablation studies revealed substantial redundancy across EHR modalities, with laboratory values being particularly important for lab prediction tasks, but no single modality matched the full representation. Overall, these findings suggest that LLM embeddings of EHR data depend less on elaborate input engineering and more on

model-specific capabilities, particularly robustness to long contexts and sensitivity to clinically relevant signals.

Conventional baselines provide important context for interpreting our results. Encoder-only language models remain a common approach for EHR representation learning [34, 53], but they required input chunking to handle long sequences, which increases computational cost and may limit performance. Across 14 evaluated configurations, BioClinicalBERT with mean pooling over 512-token chunks performed best among encoder models [54]. In our setting, LLM embedding models consistently outperformed BioClinicalBERT across multiple few-shot regimes and several tasks with statistically significant differences, although at substantially higher computational cost. This suggests that LLM embeddings are a stronger option than encoder-only models for long-context EHR representation learning. At the same time, the count-based model with ontology expansion, string and numeric values, and time binning remained highly competitive when trained on all available data [6, 55]. However, its performance deteriorated in few-shot settings, indicating lower data efficiency than pretrained representations. These findings indicate that the benefits of pretraining are most pronounced under limited supervision and diminish as more labeled data become available. They also underscore the importance of including strong count-based baselines in EHR prediction studies.

We also compared frozen LLM embeddings, decoder ICL, and parameter-efficiently fine-tuned variants of both model families with two main observations. First, a small number of in-context examples improved the decoder relative to pure zero-shot prompting, likely because decoder-style models can directly exploit pretrained logits for the constrained `Yes`/`No` outputs. These gains plateaued for 4 to 6 examples, and larger ICL settings were not computationally feasible for our long-context EHR inputs. Second, decoder fine-tuning and encoder fine-tuning both improved steadily with additional labels, but neither tuned variant exceeded the frozen Qwen3-Emb-8B baseline within the explored budgets. This supports using a frozen embedding model with a simple classifier as the default configuration for LLM-based EHR prediction. Decoder ICL and decoder fine-tuning might remain viable alternatives when very-few-shot performance or task-specific generative behavior justifies their higher optimization and inference costs.

This study has several limitations. First, our approach relies on a manually designed text-based EHR serialization and task-specific instructions, and only captures the most recent occurrence of each code. Second, comparisons between CLMBR-T-Base and Qwen3-Emb-8B are confounded by large differences in architecture, model scale, and pretraining data, making it difficult to isolate the contribution of each factor. Third, LLM embedding models incur substantially higher computational costs, with large memory requirements and long runtimes, and our analyses were limited to contexts of up to 4,096 to 8,192 tokens and three LLM embedding models. In addition, the hyperparameter tuning for our fine-tuning experiments was limited to two task groups and two shot sizes due to computational constraints, and we only used a decoder with simple token logits for comparison. Finally, we evaluated two large cohorts, EHRSHOT and UKB, but further validation across diverse healthcare systems will be necessary to assess generalizability, robustness, and fairness at scale.

Future work should address these limitations by improving long-context modeling and temporal reasoning in LLM embeddings. Serialization-free approaches that allow models to process raw EHR tables and timelines may reduce bias introduced by manual text transformation. Scaling to larger models may provide additional gains in long-context understanding. At the same time, improving efficiency through distillation or smaller architectures will be important for practical deployment. It will also be important to evaluate LLM embedding models on combined structured and unstructured clinical data, including notes, imaging, and reports. Future work should also evaluate decoder LLMs with stronger learning signals such as LLM-JEPA [56] instead of using only simple token logits. Finally, expanding evaluations to real-world deployments and investigating how to combine the complementary strengths of domain-specific EHR models and general-purpose LLMs will be essential for building robust and scalable EHR foundation models.

4 Methods

4.1 EHRSHOT Database and Prediction Task

The EHR data used in our experiments are from the EHRSHOT benchmark for few-shot evaluation of clinical EHR prediction [45]. We obtained version 2.1 of the dataset, which is accessible via gated access under a research data use agreement. This dataset comprises longitudinal records for 6,739 patients, 921,499 visits, and 41,661,637 clinical events collected between 1990 and February 8, 2023 (Table 1). Each clinical event is linked to a specific patient and includes information such as start time, end time, a semantic code, a value, unit, visit ID, and the corresponding Observational Medical Outcomes Partnership (OMOP) source table. We used the official ehrshot-benchmark GitHub repository as a starting point to design our experiments [45], enabling us to build on existing functionalities and facilitate comparisons with prior methods. The benchmark uses the Framework for Electronic Medical Records (FEMR) GitHub repository, which provides Python classes for efficient loading and processing of EHR data. All extensions and experiments conducted for this paper are publicly available via our GitHub repository: https://github.com/stefanhgm/ehrshot-benchmark. The EHRSHOT benchmark defines a rigorous evaluation including 15 clinical prediction tasks categorized into four groups: operational outcomes, anticipating lab-test results, assignment of new diagnoses, and anticipating chest X-ray findings [45]. Task labels are derived from clinical events, so a single patient can contribute multiple labels per task, resulting in substantial variation in task-specific sample sizes (Table 2). For instance, frequent events such as laboratory tests yield many more examples than rarer events such as incident diagnoses. The benchmark focuses on analyzing model performance in a few-shot setting, which is particularly relevant for large pretrained foundation models [14]. Specifically, for $k \in \{1, 2, 4, 8, 12, 16, 24, 32, 48, 64, 128\}$, the protocol uses k positive and k negative training examples and k positive and k negative validation examples sampled with replacement to train and tune supervised classifiers. If fewer than k positive or negative training examples were available, the next larger shot size was used with resampling. Using the full data for training and validation, which are often unbalanced, is included for all tasks. Testing is always performed on

the full set of available examples for each task. The classifiers evaluated within the EHRSHOT framework include logistic regression, random forests, and GBMs [57]. Performance is reported using the AUROC, the AUPRC, and the Brier score. For few-shot settings, results are averaged over multiple runs with different random seeds, and variability across runs is summarized using the standard deviation of the test set performance [45]. For each individual task, uncertainty is additionally estimated via bootstrap resampling of the test set to obtain standard deviations and percentile-based 95% confidence intervals. For task groups, mean performance is computed by averaging across tasks, and approximate 95% confidence intervals are derived from the uncertainties of the individual task estimates by combining their variances and applying a normal approximation. An overall macro average is computed by averaging across task groups, with corresponding uncertainty estimated analogously.

4.2 EHR Text Serialization

To apply LLMs embedding models to EHR data, we serialized each patient record into task-agnostic text. Following EHRSHOT, we included all events occurring before the label time and truncated inputs to 8,192 tokens (approximately 32,000 characters) due to computational constraints (Section 4.8). Each clinical event in EHRSHOT is represented by a semantic identifier of the form "ontology/code". We resolved these identifiers to text using the provided vocabularies and custom mappings. To assess ontology coverage, we analyzed events from 200 patients across the operational-outcomes and new-diagnoses task groups (2,968 labels). We observed events from the following ontologies: Logical Observation Identifiers Names and Codes (LOINC), SNOMED, RxNorm, CPT4, Domain, CARE_SITE, RxNorm Extension, Medicare Specialty, ICD10PCS, CMS Place of Service, Cancer Modifier, ICD9Proc, CVX, ICDO3, HCPCS, OMOP Extension, and Condition Type. Codes from CPT4, CARE_SITE, ICD10PCS, Cancer Modifier, CVX, and ICDO3 were not fully resolved by the provided resources. We parsed UICC cancer stages from Cancer Modifier codes and added manual mapping files for CPT4, ICD10PCS, and CVX. We excluded CARE_SITE and ICDO3 because we could not map them to useful descriptions.

We used a simple newline-separated list of event descriptions with minimal preprocessing to emphasize the embedding model's ability to interpret raw clinical content. To remain within the token budget, we kept only the most recent occurrence of each code. This default serialization therefore corresponds to a list of unique codes per patient record with code-to-description mapping and deduplication as the only mandatory preprocessing steps. When available, we appended values and units in brackets, and values of datatype float were rounded to two decimals. We also evaluated variants that kept the first occurrence of each code and that added date and time information, but these did not improve performance (Table 6).

4.3 Testing Alternative EHR Text Serializations

To evaluate whether more structured inputs improve performance, we implemented an alternative Markdown-based serialization, a common LLM input format [58]. We included visit dates and the number of days before prediction time, normalizing all

dates relative to January 1, 2024, the prediction reference time. The serialization started with demographics, and birthdates were converted to age in years. Because 65% of events were LOINC-coded time series, we aggregated LOINC events. Using the same 200-patient subset as above, we selected the 24 most frequent concepts across vital signs, body metrics, and laboratory values and merged synonymous codes (Table S2). For each concept, we reported the last three values and removed implausible measurements. We additionally added default units and categorical interpretations (low, normal, high) based on standard ranges (Table S2). Following the aggregated data, a summary of all visits was included to address the potential truncation of older visits. Events not associated with visits were then presented, using the same aggregation logic to display the last three values where applicable. Finally, a detailed reverse-chronological presentation of all visits was included, with events categorized into conditions (SNOMED, Visit, Cancer Modifier, CVX, HCPCS), medications (RxNorm, RxNorm Extension), and procedures (CPT4, ICD10PCS, ICD9Proc).

Additionally, we converted the Markdown serialization into JSON, XML, and YAML using standard Python libraries to assess format effects under a fixed token budget. Because these formats have different overhead, the amount of clinical content retained can vary for the same token limit.

4.4 LLM Embedding Models and Baselines

We evaluated three LLM embedding models: Qwen3-Embedding-8B (Qwen3-Emb-8B) [39, 44], GTE-Qwen2-7B-Instruct (Qwen2-Emb-7B) [38, 43], and LLM2Vec-Llama-3.1-8B-Instruct (Llama3.1-LLM2Vec-8B) [40, 49], based on state-of-the-art decoder-only LLMs. We selected these models for their ability to handle the 8,192-token EHR serializations used in our experiments. For comparison, we also tested smaller variants of Qwen3-Emb-8B and Qwen2-Emb-7B. All LLM-based models received task-specific instructions prepended to the EHR serialization (Section 4.5), and we used each model's default embedding configuration. For Qwen-based embedding models, we used the last-layer hidden state of the final `[EOS]` token as the patient embedding [38, 44]. For LLM2Vec models, we applied mean pooling over the last-layer hidden states corresponding to the EHR serialization, excluding the instruction tokens from pooling [40]. Importantly, the instruction still conditions the internal representation and thus influences the resulting embedding.

As additional baselines, we included commonly used encoder-only embedding models with shorter input limits of 512 tokens. To apply them to 8,192-token inputs, we split each input into up to 16 chunks of 512 tokens and evaluated mean pooling and concatenation of these chunk embeddings to obtain a single representation. For the biomedical fine-tuned encoders MedBERT and BioClinicalBERT, we also tested the MEME method to encode domain-specific data separately with a logistic regression classification head to follow our study setup [34]. Overall, this yielded 14 encoder-only baseline configurations for long-context EHR prediction. Encoder-only models did not use task instructions. Below is an overview of all models.

Qwen3-Embedding-8B/4B/0.6B is a model family built on the Qwen3 foundation LLMs [39] and trained as instruction-aware embedding models via a multi-stage recipe [44]. All variants use decoder-only Transformers with causal attention and produce

embeddings from the last-layer hidden state of the final `[EOS]` token (Section 4.5). The 8B and 4B models have 36 layers, while the 0.6B model has 28 layers, and all support a context window of up to 32,000 tokens. By default, the embedding dimensionalities are 4,096 (8B), 2,560 (4B), and 1,024 (0.6B), with support for flexible output dimensions. The base model Qwen3 was trained on a multilingual corpus of 36T tokens [39]. Training of the embedding models comprises large-scale weakly supervised pretraining on synthetic query–document pairs, followed by supervised fine-tuning on labeled and filtered synthetic data, optimizing a contrastive learning objective. Finally, different checkpoints are merged to improve robustness [44].

Qwen2-Embedding-7B/1.5B is based on GTE-Qwen2-7B-Instruct and GTE-Qwen2-1.5B-Instruct [38]. These models use decoder-only Transformers (7B: 28 layers, 28 heads, hidden size 3,584; 1.5B: 28 layers, 12 heads, hidden size 1,536). They are first trained with autoregressive next-token prediction and then converted to embedding models via the General Text Embedding (GTE) procedure [43], which replaces the causal mask with BERT-like bidirectional attention during embedding extraction. Contrastive learning is applied using a mixture of private datasets to enhance embedding performance. The models also incorporate instructions tailored for embedding tasks and support a context size of up to 32,000 tokens.

Llama3.1-LLM2Vec-8B is built upon the Llama-3.1-8B-Instruct LLM [49], which has a decoder-only Transformer architecture with 32 layers, 32 attention heads, and a hidden size of 4,096 (Hugging Face identifier: `McGill-NLP/LLM2Vec-Meta-Llama-31-8B-Instruct-mntp-supervised`). Initially trained for next-token prediction, it was converted to an embedding model using the LLM2Vec method [40]. This method adds bidirectional attention and fine-tunes the model with supervised contrastive learning on embedding tasks. Fine-tuning used curated data from the public E5 dataset [59, 60], containing approximately 1.5 million entries. The model supports task-specific instructions and a context size of up to 128,000 tokens.

DeBERTa v3 base/large are encoder-only Transformer models designed for token embeddings [61]. They improve upon their predecessor by replacing the masked language modeling objective with replaced token detection and using Gradient-Disentangled Embedding Sharing. We evaluated the base variant (12 layers, 12 attention heads, 768 hidden size) and the large variant (24 layers, 16 attention heads, 1,024 hidden size), with parameter counts of 183M and 434M, respectively (Hugging Face identifier: `microsoft/deberta-v3-{base,large}`).

BERT base/large: BERT is a well-established text embedding model using an encoder-only Transformer trained with the masked language modeling objective [15]. We included both the base (12 layers, 12 attention heads, 768 hidden size, 110M parameters) and large (24 layers, 16 attention heads, 1,024 hidden size, 340M parameters) variants as benchmarks (Hugging Face identifier: `google-bert/bert-{base,large}-uncased`). While not state of the art, BERT models remain widely used in embedding tasks.

Bio_ClinicalBERT builds on BERT-Base, further fine-tuned on biomedical [62] and clinical data [54]. It is a widely adopted embedding model for medical

text and was included as a baseline for comparison (Hugging Face identifier: `emilyalsentzer/Bio_ClinicalBERT`).

MedBERT builds on Bio_ClinicalBERT through continued domain pretraining on heterogeneous biomedical corpora (N2C2, BioNLP, CRAFT, and biomedical Wikipedia) and was originally introduced for biomedical NER [63]. We include it as a domain-adapted baseline for comparison (Hugging Face identifier: `Charangan/MedBERT`).

CLMBR-T-Base is a specialized EHR foundation model trained on 2.57 million de-identified EHRs from Stanford Medicine with autoregressive next-code prediction [13, 45]. With the estimated 706 mean clinical events per patient [45], this leads to approximately 1.8B clinical events for training. CLMBR-T-Base has 12 transformer layers and a hidden dimension of 768 (Hugging Face identifier: `StanfordShahLab/clmbr-t-base`). The model has 141M parameters and allows for a context window of 496 codes. CLMBR-T-Base has demonstrated improvements over count-based baselines across a variety of clinical prediction tasks [45]. It serves as the main baseline for our experiments to test specialized EHR models against general-purpose text embedding models for representing EHR records.

LLM Embedding Model and CLMBR-T-Base is a model combination used to test whether the LLM embedding models and the EHR foundation model learn orthogonal information. To this end, we simply appended both embeddings. The resulting embeddings have dimensions of 4,864 for Qwen3-Emb-8B.

Count-based Models have proven to be strong baselines for EHR prediction tasks [6, 12, 13]. All EHR events of a patient are encoded in a single vector, where each entry represents the number of occurrences of a medical concept. We used the count-based baseline introduced in [45], which uses counts for all clinical events that occurred in a patient's timeline prior to the prediction time and extends this approach with ontology expansion, enriching the vectors with parent and child concepts. We also included three extensions of the above count baseline implemented in the Electronic Medical Records (FEMR) toolkit [13], using (1) time binning of 0–30, 30–180, 180–365, and 365+ days [13], (2) numeric values partitioned into deciles [6], (3) string values [6], and a combination of all three (Table S6).

Based on the embeddings or count vectors generated by the methods described above, a classification head was trained and validated for each prediction task. For the embedding models, we used a logistic regression head as default. For the count-based model, we used a GBM [57] as the primary classifier because it performs better for high-dimensional count features (Table S4). For completeness, we also report count-based results with a logistic regression head. We adopted the parameter tuning of the classification heads from the EHRSHOT benchmark to ensure comparability [45].

4.5 Instructions for LLM Embedding Models

The Qwen2, Qwen3, and LLM2Vec models use instruction-tuned embeddings. We therefore added simple prompts for each prediction task based on their respective templates. For instance, for prediction of anemia, we added "Given a patient's electronic healthcare record (EHR) as a newline-separated list, retrieve relevant passages that answer the query: has the patient anemia". The existing EHRSHOT benchmark

encodes EHRs for the same patient and identical prediction times only once for efficiency. To support task-specific instructions, we changed this behavior and encoded each (patient, task, prediction time) instance, resulting in 1,161,412 instead of 406,379 EHRs and longer processing times. The difference between the 1,161,412 labels used in our experiments and the total number of 1,178,665 labels (Table 2) arises because some labels share the same task and prediction time and are therefore merged. For experiments in UKB, we designed analogous instructions. We list all instructions in Table S3 and perform ablations to test their effect.

4.6 Fine-Tuned LLM Embedding and LLM Decoder Models

The main approach evaluated in this paper used LLM embedding models that encode the EHR serialization into a fixed-length vector prior to classification. For comparison, we also tested LLM decoder models that generate text whose token probabilities are used for classification. We further assessed the effect of fine-tuning for both approaches. For comparability, all encoder, decoder, and decoder-ICL experiments used the same default list-based EHR serialization and the same task-specific instructions. In contrast to the other experiments, inputs were truncated to 4,096 tokens due to computational restrictions.

For the encoder setting, we fine-tuned Qwen3-Emb-8B [39, 44] with LoRA adapters [64] applied to the attention and MLP projection modules (`q_proj`, `k_proj`, `v_proj`, `o_proj`, `up_proj`, `down_proj`, `gate_proj`). The encoder was paired with a lightweight classification head consisting of a dropout layer and a linear projection, and optimized end-to-end with cross-entropy loss. Inputs were created by prepending the task-specific instruction to the serialized EHR and using tokenization with left padding to preserve recency under truncation.

For the decoder setting, we adapted the instruction-tuned causal language model Qwen3-8B (Hugging Face identifier: `Qwen/Qwen3-8B`) with LoRA adapters on the same projection modules. The decoder received a chat-style prompt containing the task instruction and the serialized EHR (Table S3), and was trained to predict the literal next token `Yes` or `No`. At evaluation time, we scored each example by aggregating the probability mass assigned to single-token variants of `Yes` and `No`, including capitalization and punctuation variants, and then normalizing to a two-way probability.

We also evaluated decoder ICL without weight updates. These prompts used the same task-specific instruction and deterministic balanced example selection. We evaluated 0-, 2-, 4-, and 6-shot ICL only; larger ICL settings were not computationally feasible. To limit prompt growth, we applied separate 4,096-token caps to the rendered ICL examples block and to the base prompt containing the target patient record.

For both fine-tuned model families, we kept the optimizer and most training settings fixed and tuned only the main adaptation hyperparameters. The tuning grid covered learning rates of 5×10^{-5}, 10^{-4}, and 2×10^{-4}, LoRA ranks of 8, 16, and 64, and LoRA dropout values of 0.0, 0.05, and 0.1, yielding 27 configurations per model family. We fixed LoRA $\alpha = 32$, warmup ratio 0.03, a maximum of 20 epochs, AdamW optimization via the Hugging Face `Trainer`, cosine learning-rate decay, early stopping with patience 5, gradient checkpointing, and an effective batch size of 8. Per-task

tuning across all EHRSHOT subtasks was computationally infeasible. We therefore performed tuning on the operational-outcomes and new-diagnosis tasks only (`guo_*` and `new_*`) at $k \in \{8, 16\}$ using validation AUROC as the selection criterion, and then chose one shared setting per model family based on mean validation AUROC across those tasks (Table S13). This selected an encoder setting with learning rate 5×10^{-5}, LoRA rank 8, and dropout 0.1, and a decoder setting with learning rate 2×10^{-4}, LoRA rank 8, and dropout 0.05. Using these fixed settings, we reran the full fine-tuning matrix across all EHRSHOT subtasks, $k \in \{1, 2, 4, 8, 16, 32, 64, 128\}$, and five replicates. For both model families, evaluation computed AUROC, AUPRC, and Brier score on the held-out test set together with 1,000 patient-level bootstrap replicates to estimate standard deviations and 95% confidence intervals.

4.7 Existing Methods Using Language Models for EHR Prediction

Two broad approaches have emerged for leveraging language models with structured EHR data: generation-based prediction and embedding-based prediction. Early work on generation-based approaches converted structured claims into short text snippets and queried encoder–decoder models with a 512-token context limit, showing improvements in few-shot regimes (16–64 examples) for end-of-life, surgery, and length-of-stay tasks [26]. Subsequent studies explored larger LLMs, prompt design, and fine-tuning strategies on serialized EHR inputs, typically treating prediction as text generation or calibrated scoring [27–32]. One variant constrains the model's output space to medical codes to better align free-text reasoning with code-based clinical labels, thereby bridging the gap between general-purpose language models and EHR-specific foundation models [65].

Embedding-based methods instead extract fixed-dimensional representations for downstream classifiers [33–36]. Gao et al. provide a systematic comparison across serialization formats, LLMs, and embedding strategies on MIMIC-III and a private 660-patient clinical-deterioration dataset, reporting that LLM embeddings paired with a prediction head can be competitive in some settings, while raw numerical features remain strong baselines [33]. They also evaluate a decoder-based approach producing `Yes` and `No` tokens in the zero-shot setting but find no discriminatory ability for Mistral-7B-Instruct and Llama3-8B-Instruct. The GRASP framework shows that combining LLM-derived embeddings of medical codes with transformer predictors improves cross-dataset generalization [36]. The DeLLiriuM method introduced in [35] also evaluates embeddings derived from different LLMs for delirium prediction and performs detailed model introspection via a SHAP analysis. Most similar to our work is the MEME method, which encodes different EHR modalities such as vitals, medications, and diagnoses into separate embeddings and fuses them with a self-attention layer [34]. This framework uses the relatively small and efficient MedBERT language model for embedding creation and reports superior performance to GPT-4 [34].

Our study follows the embedding paradigm but differs from prior work in three ways. First, we use LLMs explicitly adapted for embedding via contrastive learning. Second, we operate with substantially longer inputs (up to 8,192 tokens), which is important for longitudinal EHR serialization where earlier studies often processed up

to 3,076 tokens [33] or relied on chunking [34]. Third, we evaluate on large public longitudinal cohorts and standardized benchmarks from EHRSHOT and UKB. We also include a MEME-style baseline with a linear head in place of self-attention due to data sparsity [34]. Finally, consistent with [33], we explicitly compare embeddings to direct LLM outputs and examine parameter-efficient fine-tuning to assess robustness and practical trade-offs (Section 2.6).

4.8 Computational Setup and Runtime

All experiments were conducted on the Charité High-Performance Cluster offering different GPU setups. Due to the larger memory requirements of the LLMs, we used a smaller batch size for inference compared to encoder-based models and CLMBR-T-Base. For the Llama3.1-LLM2Vec-8B model, runtime errors occurred during multi-GPU experiments with the full dataset. These issues were resolved by splitting the data into smaller batches, which introduced additional overhead. Additionally, we optimized the LLM2Vec code by removing an initial word-boundary token-limit routine that iteratively re-tokenizes to ensure the final cut occurs at a word boundary, with minimal effect on performance limited to a potentially incomplete trailing word. To quantify runtime differences, we measured the wall-clock encoding time for the EHRSHOT benchmark on the same 8-GPU Nvidia H200 cluster for CLMBR-T-Base, LLM embedding models, and encoder-based models (Table S12). We tried to use the maximum possible batch sizes. Encoder-based models used 512-token chunks of the up to 8,192-token inputs, which substantially increased their runtime. On the UKB, encoding all 387,464 UKB patients for one task with a maximum context length of 8,192 on the same H200 cluster took 4:46:34 hours for Qwen3-Emb-8B, 3:49:21 hours for Qwen2-Emb-7B, and 3:55:12 hours for Llama3.1-LLM2Vec-8B.

4.9 Performance Results on EHRSHOT Prediction Tasks and Few-Shot Setting

Following the EHRSHOT benchmark, we evaluated all models across 15 prediction tasks under various few-shot settings. The benchmark includes a modular pipeline designed to execute key tasks, with the flexibility to optionally use a Slurm cluster for distributed execution. Running all steps within this pipeline ensures full reproducibility of results. Step four of the pipeline, which generates EHR representations with CLMBR-T-Base and the count-based model, was extended to incorporate our method for creating language model-based EHR representations. This adaptation allowed reuse of significant portions of the existing code, including the task evaluation framework. Additionally, we implemented new functionality for EHR serialization and slightly modified other steps of the benchmark to accommodate our experimental setup. For instance, the label creation process was adjusted (step three) to enable task-specific instructions for the LLM embedding models. All modifications have been documented and can be tracked in our public GitHub repository.

4.10 External Validation on UK Biobank

External validation was performed using data from the UKB, a large-scale prospective cohort study comprising 502,489 UK participants recruited between 2006 and 2010, with a median follow-up of 13.8 years (Table 1). We used linked EHR data from primary care (General Practitioner (GP)) and secondary care (Hospital Episode Statistics (HES)), providing information on diagnoses, procedures, and prescriptions. We aimed to closely replicate the experimental setup of the EHRSHOT benchmark by using predefined splits of training, validation, and test data (Table S1), defining tasks and task groups accordingly, and applying the same few-shot analysis, hyperparameter tuning scheme, and statistical evaluation.

Initial data preprocessing, including cleaning, feature extraction, missing-value imputation, and endpoint selection, followed the methodology described in [46]. All health records were mapped to the OMOP CDM using mapping tables provided by the UKB, SNOMED International, and the OHDSI community for mapping concepts from provider- and country-specific non-standard vocabularies to OMOP standard vocabularies. Participants not having full demographic information were excluded. Participants lacking any recorded GP or HES events either before or after their recruitment date were excluded, resulting in a validation cohort of 387,464 individuals. Diagnostic codes were mapped to Phecodes X [66, 67] primarily for standardized endpoint definition and cohort selection. To avoid redundancy with medical codes used as features, the Phecodes were excluded during the creation of patient representations. Due to significant challenges in mapping and harmonizing UKB laboratory values [68], and to ensure comparability across models and tasks, medical codes of laboratory values were used without numerical values [46]. The final feature set comprised conditions (SNOMED, CVX), medications (RxNorm), and procedures (SNOMED).

We defined the following tasks for the UKB: (1) prediction of all-cause hospitalization within the next year (operational outcomes), (2) prediction of all-cause mortality (mortality prediction), and (3) prediction of incident diagnoses for a set of selected conditions (assignment of new diagnoses). The selection of diseases for the assignment of new diagnoses task group largely followed [46], focusing on common conditions, diseases lacking established risk stratification tools, and specific cardiovascular conditions. From the initial 24 endpoints proposed in [46], we treated all-cause mortality as a separate task, leading to a total of 25 tasks. For the assignment of new diagnoses and mortality tasks, patients with a diagnosis of the respective endpoint recorded prior to and on the day of their UKB recruitment date were excluded. This exclusion was not applied to the hospitalization task due to the high incidence of hospitalization events before the recruitment date (Table S1). In the external validation on UKB, each patient had only one prediction date, which was marked by their recruitment date. Analogously to the main experiments, we used a simple EHR list serialization of the most recent occurrence of each medical code, with birth and race events added at the time of birth.

The pretrained CLMBR-T-Base model operates with a fixed vocabulary of 26,249 unique codes. To use this model, we mapped the 50,702 unique medical codes (SNOMED CT, RxNorm, CVX) present in our processed UKB cohort to the CLMBR-T-Base vocabulary. This mapping followed steps similar to those implemented in the

FEMR package, involving direct code matching where possible, supplemented by indirect mapping via the OHDSI ATHENA vocabulary using "Maps to" relationships and inclusion of ancestor concepts. This process constituted a major effort and required approximately two weeks to complete. Overall, 7,969 (16%) unique UKB codes were successfully mapped to the CLMBR-T-Base vocabulary (in the format ontology/code), which were responsible for 25% of medical events in the UKB. The relatively low mapping coverage can be attributed to differences in underlying hospital systems and the distinct purposes of the datasets. Unmapped codes were excluded for CLMBR-T-Base. Additionally, UKB ethnicities were converted to the ethnicity groups used by CLMBR-T-Base. The final data of mapped medical events, birth date, ethnicity, and visits were converted into the MEDS standard [69]. For transforming patient information into embeddings, we mainly followed the code provided by FEMR, primarily using the `convert_patient` function with minor modifications to enable batch processing. To disentangle effects of vocabulary coverage from generalization capabilities, we performed a sensitivity analysis on UKB by restricting Qwen3-Emb-8B to CLMBR-T-Base-mappable codes. We performed the same few-shot experiments and statistical analyses as for the main experiments to compare Qwen3-Emb-8B with all UKB codes, Qwen3-Emb-8B restricted to CLMBR-T-Base-mappable codes, and CLMBR-T-Base (Table 4, Fig. S13, and Table S17).

Analogously to the best count-based model for EHRSHOT, the count model for the UKB included ontology expansion [45], increasing the number of unique codes from 50,702 to 71,393, and time binning of 0–30, 30–180, 180–365, and 365+ days [13]. In contrast to the EHRSHOT experiments, the count-based model did not include string or numeric values because the UKB did not provide them. We also added normalized age at prediction time and coded sex as additional features. Lastly, we evaluated the best encoder-based language model from the EHRSHOT experiments, BioClinicalBERT, on the UKB.

4.11 Statistical Testing

To assess the significance of performance differences between the best LLM embedding model, Qwen3-Emb-8B, the EHR foundation model CLMBR-T-Base, the encoder-only model BioClinicalBERT, and the count-based baseline, we performed statistical tests for per-task performance on EHRSHOT and the UKB. We evaluated three training regimes: a very few-shot setting with 8 positive and 8 negative examples, a few-shot setting with 64 positive and 64 negative examples, and training on all available data. We excluded tasks with insufficient training data for the 64-shot setting. Few-shot experiments with five-fold cross-validation already evaluate learning efficiency and robustness under limited training data, whereas the statistical tests assess whether the final trained models differ significantly in population-level task performance. Statistical significance of AUROC differences between models was assessed using a paired, patient-level bootstrap on the held-out test set with 10,000 bootstrap replicates. For each shot setting, we used all evaluation replicates by averaging predicted probabilities across replicates for each test example before computing the bootstrap statistic. For the chest X-ray findings task, which comprises 14 binary sub-tasks, the bootstrap statistic is the macro-averaged AUROC, defined as the mean of per-sub-task

AUROCs computed within each bootstrap replicate, matching the macro-average metric reported in the main results. We report 95% percentile confidence intervals and two-sided p-values computed from the bootstrap ΔAUROC distribution. For each shot setting, p-values were adjusted jointly across all tasks and baseline comparisons using Holm's procedure to control the family-wise error rate. This corresponds to a correction over 45 hypotheses per shot setting for 15 tasks and three model comparisons on EHRSHOT, and 75 (8-shot, all data) and 60 (64-shot) hypotheses for the UKB (Table S5 and Table S15). We also performed an analogous statistical test for the sensitivity analysis of Qwen3-Emb-8B restricted to CLMBR-T-Base-mappable codes on the UKB (Table S17).

4.12 Ablation Studies of EHR Serialization

To better understand the contribution of various components in the EHR serialization process to the performance of the LLM embedding models, we conducted a series of ablation studies. These ablations used Qwen3-Emb-8B with the default list serialization and a 8,192-token limit. We first examined the role of task-specific instructions by replacing them with a generic prompt (Table S3) or removing instructions entirely, thereby isolating their contribution to the resulting embeddings. Next, we systematically excluded medical events from six different categories: demographics, visits, medications, procedures, labs, and conditions. To this end, we grouped medical codes into six mutually exclusive categories based on ontology prefixes and hierarchical SNOMED parent concepts (Table S8). Finally, we constructed serializations that retained only medical events from one category.

4.13 Effect of Different Time Windows

To examine the influence of recency on predictive performance, we varied the time window preceding the prediction date used during EHR text serialization with a maximum context size of 8,192 tokens. We evaluated Qwen3-Emb-8B, Qwen2-Emb-7B, Llama3.1-LLM2Vec-8B, and the count-based baseline with a GBM head across seven intervals: one hour, one day, one week (7 days), one month (30 days), one year (365 days), three years (1,095 days), and full history. For each window, only events occurring within the specified interval before the prediction time were included. Thus, only data from the respective time window contributed to the aggregated information and visit data in the EHR serialization. All other aspects of the serialization, including structure, formatting, and instruction prompts, remained unchanged to isolate the effect of the temporal window.

4.14 Effect of Different Context Sizes

We investigated the impact of varying context sizes in the LLM embedding models. Specifically, we evaluated Qwen3-Emb-8B, Qwen2-Emb-7B, and Llama3.1-LLM2Vec-8B with input token limits of 512, 1,024, 2,048, 4,096, and 8,192 tokens. Input tokens exceeding these thresholds were discarded. Due to the EHR list serialization including the most recent occurrences of each medical code, additional input tokens primarily consisted of earlier medical concepts. All other preprocessing choices and task-specific

instructions were held fixed across context-size settings. By testing these varying context sizes, we aimed to assess the balance between capturing historical medical data and preserving the clarity of high-priority information within the embeddings.

Data Availability

The EHRSHOT data are available through gated access via https://doi.org/10.57761/0gv9-nd83. UK Biobank data, including all linked routine health records, are publicly available to bona fide researchers upon application at http://www.ukbiobank.ac.uk/using-the-resource. In this study, only primary care data not subject to the Government's Control of Patient Information (COPI) notice were used (UK Biobank Category 3000).

Code Availability

All extensions and experiments conducted for this paper are publicly available via our GitHub repository: https://github.com/stefanhgm/ehrshot-benchmark.

Acknowledgements

This work was funded by the Deutsche Forschungsgemeinschaft (DFG, German Research Foundation) – Project-ID 437531118 – SFB 1470 and the German Federal Ministry of Education and Research (BMBF) Project-ID 01ZZ2317G. Stefan Hegselmann is a participant in the BIH Charité Junior Digital Clinician Scientist Program funded by Charité – Universitätsmedizin Berlin and the Berlin Institute of Health at Charité (BIH).

Author Contributions

S.H., G.v.A., and B.W. designed the study. T.R., N.K., D.S., G.H., and R.E. reviewed and revised the experimental setup. S.H. implemented and conducted the experiments on EHRSHOT. G.v.A. and B.W. implemented and conducted the experiments on the UK Biobank. S.H. and G.v.A. created the initial figures, which were revised and finalized with contributions from T.R., N.K., and B.W. S.H. drafted the initial manuscript, and G.v.A., T.R., N.K., D.S., G.H., R.E., and B.W. provided substantial feedback. S.H., G.v.A., and B.W. revised and prepared the final version of the manuscript. All authors reviewed and approved the final manuscript.

Competing Interests

The authors declare no competing interests.

References

[1] Dash, S., Shakyawar, S.K., Sharma, M., Kaushik, S.: Big data in healthcare: management, analysis and future prospects. Journal of Big Data **6**(1), 54 (2019) https://doi.org/10.1186/s40537-019-0217-0 . Accessed 2025-02-15

[2] Ahsan, H., McInerney, D.J., Kim, J., Potter, C., Young, G., Amir, S., Wallace, B.C.: Retrieving Evidence from EHRs with LLMs: Possibilities and Challenges. Proceedings of machine learning research **248**, 489–505 (2024). Accessed 2025-02-15

[3] Rajkomar, A., Dean, J., Kohane, I.: Machine Learning in Medicine. New England Journal of Medicine **380**(14), 1347–1358 (2019) https://doi.org/10.1056/NEJMra1814259 . Accessed 2020-06-05

[4] Xu, D., Wang, C., Khan, A., Shang, N., He, Z., Gordon, A., Kullo, I.J., Murphy, S., Ni, Y., Wei, W.-Q., Gharavi, A., Kiryluk, K., Weng, C., Ionita-Laza, I.: Quantitative disease risk scores from EHR with applications to clinical risk stratification and genetic studies. npj Digital Medicine **4**(1), 1–13 (2021) https://doi.org/10.1038/s41746-021-00488-3 . Publisher: Nature Publishing Group. Accessed 2025-02-15

[5] Golas, S.B., Shibahara, T., Agboola, S., Otaki, H., Sato, J., Nakae, T., Hisamitsu, T., Kojima, G., Felsted, J., Kakarmath, S., Kvedar, J., Jethwani, K.: A machine learning model to predict the risk of 30-day readmissions in patients with heart failure: a retrospective analysis of electronic medical records data. BMC Medical Informatics and Decision Making **18**(1), 44 (2018) https://doi.org/10.1186/s12911-018-0620-z . Accessed 2024-12-14

[6] Rajkomar, A., Oren, E., Chen, K., Dai, A.M., Hajaj, N., Hardt, M., Liu, P.J., Liu, X., Marcus, J., Sun, M., Sundberg, P., Yee, H., Zhang, K., Zhang, Y., Flores, G., Duggan, G.E., Irvine, J., Le, Q., Litsch, K., Mossin, A., Tansuwan, J., Wang, D., Wexler, J., Wilson, J., Ludwig, D., Volchenboum, S.L., Chou, K., Pearson, M., Madabushi, S., Shah, N.H., Butte, A.J., Howell, M.D., Cui, C., Corrado, G.S., Dean, J.: Scalable and accurate deep learning with electronic health records. npj Digital Medicine **1**(1), 1–10 (2018) https://doi.org/10.1038/s41746-018-0029-1 . Publisher: Nature Publishing Group. Accessed 2024-12-15

[7] Lauritsen, S.M., Kalør, M.E., Kongsgaard, E.L., Lauritsen, K.M., Jørgensen, M.J., Lange, J., Thiesson, B.: Early detection of sepsis utilizing deep learning on electronic health record event sequences. Artificial Intelligence in Medicine **104**, 101820 (2020) https://doi.org/10.1016/j.artmed.2020.101820 . Accessed 2024-12-15

[8] Moor, M., Bennett, N., Plečko, D., Horn, M., Rieck, B., Meinshausen, N., Bühlmann, P., Borgwardt, K.: Predicting sepsis using deep learning across

international sites: a retrospective development and validation study. eClinicalMedicine **62** (2023) https://doi.org/10.1016/j.eclinm.2023.102124 . Publisher: Elsevier. Accessed 2024-12-15

[9] Thorsen-Meyer, H.-C., Nielsen, A.B., Nielsen, A.P., Kaas-Hansen, B.S., Toft, P., Schierbeck, J., Strøm, T., Chmura, P.J., Heimann, M., Dybdahl, L., Spangsege, L., Hulsen, P., Belling, K., Brunak, S., Perner, A.: Dynamic and explainable machine learning prediction of mortality in patients in the intensive care unit: a retrospective study of high-frequency data in electronic patient records. The Lancet. Digital Health **2**(4), 179–191 (2020) https://doi.org/10.1016/S2589-7500(20)30018-2

[10] Desai, R.J., Wang, S.V., Vaduganathan, M., Evers, T., Schneeweiss, S.: Comparison of Machine Learning Methods With Traditional Models for Use of Administrative Claims With Electronic Medical Records to Predict Heart Failure Outcomes. JAMA Network Open **3**(1), 1918962 (2020) https://doi.org/10.1001/jamanetworkopen.2019.18962 . Accessed 2024-12-15

[11] Kim, E., Rubinstein, S.M., Nead, K.T., Wojcieszynski, A.P., Gabriel, P.E., Warner, J.L.: The Evolving Use of Electronic Health Records (EHR) for Research. Seminars in Radiation Oncology **29**(4), 354–361 (2019) https://doi.org/10.1016/j.semradonc.2019.05.010 . Accessed 2025-02-15

[12] Rasmy, L., Xiang, Y., Xie, Z., Tao, C., Zhi, D.: Med-BERT: pretrained contextualized embeddings on large-scale structured electronic health records for disease prediction. npj Digital Medicine **4**(1), 1–13 (2021) https://doi.org/10.1038/s41746-021-00455-y . Publisher: Nature Publishing Group. Accessed 2024-12-15

[13] Steinberg, E., Jung, K., Fries, J.A., Corbin, C.K., Pfohl, S.R., Shah, N.H.: Language models are an effective representation learning technique for electronic health record data. Journal of Biomedical Informatics **113**, 103637 (2021) https://doi.org/10.1016/j.jbi.2020.103637 . Accessed 2024-06-12

[14] Bommasani, R., Hudson, D.A., Adeli, E., Altman, R., Arora, S., Arx, S.v., Bernstein, M.S., Bohg, J., Bosselut, A., Brunskill, E., Brynjolfsson, E., Buch, S., Card, D., Castellon, R., Chatterji, N., Chen, A., Creel, K., Davis, J.Q., Demszky, D., Donahue, C., Doumbouya, M., Durmus, E., Ermon, S., Etchemendy, J., Ethayarajh, K., Fei-Fei, L., Finn, C., Gale, T., Gillespie, L., Goel, K., Goodman, N., Grossman, S., Guha, N., Hashimoto, T., Henderson, P., Hewitt, J., Ho, D.E., Hong, J., Hsu, K., Huang, J., Icard, T., Jain, S., Jurafsky, D., Kalluri, P., Karamcheti, S., Keeling, G., Khani, F., Khattab, O., Koh, P.W., Krass, M., Krishna, R., Kuditipudi, R., Kumar, A., Ladhak, F., Lee, M., Lee, T., Leskovec, J., Levent, I., Li, X.L., Li, X., Ma, T., Malik, A., Manning, C.D., Mirchandani, S., Mitchell, E., Munyikwa, Z., Nair, S., Narayan, A., Narayanan, D., Newman, B., Nie, A., Niebles, J.C., Nilforoshan, H., Nyarko, J., Ogut, G., Orr, L., Papadimitriou, I., Park, J.S., Piech, C., Portelance, E., Potts, C., Raghunathan, A., Reich, R., Ren,

H., Rong, F., Roohani, Y., Ruiz, C., Ryan, J., Ré, C., Sadigh, D., Sagawa, S., Santhanam, K., Shih, A., Srinivasan, K., Tamkin, A., Taori, R., Thomas, A.W., Tramèr, F., Wang, R.E., Wang, W., Wu, B., Wu, J., Wu, Y., Xie, S.M., Yasunaga, M., You, J., Zaharia, M., Zhang, M., Zhang, T., Zhang, X., Zhang, Y., Zheng, L., Zhou, K., Liang, P.: On the Opportunities and Risks of Foundation Models. arXiv. arXiv:2108.07258 [cs] (2022). https://doi.org/10.48550/arXiv.2108.07258 . http://arxiv.org/abs/2108.07258 Accessed 2024-12-16

[15] Devlin, J., Chang, M.-W., Lee, K., Toutanova, K.: BERT: Pre-training of Deep Bidirectional Transformers for Language Understanding. Proceedings of the 2019 Conference of the North American Chapter of the Association for Computational Linguistics: Human Language Technologies, Volume 1 (Long and Short Papers), 4171–4186 (2019) https://doi.org/10.18653/v1/N19-1423 . Accessed 2022-04-22

[16] Radford, A., Wu, J., Child, R., Luan, D., Amodei, D., Sutskever, I.: Language Models are Unsupervised Multitask Learners. Technical report, OpenAi, 24 (2019)

[17] Odgaard, M., Klein, K.V., Thysen, S.M., Jimenez-Solem, E., Sillesen, M., Nielsen, M.: CORE-BEHRT: A Carefully Optimized and Rigorously Evaluated BEHRT. arXiv. arXiv:2404.15201 [cs] (2024). https://doi.org/10.48550/arXiv.2404.15201 . http://arxiv.org/abs/2404.15201 Accessed 2024-12-16

[18] Pang, C., Jiang, X., Kalluri, K.S., Spotnitz, M., Chen, R., Perotte, A., Natarajan, K.: CEHR-BERT: Incorporating temporal information from structured EHR data to improve prediction tasks. arXiv. arXiv:2111.08585 [cs] (2021). https://doi.org/10.48550/arXiv.2111.08585 . http://arxiv.org/abs/2111.08585 Accessed 2024-12-16

[19] Li, Y., Rao, S., Solares, J.R.A., Hassaine, A., Ramakrishnan, R., Canoy, D., Zhu, Y., Rahimi, K., Salimi-Khorshidi, G.: BEHRT: Transformer for Electronic Health Records. Scientific Reports **10**(1), 7155 (2020) https://doi.org/10.1038/s41598-020-62922-y . Publisher: Nature Publishing Group. Accessed 2024-12-16

[20] Waxler, S., Blazek, P., White, D., Sneider, D., Chung, K., Nagarathnam, M., Williams, P., Voeller, H., Wong, K., Swanhorst, M., Zhang, S., Usuyama, N., Wong, C., Naumann, T., Poon, H., Loza, A., Meeker, D., Hain, S., Shah, R.: Generative Medical Event Models Improve with Scale. arXiv. arXiv:2508.12104 [cs] version: 1 (2025). https://doi.org/10.48550/arXiv.2508.12104 . http://arxiv.org/abs/2508.12104 Accessed 2025-09-16

[21] Shmatko, A., Jung, A.W., Gaurav, K., Brunak, S., Mortensen, L.H., Birney, E., Fitzgerald, T., Gerstung, M.: Learning the natural history of human disease with generative transformers. Nature, 1–9 (2025) https://doi.org/10.1038/s41586-025-09529-3 . Publisher: Nature Publishing Group. Accessed 2025-10-04

[22] Penedo, G., Malartic, Q., Hesslow, D., Cojocaru, R., Alobeidli, H., Cappelli, A.,

Pannier, B., Almazrouei, E., Launay, J.: The RefinedWeb Dataset for Falcon LLM: Outperforming Curated Corpora with Web Data Only. Advances in Neural Information Processing Systems **36**, 79155–79172 (2023). Accessed 2025-05-01

[23] Raffel, C., Shazeer, N., Roberts, A., Lee, K., Narang, S., Matena, M., Zhou, Y., Li, W., Liu, P.J.: Exploring the limits of transfer learning with a unified text-to-text transformer. J. Mach. Learn. Res. **21**(1), 140–54851405551 (2020)

[24] Agrawal, M., Hegselmann, S., Lang, H., Kim, Y., Sontag, D.: Large Language Models are Few-Shot Clinical Information Extractors. Proceedings of the 2022 Conference on Empirical Methods in Natural Language Processing, 1998–2022 (2022) https://doi.org/10.18653/v1/2022.emnlp-main.130 . Accessed 2024-04-12

[25] Van Veen, D., Van Uden, C., Blankemeier, L., Delbrouck, J.-B., Aali, A., Bluethgen, C., Pareek, A., Polacin, M., Reis, E.P., Seehofnerová, A., Rohatgi, N., Hosamani, P., Collins, W., Ahuja, N., Langlotz, C.P., Hom, J., Gatidis, S., Pauly, J., Chaudhari, A.S.: Adapted large language models can outperform medical experts in clinical text summarization. Nature Medicine, 1–9 (2024) https://doi.org/10.1038/s41591-024-02855-5 . Publisher: Nature Publishing Group. Accessed 2024-04-11

[26] Hegselmann, S., Buendia, A., Lang, H., Agrawal, M., Jiang, X., Sontag, D.: TabLLM: Few-shot Classification of Tabular Data with Large Language Models. Proceedings of The 26th International Conference on Artificial Intelligence and Statistics, 5549–5581 (2023). Accessed 2024-04-12

[27] Shoham, O.B., Rappoport, N.: CPLLM: Clinical prediction with large language models. PLOS Digital Health **3**(12), 0000680 (2024) https://doi.org/10.1371/journal.pdig.0000680 . Publisher: Public Library of Science. Accessed 2025-09-22

[28] Zhu, Y., Wang, Z., Gao, J., Tong, Y., An, J., Liao, W., Harrison, E.M., Ma, L., Pan, C.: Prompting Large Language Models for Zero-Shot Clinical Prediction with Structured Longitudinal Electronic Health Record Data. arXiv. arXiv:2402.01713 [cs] (2024). https://doi.org/10.48550/arXiv.2402.01713 . http://arxiv.org/abs/2402.01713 Accessed 2025-09-22

[29] Cui, H., Shen, Z., Zhang, J., Shao, H., Qin, L., Ho, J.C., Yang, C.: LLMs-based Few-Shot Disease Predictions using EHR: A Novel Approach Combining Predictive Agent Reasoning and Critical Agent Instruction. arXiv. arXiv:2403.15464 [cs] (2024). https://doi.org/10.48550/arXiv.2403.15464 . http://arxiv.org/abs/2403.15464 Accessed 2024-12-16

[30] Acharya, A., Shrestha, S., Chen, A., Conte, J., Avramovic, S., Sikdar, S., Anastasopoulos, A., Das, S.: Clinical risk prediction using language models: benefits and considerations. Journal of the American Medical Informatics Association **31**(9), 1856–1864 (2024) https://doi.org/10.1093/jamia/ocae030 . Accessed 2025-09-22

[31] Chen, C., Yu, J., Chen, S., Liu, C., Wan, Z., Bitterman, D., Wang, F., Shu, K.: ClinicalBench: Can LLMs Beat Traditional ML Models in Clinical Prediction? arXiv. arXiv:2411.06469 [cs] (2024). https://doi.org/10.48550/arXiv.2411.06469 . http://arxiv.org/abs/2411.06469 Accessed 2025-09-22

[32] Makarov, N., Bordukova, M., Quengdaeng, P., Garger, D., Rodriguez-Esteban, R., Schmich, F., Menden, M.P.: Large language models forecast patient health trajectories enabling digital twins. npj Digital Medicine **8**(1), 588 (2025) https://doi.org/10.1038/s41746-025-02004-3 . Publisher: Nature Publishing Group. Accessed 2025-10-09

[33] Gao, Y., Myers, S., Chen, S., Dligach, D., Miller, T.A., Bitterman, D., Churpek, M., Afshar, M.: When Raw Data Prevails: Are Large Language Model Embeddings Effective in Numerical Data Representation for Medical Machine Learning Applications? In: Al-Onaizan, Y., Bansal, M., Chen, Y.-N. (eds.) Findings of the Association for Computational Linguistics: EMNLP 2024, pp. 5414–5428. Association for Computational Linguistics, Miami, Florida, USA (2024). https://doi.org/10.18653/v1/2024.findings-emnlp.311 . https://aclanthology.org/2024.findings-emnlp.311/ Accessed 2025-09-22

[34] Lee, S.A., Jain, S., Chen, A., Ono, K., Biswas, A., Rudas, A., Fang, J., Chiang, J.N.: Clinical decision support using pseudo-notes from multiple streams of EHR data. npj Digital Medicine **8**(1), 394 (2025) https://doi.org/10.1038/s41746-025-01777-x . Publisher: Nature Publishing Group. Accessed 2025-09-16

[35] Contreras, M., Kapoor, S., Zhang, J., Davidson, A., Ren, Y., Guan, Z., Ozrazgat-Baslanti, T., Nerella, S., Bihorac, A., Rashidi, P.: DeLLiriuM: A large language model for delirium prediction in the ICU using structured EHR. arXiv. arXiv:2410.17363 [cs] (2024). https://doi.org/10.48550/arXiv.2410.17363 . http://arxiv.org/abs/2410.17363 Accessed 2025-09-22

[36] Kirchler, M., Ferro, M., Lorenzini, V., Water, R.P., Christoph Lippert, Ganna, A.: Large language models improve transferability of electronic health record-based predictions across countries and coding systems. npj Digital Medicine **9**(1), 177 (2026) https://doi.org/10.1038/s41746-026-02363-5 . Publisher: Nature Publishing Group. Accessed 2026-03-30

[37] Brown, T., Mann, B., Ryder, N., Subbiah, M., Kaplan, J.D., Dhariwal, P., Neelakantan, A., Shyam, P., Sastry, G., Askell, A., Agarwal, S., Herbert-Voss, A., Krueger, G., Henighan, T., Child, R., Ramesh, A., Ziegler, D., Wu, J., Winter, C., Hesse, C., Chen, M., Sigler, E., Litwin, M., Gray, S., Chess, B., Clark, J., Berner, C., McCandlish, S., Radford, A., Sutskever, I., Amodei, D.: Language Models are Few-Shot Learners. Advances in Neural Information Processing Systems **33**, 1877–1901 (2020). Accessed 2024-05-22

[38] Yang, A., Yang, B., Hui, B., Zheng, B., Yu, B., Zhou, C., Li, C., Li, C., Liu, D., Huang, F., Dong, G., Wei, H., Lin, H., Tang, J., Wang, J., Yang, J., Tu, J., Zhang,

J., Ma, J., Yang, J., Xu, J., Zhou, J., Bai, J., He, J., Lin, J., Dang, K., Lu, K., Chen, K., Yang, K., Li, M., Xue, M., Ni, N., Zhang, P., Wang, P., Peng, R., Men, R., Gao, R., Lin, R., Wang, S., Bai, S., Tan, S., Zhu, T., Li, T., Liu, T., Ge, W., Deng, X., Zhou, X., Ren, X., Zhang, X., Wei, X., Ren, X., Liu, X., Fan, Y., Yao, Y., Zhang, Y., Wan, Y., Chu, Y., Liu, Y., Cui, Z., Zhang, Z., Guo, Z., Fan, Z.: Qwen2 Technical Report. arXiv. arXiv:2407.10671 [cs] (2024). https://doi.org/10.48550/arXiv.2407.10671 . http://arxiv.org/abs/2407.10671 Accessed 2025-01-08

[39] Yang, A., Li, A., Yang, B., Zhang, B., Hui, B., Zheng, B., Yu, B., Gao, C., Huang, C., Lv, C., Zheng, C., Liu, D., Zhou, F., Huang, F., Hu, F., Ge, H., Wei, H., Lin, H., Tang, J., Yang, J., Tu, J., Zhang, J., Yang, J., Yang, J., Zhou, J., Zhou, J., Lin, J., Dang, K., Bao, K., Yang, K., Yu, L., Deng, L., Li, M., Xue, M., Li, M., Zhang, P., Wang, P., Zhu, Q., Men, R., Gao, R., Liu, S., Luo, S., Li, T., Tang, T., Yin, W., Ren, X., Wang, X., Zhang, X., Ren, X., Fan, Y., Su, Y., Zhang, Y., Zhang, Y., Wan, Y., Liu, Y., Wang, Z., Cui, Z., Zhang, Z., Zhou, Z., Qiu, Z.: Qwen3 Technical Report. arXiv. arXiv:2505.09388 [cs] (2025). https://doi.org/10.48550/arXiv.2505.09388 . http://arxiv.org/abs/2505.09388 Accessed 2025-10-04

[40] BehnamGhader, P., Adlakha, V., Mosbach, M., Bahdanau, D., Chapados, N., Reddy, S.: LLM2Vec: Large Language Models Are Secretly Powerful Text Encoders. (2024). https://openreview.net/forum?id=IW1PR7vEBf Accessed 2025-03-09

[41] Lee, C., Roy, R., Xu, M., Raiman, J., Shoeybi, M., Catanzaro, B., Ping, W.: NV-Embed: Improved Techniques for Training LLMs as Generalist Embedding Models. arXiv. arXiv:2405.17428 [cs] (2024). http://arxiv.org/abs/2405.17428 Accessed 2024-08-02

[42] Muennighoff, N., Su, H., Wang, L., Yang, N., Wei, F., Yu, T., Singh, A., Kiela, D.: Generative Representational Instruction Tuning. arXiv. arXiv:2402.09906 [cs] (2024). http://arxiv.org/abs/2402.09906 Accessed 2024-08-01

[43] Li, Z., Zhang, X., Zhang, Y., Long, D., Xie, P., Zhang, M.: Towards General Text Embeddings with Multi-stage Contrastive Learning. arXiv. arXiv:2308.03281 [cs] (2023). https://doi.org/10.48550/arXiv.2308.03281 . http://arxiv.org/abs/2308.03281 Accessed 2024-08-02

[44] Zhang, Y., Li, M., Long, D., Zhang, X., Lin, H., Yang, B., Xie, P., Yang, A., Liu, D., Lin, J., Huang, F., Zhou, J.: Qwen3 Embedding: Advancing Text Embedding and Reranking Through Foundation Models. arXiv. arXiv:2506.05176 [cs] (2025). https://doi.org/10.48550/arXiv.2506.05176 . http://arxiv.org/abs/2506.05176 Accessed 2025-09-28

[45] Wornow, M., Thapa, R., Steinberg, E., Fries, J.A., Shah, N.: EHRSHOT: An EHR Benchmark for Few-Shot Evaluation of Foundation Models. In: Thirty-seventh Conference on Neural Information Processing Systems Datasets and Benchmarks Track (2023). https://openreview.net/forum?id=CsXC6lcdwI Accessed 2024-06-12

[46] Steinfeldt, J., Wild, B., Buergel, T., Pietzner, M., Belzen, J., Vauvelle, A., Hegselmann, S., Denaxas, S., Hemingway, H., Langenberg, C., Landmesser, U., Deanfield, J., Eils, R.: Medical history predicts phenome-wide disease onset and enables the rapid response to emerging health threats. Nature Communications **16**(1), 585 (2025) https://doi.org/10.1038/s41467-025-55879-x . Publisher: Nature Publishing Group. Accessed 2025-02-15

[47] Sudlow, C., Gallacher, J., Allen, N., Beral, V., Burton, P., Danesh, J., Downey, P., Elliott, P., Green, J., Landray, M., Liu, B., Matthews, P., Ong, G., Pell, J., Silman, A., Young, A., Sprosen, T., Peakman, T., Collins, R.: UK Biobank: An Open Access Resource for Identifying the Causes of a Wide Range of Complex Diseases of Middle and Old Age. PLOS Medicine **12**(3), 1001779 (2015) https://doi.org/10.1371/journal.pmed.1001779 . Publisher: Public Library of Science. Accessed 2025-05-01

[48] Bycroft, C., Freeman, C., Petkova, D., Band, G., Elliott, L.T., Sharp, K., Motyer, A., Vukcevic, D., Delaneau, O., O'Connell, J., Cortes, A., Welsh, S., Young, A., Effingham, M., McVean, G., Leslie, S., Allen, N., Donnelly, P., Marchini, J.: The UK Biobank resource with deep phenotyping and genomic data. Nature **562**(7726), 203–209 (2018) https://doi.org/10.1038/s41586-018-0579-z . Number: 7726 Publisher: Nature Publishing Group. Accessed 2022-11-21

[49] Grattafiori, A., Dubey, A., Jauhri, A., Pandey, A., Kadian, A., Al-Dahle, A., Letman, A., Mathur, A., Schelten, A., Vaughan, A., Yang, A., Fan, A., Goyal, A., Hartshorn, A., Yang, A., Mitra, A., Sravankumar, A., Korenev, A., Hinsvark, A., Rao, A., Zhang, A., Rodriguez, A., Gregerson, A., Spataru, A., Roziere, B., Biron, B., Tang, B., Chern, B., Caucheteux, C., Nayak, C., Bi, C., Marra, C., McConnell, C., Keller, C., Touret, C., Wu, C., Wong, C., Ferrer, C.C., Nikolaidis, C., Allonsius, D., Song, D., Pintz, D., Livshits, D., Wyatt, D., Esiobu, D., Choudhary, D., Mahajan, D., Garcia-Olano, D., Perino, D., Hupkes, D., Lakomkin, E., AlBadawy, E., Lobanova, E., Dinan, E., Smith, E.M., Radenovic, F., Guzmán, F., Zhang, F., Synnaeve, G., Lee, G., Anderson, G.L., Thattai, G., Nail, G., Mialon, G., Pang, G., Cucurell, G., Nguyen, H., Korevaar, H., Xu, H., Touvron, H., Zarov, I., Ibarra, I.A., Kloumann, I., Misra, I., Evtimov, I., Zhang, J., Copet, J., Lee, J., Geffert, J., Vranes, J., Park, J., Mahadeokar, J., Shah, J., Linde, J.v.d., Billock, J., Hong, J., Lee, J., Fu, J., Chi, J., Huang, J., Liu, J., Wang, J., Yu, J., Bitton, J., Spisak, J., Park, J., Rocca, J., Johnstun, J., Saxe, J., Jia, J., Alwala, K.V., Prasad, K., Upasani, K., Plawiak, K., Li, K., Heafield, K., Stone, K., El-Arini, K., Iyer, K., Malik, K., Chiu, K., Bhalla, K., Lakhotia, K., Rantala-Yeary, L., Maaten, L.v.d., Chen, L., Tan, L., Jenkins, L., Martin, L., Madaan, L., Malo, L., Blecher, L., Landzaat, L., Oliveira, L.d., Muzzi, M., Pasupuleti, M., Singh, M., Paluri, M., Kardas, M., Tsimpoukelli, M., Oldham, M., Rita, M., Pavlova, M., Kambadur, M., Lewis, M., Si, M., Singh, M.K., Hassan, M., Goyal, N., Torabi, N., Bashlykov, N., Bogoychev, N., Chatterji, N., Zhang, N., Duchenne, O., Çelebi, O., Alrassy, P., Zhang, P., Li, P., Vasic, P., Weng, P., Bhargava, P., Dubal, P., Krishnan, P., Koura, P.S., Xu, P., He, Q., Dong, Q., Srinivasan, R., Ganapathy,

R., Calderer, R., Cabral, R.S., Stojnic, R., Raileanu, R., Maheswari, R., Girdhar, R., Patel, R., Sauvestre, R., Polidoro, R., Sumbaly, R., Taylor, R., Silva, R., Hou, R., Wang, R., Hosseini, S., Chennabasappa, S., Singh, S., Bell, S., Kim, S.S., Edunov, S., Nie, S., Narang, S., Raparthy, S., Shen, S., Wan, S., Bhosale, S., Zhang, S., Vandenhende, S., Batra, S., Whitman, S., Sootla, S., Collot, S., Gururangan, S., Borodinsky, S., Herman, T., Fowler, T., Sheasha, T., Georgiou, T., Scialom, T., Speckbacher, T., Mihaylov, T., Xiao, T., Karn, U., Goswami, V., Gupta, V., Ramanathan, V., Kerkez, V., Gonguet, V., Do, V., Vogeti, V., Albiero, V., Petrovic, V., Chu, W., Xiong, W., Fu, W., Meers, W., Martinet, X., Wang, X., Wang, X., Tan, X.E., Xia, X., Xie, X., Jia, X., Wang, X., Goldschlag, Y., Gaur, Y., Babaei, Y., Wen, Y., Song, Y., Zhang, Y., Li, Y., Mao, Y., Coudert, Z.D., Yan, Z., Chen, Z., Papakipos, Z., Singh, A., Srivastava, A., Jain, A., Kelsey, A., Shajnfeld, A., Gangidi, A., Victoria, A., Goldstand, A., Menon, A., Sharma, A., Boesenberg, A., Baevski, A., Feinstein, A., Kallet, A., Sangani, A., Teo, A., Yunus, A., Lupu, A., Alvarado, A., Caples, A., Gu, A., Ho, A., Poulton, A., Ryan, A., Ramchandani, A., Dong, A., Franco, A., Goyal, A., Saraf, A., Chowdhury, A., Gabriel, A., Bharambe, A., Eisenman, A., Yazdan, A., James, B., Maurer, B., Leonhardi, B., Huang, B., Loyd, B., Paola, B.D., Paranjape, B., Liu, B., Wu, B., Ni, B., Hancock, B., Wasti, B., Spence, B., Stojkovic, B., Gamido, B., Montalvo, B., Parker, C., Burton, C., Mejia, C., Liu, C., Wang, C., Kim, C., Zhou, C., Hu, C., Chu, C.-H., Cai, C., Tindal, C., Feichtenhofer, C., Gao, C., Civin, D., Beaty, D., Kreymer, D., Li, D., Adkins, D., Xu, D., Testuggine, D., David, D., Parikh, D., Liskovich, D., Foss, D., Wang, D., Le, D., Holland, D., Dowling, E., Jamil, E., Montgomery, E., Presani, E., Hahn, E., Wood, E., Le, E.-T., Brinkman, E., Arcaute, E., Dunbar, E., Smothers, E., Sun, F., Kreuk, F., Tian, F., Kokkinos, F., Ozgenel, F., Caggioni, F., Kanayet, F., Seide, F., Florez, G.M., Schwarz, G., Badeer, G., Swee, G., Halpern, G., Herman, G., Sizov, G., Guangyi, Zhang, Lakshminarayanan, G., Inan, H., Shojanazeri, H., Zou, H., Wang, H., Zha, H., Habeeb, H., Rudolph, H., Suk, H., Aspegren, H., Goldman, H., Zhan, H., Damlaj, I., Molybog, I., Tufanov, I., Leontiadis, I., Veliche, I.-E., Gat, I., Weissman, J., Geboski, J., Kohli, J., Lam, J., Asher, J., Gaya, J.-B., Marcus, J., Tang, J., Chan, J., Zhen, J., Reizenstein, J., Teboul, J., Zhong, J., Jin, J., Yang, J., Cummings, J., Carvill, J., Shepard, J., McPhie, J., Torres, J., Ginsburg, J., Wang, J., Wu, K., U, K.H., Saxena, K., Khandelwal, K., Zand, K., Matosich, K., Veeraraghavan, K., Michelena, K., Li, K., Jagadeesh, K., Huang, K., Chawla, K., Huang, K., Chen, L., Garg, L., A, L., Silva, L., Bell, L., Zhang, L., Guo, L., Yu, L., Moshkovich, L., Wehrstedt, L., Khabsa, M., Avalani, M., Bhatt, M., Mankus, M., Hasson, M., Lennie, M., Reso, M., Groshev, M., Naumov, M., Lathi, M., Keneally, M., Liu, M., Seltzer, M.L., Valko, M., Restrepo, M., Patel, M., Vyatskov, M., Samvelyan, M., Clark, M., Macey, M., Wang, M., Hermoso, M.J., Metanat, M., Rastegari, M., Bansal, M., Santhanam, N., Parks, N., White, N., Bawa, N., Singhal, N., Egebo, N., Usunier, N., Mehta, N., Laptev, N.P., Dong, N., Cheng, N., Chernoguz, O., Hart, O., Salpekar, O., Kalinli, O., Kent, P., Parekh, P., Saab, P., Balaji, P., Rittner, P., Bontrager, P., Roux, P., Dollar, P., Zvyagina, P., Ratanchandani, P., Yuvraj, P., Liang, Q., Alao, R.,

Rodriguez, R., Ayub, R., Murthy, R., Nayani, R., Mitra, R., Parthasarathy, R., Li, R., Hogan, R., Battey, R., Wang, R., Howes, R., Rinott, R., Mehta, S., Siby, S., Bondu, S.J., Datta, S., Chugh, S., Hunt, S., Dhillon, S., Sidorov, S., Pan, S., Mahajan, S., Verma, S., Yamamoto, S., Ramaswamy, S., Lindsay, S., Lindsay, S., Feng, S., Lin, S., Zha, S.C., Patil, S., Shankar, S., Zhang, S., Zhang, S., Wang, S., Agarwal, S., Sajuyigbe, S., Chintala, S., Max, S., Chen, S., Kehoe, S., Satterfield, S., Govindaprasad, S., Gupta, S., Deng, S., Cho, S., Virk, S., Subramanian, S., Choudhury, S., Goldman, S., Remez, T., Glaser, T., Best, T., Koehler, T., Robinson, T., Li, T., Zhang, T., Matthews, T., Chou, T., Shaked, T., Vontimitta, V., Ajayi, V., Montanez, V., Mohan, V., Kumar, V.S., Mangla, V., Ionescu, V., Poenaru, V., Mihailescu, V.T., Ivanov, V., Li, W., Wang, W., Jiang, W., Bouaziz, W., Constable, W., Tang, X., Wu, X., Wang, X., Wu, X., Gao, X., Kleinman, Y., Chen, Y., Hu, Y., Jia, Y., Qi, Y., Li, Y., Zhang, Y., Zhang, Y., Adi, Y., Nam, Y., Yu, Wang, Zhao, Y., Hao, Y., Qian, Y., Li, Y., He, Y., Rait, Z., DeVito, Z., Rosnbrick, Z., Wen, Z., Yang, Z., Zhao, Z., Ma, Z.: The Llama 3 Herd of Models. arXiv. arXiv:2407.21783 [cs] (2024). https://doi.org/10.48550/arXiv.2407.21783 . http://arxiv.org/abs/2407.21783 Accessed 2025-01-08

[50] Papez, V., Moinat, M., Voss, E.A., Bazakou, S., Van Winzum, A., Peviani, A., Payralbe, S., Lara, E.G., Kallfelz, M., Asselbergs, F.W., Prieto-Alhambra, D., Dobson, R.J.B., Denaxas, S.: Transforming and evaluating the UK Biobank to the OMOP Common Data Model for COVID-19 research and beyond. Journal of the American Medical Informatics Association **30**(1), 103–111 (2023) https://doi.org/10.1093/jamia/ocac203 . Accessed 2026-03-30

[51] Lehne, M., Sass, J., Essenwanger, A., Schepers, J., Thun, S.: Why digital medicine depends on interoperability. npj Digital Medicine **2**(1), 1–5 (2019) https://doi.org/10.1038/s41746-019-0158-1 . Publisher: Nature Publishing Group. Accessed 2025-02-15

[52] Moor, M., Banerjee, O., Abad, Z.S.H., Krumholz, H.M., Leskovec, J., Topol, E.J., Rajpurkar, P.: Foundation models for generalist medical artificial intelligence. Nature **616**(7956), 259–265 (2023) https://doi.org/10.1038/s41586-023-05881-4 . Publisher: Nature Publishing Group. Accessed 2025-02-15

[53] Jiang, L.Y., Liu, X.C., Nejatian, N.P., Nasir-Moin, M., Wang, D., Abidin, A., Eaton, K., Riina, H.A., Laufer, I., Punjabi, P., Miceli, M., Kim, N.C., Orillac, C., Schnurman, Z., Livia, C., Weiss, H., Kurland, D., Neifert, S., Dastagirzada, Y., Kondziolka, D., Cheung, A.T.M., Yang, G., Cao, M., Flores, M., Costa, A.B., Aphinyanaphongs, Y., Cho, K., Oermann, E.K.: Health system-scale language models are all-purpose prediction engines. Nature **619**(7969), 357–362 (2023) https://doi.org/10.1038/s41586-023-06160-y . Publisher: Nature Publishing Group. Accessed 2024-07-31

[54] Alsentzer, E., Murphy, J., Boag, W., Weng, W.-H., Jindi, D., Naumann, T., McDermott, M.: Publicly Available Clinical BERT Embeddings. In: Rumshisky,

A., Roberts, K., Bethard, S., Naumann, T. (eds.) Proceedings of the 2nd Clinical Natural Language Processing Workshop, pp. 72–78. Association for Computational Linguistics, Minneapolis, Minnesota, USA (2019). https://doi.org/10.18653/v1/W19-1909 . https://aclanthology.org/W19-1909/ Accessed 2025-01-19

[55] Razavian, N., Blecker, S., Schmidt, A.M., Smith-McLallen, A., Nigam, S., Sontag, D.: Population-Level Prediction of Type 2 Diabetes From Claims Data and Analysis of Risk Factors. Big Data **3**(4), 277–287 (2015) https://doi.org/10.1089/big.2015.0020 . Publisher: Mary Ann Liebert, Inc., publishers. Accessed 2022-08-01

[56] Huang, H., LeCun, Y., Balestriero, R.: LLM-JEPA: Large Language Models Meet Joint Embedding Predictive Architectures. (2025). https://openreview.net/forum?id=GbXKPo9QfH Accessed 2026-04-13

[57] Ke, G., Meng, Q., Finley, T., Wang, T., Chen, W., Ma, W., Ye, Q., Liu, T.-Y.: LightGBM: A Highly Efficient Gradient Boosting Decision Tree. Advances in Neural Information Processing Systems **30** (2017). Accessed 2022-08-01

[58] Sui, Y., Zhou, M., Zhou, M., Han, S., Zhang, D.: Table Meets LLM: Can Large Language Models Understand Structured Table Data? A Benchmark and Empirical Study. In: Proceedings of the 17th ACM International Conference on Web Search and Data Mining, pp. 645–654. ACM, Merida Mexico (2024). https://doi.org/10.1145/3616855.3635752 . https://dl.acm.org/doi/10.1145/3616855.3635752 Accessed 2025-01-18

[59] Springer, J.M., Kotha, S., Fried, D., Neubig, G., Raghunathan, A.: Repetition Improves Language Model Embeddings. arXiv. arXiv:2402.15449 [cs] (2024). https://doi.org/10.48550/arXiv.2402.15449 . http://arxiv.org/abs/2402.15449 Accessed 2024-08-01

[60] Wang, A., Liu, C., Yang, J., Weng, C.: Fine-tuning Large Language Models for Rare Disease Concept Normalization. bioRxiv. Pages: 2023.12.28.573586 Section: New Results (2024). https://doi.org/10.1101/2023.12.28.573586 . https://www.biorxiv.org/content/10.1101/2023.12.28.573586v3 Accessed 2024-07-26

[61] He, P., Gao, J., Chen, W.: DeBERTaV3: Improving DeBERTa using ELECTRA-Style Pre-Training with Gradient-Disentangled Embedding Sharing. (2022). https://openreview.net/forum?id=sE7-XhLxHA Accessed 2025-01-19

[62] Lee, J., Yoon, W., Kim, S., Kim, D., Kim, S., So, C.H., Kang, J.: BioBERT: a pre-trained biomedical language representation model for biomedical text mining. Bioinformatics **36**(4), 1234–1240 (2020) https://doi.org/10.1093/bioinformatics/btz682 . Accessed 2022-04-26

[63] Vasantharajan, C., Tun, K.Z., Thi-Nga, H., Jain, S., Rong, T., Siong, C.E.: MedBERT: A Pre-trained Language Model for Biomedical Named Entity Recognition. In: 2022 Asia-Pacific Signal and Information Processing Association

Annual Summit and Conference (APSIPA ASC), pp. 1482–1488. IEEE, Chiang Mai, Thailand (2022). https://doi.org/10.23919/APSIPAASC55919.2022.9980157 . https://ieeexplore.ieee.org/document/9980157/ Accessed 2025-10-05

[64] Hu, E.J., Shen, Y., Wallis, P., Allen-Zhu, Z., Li, Y., Wang, S., Wang, L., Chen, W.: LoRA: Low-Rank Adaptation of Large Language Models. arXiv preprint arXiv:2106.09685 (2021). Accessed 2023-11-10

[65] Ma, M.D., Wang, X., Xiao, Y., Cuturrufo, A., Nori, V.S., Halperin, E., Wang, W.: Memorize and Rank: Elevating Large Language Models for Clinical Diagnosis Prediction. Proceedings of the AAAI Conference on Artificial Intelligence **39**(23), 24786–24794 (2025) https://doi.org/10.1609/aaai.v39i23.34660 . Accessed 2025-09-22

[66] Wu, P., Gifford, A., Meng, X., Li, X., Campbell, H., Varley, T., Zhao, J., Carroll, R., Bastarache, L., Denny, J.C., Theodoratou, E., Wei, W.-Q.: Mapping ICD-10 and ICD-10-CM Codes to Phecodes: Workflow Development and Initial Evaluation. JMIR Medical Informatics **7**(4), 14325 (2019) https://doi.org/10.2196/14325 . Company: JMIR Medical Informatics Distributor: JMIR Medical Informatics Institution: JMIR Medical Informatics Label: JMIR Medical Informatics Publisher: JMIR Publications Inc., Toronto, Canada. Accessed 2025-05-01

[67] Wei, W.-Q., Bastarache, L.A., Carroll, R.J., Marlo, J.E., Osterman, T.J., Gamazon, E.R., Cox, N.J., Roden, D.M., Denny, J.C.: Evaluating phecodes, clinical classification software, and ICD-9-CM codes for phenome-wide association studies in the electronic health record. PLOS ONE **12**(7), 0175508 (2017) https://doi.org/10.1371/journal.pone.0175508 . Publisher: Public Library of Science. Accessed 2025-05-01

[68] Denaxas, S., Shah, A.D., Mateen, B.A., Kuan, V., Quint, J.K., Fitzpatrick, N., Torralbo, A., Fatemifar, G., Hemingway, H.: A semi-supervised approach for rapidly creating clinical biomarker phenotypes in the UK Biobank using different primary care EHR and clinical terminology systems. JAMIA Open **3**(4), 545–556 (2020) https://doi.org/10.1093/jamiaopen/ooaa047 . Accessed 2025-05-01

[69] Arnrich, B., Choi, E., Fries, J.A., McDermott, M.B.A., Oh, J., Pollard, T.J., Shah, N., Steinberg, E., Wornow, M., Water, R.: Medical Event Data Standard (MEDS): Facilitating Machine Learning for Health. In: ICLR 2024 Workshop on Learning from Time Series For Health (2024). https://openreview.net/forum?id=IsHy2ebjIG

1 Supplementary Information

1.1 Additional Experimental Details

Table S1 UK Biobank Prediction Tasks Overview. The external validation on the UKB includes three task groups. Operational outcomes and mortality prediction only consist of a single prediction task, while the assignment of new diagnosis spans 23 conditions. Following [45], canonical splits for training, validation, and testing were defined.

Attribute	Train Labels (Positive)	Valid Labels (Positive)	Test Labels (Positive)	Total Labels (Positive)
Operational Outcomes				
Hospitalization	119463 (22992)	119463 (22913)	119463 (22624)	358389 (68529)
Mortality Prediction				
Death	119459 (268)	119463 (284)	119462 (250)	358384 (802)
Assignment of New Diagnoses				
Hypertension	100049 (2515)	99866 (2532)	99613 (2600)	299528 (7647)
Diabetes Mellitus	114423 (621)	114531 (616)	114380 (604)	343334 (1841)
Atrial Fibrillation	118804 (107)	118784 (94)	118704 (105)	356292 (306)
Pneumonia	117409 (270)	117527 (299)	117437 (232)	352373 (801)
Chronic Obstructive Pulmonary Disease [COPD]	117868 (305)	117899 (284)	117886 (334)	353653 (923)
Chronic Kidney Disease	117542 (308)	117512 (346)	117478 (347)	352532 (1001)
Ischemic Heart Disease	113627 (609)	113634 (583)	113467 (596)	340728 (1788)
Myocardial Infarction [heart Attack]	117049 (214)	117070 (204)	116995 (201)	351114 (619)
Cerebral Infarction [ischemic Stroke]	118788 (100)	118788 (116)	118745 (94)	356321 (310)
Heart Failure	118563 (152)	118626 (158)	118609 (125)	355798 (435)
Cardiac Arrest	119370 (25)	119362 (29)	119370 (33)	358102 (87)
Abdominal Aortic Aneurysm	119359 (17)	119352 (17)	119354 (39)	358065 (73)
Pulmonary Embolism	118750 (81)	118795 (99)	118754 (68)	356299 (248)
Aortic Stenosis	119170 (38)	119174 (37)	119179 (39)	357523 (114)
Mitral Valve Insufficiency	119003 (63)	119061 (58)	119024 (65)	357088 (186)
Endocarditis	119005 (24)	119012 (24)	118998 (31)	357015 (79)
Rheumatic Fever And Chronic Rheumatic Heart Diseases	119047 (51)	119073 (46)	119083 (57)	357203 (154)
Anemia	114135 (606)	114119 (587)	114142 (620)	342396 (1813)
Back Pain	100129 (1323)	99663 (1322)	99876 (1285)	299668 (3930)
Parkinson's Disease (primary)	119278 (27)	119306 (31)	119284 (28)	357868 (86)
Rheumatoid Arthritis	118392 (117)	118400 (107)	118380 (92)	355172 (316)
Psoriasis	117482 (148)	117461 (119)	117594 (142)	352537 (409)
Suicide Ideation And Attempt Or Self Harm	118953 (62)	118896 (60)	118943 (53)	356792 (175)

Table S2 Semantic Codes for Aggregated Concepts in EHR Markdown Serialization. We aggregated time-series data encoded via LOINC concepts and identified the most frequent concepts from which we selected 24 key medical concepts. To reduce duplicate information, we merged synonymous semantic codes. The primary LOINC code is presented first in the column Semantic Codes followed by identified duplicates. We also defined a unit, minimum and maximum allowed values for filtering, a normal range to classify values in low, normal, and high, and a formatting strategy to create our EHR serialization.

Medical Concept	Semantic Codes	Unit	Min-Max Range	Normal Range	Formatting
Recent Body Metrics					
Body weight	LOINC/29463-7	oz	350-10000		One decimal
Body height	LOINC/8302-2	inch	5-100		One decimal
Body mass index / BMI	LOINC/39156-5	kg/m2	10-100	18.5-24.9	One decimal
Body surface area	LOINC/8277-6, SNOMED/301898006	m2	0.1-10		Two decimals
Recent Vital Signs					
Heart rate	LOINC/8867-4, SNOMED/364075005, SNOMED/78564009	bpm	5-300	60-100	Integer
Systolic blood pressure	LOINC/8480-6, SNOMED/271649006	mmHg	20-300	90-140	Integer
Diastolic blood pressure	LOINC/8462-4, SNOMED/271650006	mmHg	20-300	60-90	Integer
Body temperature	LOINC/8310-5	°F	80-120	95-100.4	One decimal
Respiratory rate	LOINC/9279-1	breaths/min	1-100	12-18	Integer
Oxygen saturation	LOINC/LP21258-6	%	1-100	95-100	Integer
Recent Lab Results					
Hemoglobin	LOINC/718-7, SNOMED/271026005, SNOMED/441689006	g/dL	1-20	12-17	One decimal
Hematocrit	LOINC/4544-3, LOINC/20570-8, LOINC/48703-3, SNOMED/28317006	%	10-100	36-51	Integer
Erythrocytes	LOINC/789-8, LOINC/26453-1	106/uL	1-10	4.2-5.9	Two decimals
Leukocytes	LOINC/20584-9, LOINC/6690-2	103/uL	1-100	4-10	One decimal
Platelets	LOINC/777-3, SNOMED/61928009	103/uL	10-1000	150-350	Integer
Sodium	LOINC/2951-2, LOINC/2947-0, SNOMED/25197003	mmol/L	100-200	136-145	Integer
Potassium	LOINC/2823-3, SNOMED/312468003, LOINC/6298-4, SNOMED/59573005	mmol/L	0.1-10	3.5-5.0	One decimal
Chloride	LOINC/2075-0, SNOMED/104589004, LOINC/2069-3	mmol/L	50-200	98-106	Integer
Carbon dioxide, total	LOINC/2028-9	mmol/L	10-100	23-28	Integer
Calcium	LOINC/17861-6, SNOMED/271240001	mg/dL	1-20	9-10.5	One decimal
Glucose	LOINC/2345-7, SNOMED/166900001, LOINC/2339-0, SNOMED/33747003, LOINC/14749-6	mg/dL	10-1000	70-100	Integer
Urea nitrogen	LOINC/3094-0, SNOMED/105011006	mg/dL	1-200	8-20	Integer
Creatinine	LOINC/2160-0, SNOMED/113075003	mg/dL	0.1-10	0.7-1.3	One decimal
Anion gap	LOINC/33037-3, LOINC/41276-7, SNOMED/25469001	mmol/L	-20-50	3-11	Integer

Table S3 Instructions for LLM Embedding Models. The LLM embedding models were trained using instructions; hence, we also defined simple task-specific prompts for each of the 15 clinical prediction tasks. Each prompt is prepended by the prefix given below, containing a general task description. The three tasks used for the external validation on UKB use a similar design. For the decoder model we added an additional instruction to the prompt enforcing the output of `Yes` and `No` tokens used for prediction.

Task	Prompt
Prefix (for all tasks)	Given a patient's electronic healthcare record (EHR) as a newline separated list, retrieve relevant passages that answer the query:
EHRSHOT	
Long Length of Stay	will the patient stay in the hospital for more than 7 days
30-day Readmission	will the patient be readmitted to the hospital within 30 days
ICU Transfer	will the patient be transferred to the intensive care unit
Thrombocytopenia	has the patient thrombocytopenia
Hyperkalemia	has the patient hyperkalemia
Hypoglycemia	has the patient hypoglycemia
Hyponatremia	has the patient hyponatremia
Anemia	has the patient anemia
Hypertension	has the patient hypertension
Hyperlipidemia	has the patient hyperlipidemia
Pancreatic Cancer	has the patient pancreatic cancer
Celiac	has the patient celiac disease
Lupus	has the patient lupus
Acute MI	has the patient an acute myocardial infarction
Chest X-Ray Findings	what are the chest x-ray findings of the patient
Generic (ablation)	what are the key clinical features of the patient to predict future medical events
UK Biobank (UKB)	
Mortality Prediction	will the patient die within one year
Hospitalization	will the patient be admitted to the hospital within one year
Assignment of New Diagnoses	has the patient {diagnosis name}
Additional Prompt Added for Decoder Qwen3-8B	
Decoder Prompt	Answer STRICTLY with a single token: Yes or No. No punctuation, no extra words.

1.2 Full Results on EHRSHOT

Table S4 Performance for All Examples on EHRSHOT. Mean area under the receiver operating characteristic curve (AUROC) performance with approximate 95% confidence intervals of all included models for four task groups. The macro-averaged performance across all task groups is given in the right-most column. All LLM embedding models use a context size of 8,192 tokens.

Model	Operational Outcomes	Anticipating Lab Test Results	Assignment of New Diagnosis	Anticipating Chest X-ray Findings	Macro Avg. Across Task Groups
Baselines [45]					
CLMBR-T-Base	0.824 .803-.845	0.832 .824-.840	0.707 .667-.746	0.713 .702-.724	0.769 .746-.792
Count-based + GBM	0.824 .804-.844	0.841 .833-.849	0.758 .724-.793	0.686 .674-.699	0.777 .756-.799
Count-based + LR	0.764 .741-.787	0.742 .729-.756	0.734 .687-.782	0.673 .656-.690	0.728 .700-.757
LLM Embedding Models					
Qwen3-Emb-8B	0.797 .773-.820	0.842 .835-.850	0.714 .672-.757	0.722 .711-.733	0.769 .744-.794
Qwen3-Emb-4B	0.787 .764-.810	0.824 .816-.831	0.718 .667-.768	0.708 .696-.719	0.759 .730-.787
Qwen3-Emb-0.6B	0.778 .753-.803	0.742 .732-.753	0.684 .631-.737	0.705 .694-.716	0.727 .697-.758
Qwen2-Emb-7B	0.772 .749-.796	0.746 .735-.757	0.744 .705-.784	0.685 .671-.699	0.737 .712-.761
Qwen2-Emb-1.5B	0.756 .735-.778	0.710 .699-.721	0.696 .647-.744	0.680 .668-.691	0.710 .683-.738
Llama3.1-LLM2Vec-8B	0.763 .738-.787	0.726 .714-.738	0.727 .688-.766	0.686 .673-.699	0.725 .701-.750
LLM Embedding Model + EHR Foundation Model [45]					
Qwen3-Emb-8B + CLMBR-T-Base	0.821 .800-.842	0.864 .858-.871	0.736 .695-.777	0.731 .721-.742	0.788 .764-.812
LLM Embedding Model + GBM Head					
Qwen3-Emb-8B + GBM	0.774 .749-.799	0.812 .804-.820	0.685 .644-.727	0.696 .686-.706	0.742 .717-.767
Multiple Embedding Model for EHR (MEME) [34] **with Linear Head**					
Qwen3-Emb-8B MEME	0.814 .793-.834	0.845 .837-.852	0.728 .673-.784	0.717 .705-.728	0.776 .746-.806
BioClinicalBERT MEME	0.756 .733-.778	0.699 .686-.713	0.704 .651-.758	0.648 .635-.661	0.702 .671-.732
MedBERT MEME	0.759 .736-.782	0.695 .682-.708	0.715 .676-.755	0.620 .605-.635	0.697 .673-.722
Encoder Language Models with Mean Embeddings of Chunked Inputs					
BioClinicalBERT	0.738 .712-.763	0.698 .685-.711	0.707 .668-.746	0.679 .666-.691	0.705 .680-.730
MedBERT	0.742 .718-.767	0.694 .683-.706	0.663 .614-.713	0.683 .671-.696	0.696 .667-.725
DeBERTaV3 large	0.737 .713-.762	0.694 .681-.706	0.676 .629-.724	0.660 .648-.673	0.692 .664-.720
DeBERTaV3 base	0.727 .701-.753	0.680 .668-.693	0.672 .635-.710	0.659 .647-.672	0.685 .660-.709
BERT large	0.748 .725-.771	0.688 .675-.700	0.671 .625-.718	0.669 .656-.682	0.694 .667-.722
BERT base	0.748 .724-.772	0.693 .681-.706	0.685 .641-.729	0.677 .664-.690	0.701 .674-.727
Encoder Language Models with Concatenated Embeddings of Chunked Inputs					
BioClinicalBERT	0.740 .715-.764	0.707 .696-.718	0.690 .651-.730	0.653 .641-.665	0.698 .673-.722
MedBERT	0.751 .726-.775	0.712 .701-.723	0.658 .618-.698	0.658 .646-.670	0.695 .670-.720
DeBERTaV3 large	0.714 .687-.742	0.690 .679-.701	0.632 .595-.669	0.624 .612-.636	0.665 .641-.690
DeBERTaV3 base	0.675 .647-.703	0.680 .670-.690	0.623 .583-.662	0.615 .603-.628	0.648 .623-.674
BERT large	0.736 .710-.762	0.697 .686-.708	0.657 .613-.701	0.643 .631-.655	0.683 .657-.710
BERT base	0.752 .728-.776	0.705 .695-.716	0.657 .613-.701	0.650 .639-.662	0.691 .665-.717

Table S5 Per-task ΔAUROC (Qwen3-Emb-8B minus baseline) on EHRSHOT. Cells report the AUROC difference (ΔAUROC), 95% bootstrap confidence intervals, and Holm-adjusted p-values obtained from paired patient-level bootstrap tests with 10,000 resamples. Positive values indicate better performance of Qwen3-Emb-8B. Multiple testing was controlled separately for each shot setting ($k = 8$, $k = 64$, and all training data) using Holm's procedure across all tasks and baseline comparisons (45 tests per setting). Bold indicates statistically significant differences ($p_{\text{adj}} < 0.05$).

Task	CLMBR-T-Base	BioClinicalBERT	Count-based Model
8-shot (8 positive / 8 negative examples)			
Long LOS	$+0.011_{[-0.025,+0.047]}$ (1.000)	$-0.001_{[-0.034,+0.031]}$ (1.000)	$-0.042_{[-0.080,-0.002]}$ (0.677)
30-day Readmission	$+0.001_{[-0.034,+0.034]}$ (1.000)	$\mathbf{+0.079}_{[+0.038,+0.121]}$ (0.009)	$\mathbf{+0.085}_{[+0.039,+0.131]}$ (0.009)
ICU Transfer	$-0.043_{[-0.089,+0.002]}$ (1.000)	$+0.071_{[+0.009,+0.132]}$ (0.572)	$+0.069_{[-0.015,+0.151]}$ (1.000)
Thrombocytopenia	$\mathbf{+0.036}_{[+0.014,+0.057]}$ (0.041)	$\mathbf{+0.089}_{[+0.068,+0.110]}$ (0.009)	$\mathbf{+0.100}_{[+0.074,+0.123]}$ (0.009)
Hyperkalemia	$\mathbf{+0.113}_{[+0.082,+0.141]}$ (0.009)	$\mathbf{+0.197}_{[+0.160,+0.236]}$ (0.009)	$\mathbf{+0.194}_{[+0.146,+0.241]}$ (0.009)
Hypoglycemia	$-0.042_{[-0.080,-0.004]}$ (0.584)	$+0.050_{[+0.009,+0.089]}$ (0.415)	$+0.024_{[-0.021,+0.067]}$ (1.000)
Hyponatremia	$\mathbf{+0.029}_{[+0.011,+0.047]}$ (0.041)	$\mathbf{+0.085}_{[+0.061,+0.109]}$ (0.009)	$\mathbf{+0.070}_{[+0.046,+0.095]}$ (0.009)
Anemia	$\mathbf{-0.067}_{[-0.080,-0.056]}$ (0.009)	$\mathbf{+0.145}_{[+0.130,+0.161]}$ (0.009)	$\mathbf{+0.032}_{[+0.021,+0.043]}$ (0.009)
Hypertension	$-0.068_{[-0.125,-0.012]}$ (0.415)	$-0.012_{[-0.060,+0.037]}$ (1.000)	$+0.002_{[-0.065,+0.070]}$ (1.000)
Hyperlipidemia	$+0.019_{[-0.028,+0.069]}$ (1.000)	$+0.030_{[-0.027,+0.088]}$ (1.000)	$+0.076_{[+0.011,+0.141]}$ (0.474)
Pancreatic Cancer	$+0.089_{[+0.008,+0.174]}$ (0.600)	$+0.071_{[-0.024,+0.164]}$ (1.000)	$\mathbf{+0.167}_{[+0.074,+0.259]}$ (0.030)
Celiac	$+0.070_{[-0.113,+0.299]}$ (1.000)	$+0.209_{[-0.166,+0.453]}$ (1.000)	$+0.009_{[-0.262,+0.232]}$ (1.000)
Lupus	$+0.054_{[-0.088,+0.184]}$ (1.000)	$+0.123_{[-0.005,+0.270]}$ (1.000)	$+0.063_{[-0.097,+0.237]}$ (1.000)
Acute MI	$\mathbf{+0.126}_{[+0.056,+0.191]}$ (0.025)	$\mathbf{+0.161}_{[+0.081,+0.237]}$ (0.009)	$\mathbf{+0.172}_{[+0.088,+0.251]}$ (0.009)
Chest X-ray Findings	$-0.015_{[-0.028,-0.001]}$ (0.600)	$+0.024_{[+0.009,+0.037]}$ (0.062)	$\mathbf{+0.026}_{[+0.010,+0.042]}$ (0.043)
64-shot (64 positive / 64 negative examples)			
Long LOS	$-0.037_{[-0.060,-0.014]}$ (0.054)	$+0.019_{[-0.011,+0.049]}$ (1.000)	$-0.025_{[-0.054,+0.004]}$ (1.000)
30-day Readmission	$-0.010_{[-0.029,+0.009]}$ (1.000)	$\mathbf{+0.050}_{[+0.030,+0.069]}$ (0.009)	$+0.022_{[+0.002,+0.041]}$ (0.846)
ICU Transfer	$-0.069_{[-0.123,-0.014]}$ (0.418)	$+0.056_{[-0.007,+0.120]}$ (1.000)	$-0.041_{[-0.097,+0.016]}$ (1.000)
Thrombocytopenia	$\mathbf{+0.023}_{[+0.009,+0.036]}$ (0.026)	$\mathbf{+0.078}_{[+0.066,+0.092]}$ (0.009)	$\mathbf{-0.047}_{[-0.060,-0.036]}$ (0.009)
Hyperkalemia	$\mathbf{+0.044}_{[+0.026,+0.062]}$ (0.009)	$\mathbf{+0.143}_{[+0.115,+0.169]}$ (0.009)	$+0.020_{[-0.001,+0.040]}$ (1.000)
Hypoglycemia	$\mathbf{-0.044}_{[-0.070,-0.018]}$ (0.043)	$\mathbf{+0.094}_{[+0.057,+0.131]}$ (0.009)	$+0.034_{[+0.002,+0.065]}$ (1.000)
Hyponatremia	$+0.016_{[-0.003,+0.035]}$ (1.000)	$\mathbf{+0.118}_{[+0.097,+0.137]}$ (0.009)	$\mathbf{-0.072}_{[-0.091,-0.055]}$ (0.009)
Anemia	$\mathbf{-0.056}_{[-0.064,-0.049]}$ (0.009)	$\mathbf{+0.156}_{[+0.141,+0.172]}$ (0.009)	$+0.004_{[-0.003,+0.011]}$ (1.000)
Hypertension	$-0.038_{[-0.073,-0.002]}$ (1.000)	$+0.028_{[-0.018,+0.074]}$ (1.000)	$+0.002_{[-0.040,+0.045]}$ (1.000)
Hyperlipidemia	$+0.030_{[-0.009,+0.068]}$ (1.000)	$+0.037_{[-0.013,+0.087]}$ (1.000)	$+0.020_{[-0.021,+0.063]}$ (1.000)
Pancreatic Cancer	$\mathbf{+0.090}_{[+0.038,+0.148]}$ (0.038)	$+0.073_{[+0.001,+0.141]}$ (1.000)	$+0.011_{[-0.042,+0.071]}$ (1.000)
Celiac	$+0.101_{[-0.080,+0.257]}$ (1.000)	$+0.169_{[-0.121,+0.317]}$ (1.000)	$-0.029_{[-0.138,+0.100]}$ (1.000)
Lupus	$-0.079_{[-0.205,+0.040]}$ (1.000)	$+0.019_{[-0.122,+0.163]}$ (1.000)	$+0.039_{[-0.133,+0.220]}$ (1.000)
Acute MI	$-0.028_{[-0.066,+0.010]}$ (1.000)	$-0.047_{[-0.089,-0.002]}$ (1.000)	$-0.041_{[-0.083,+0.002]}$ (1.000)
Chest X-ray Findings	$+0.000_{[-0.009,+0.010]}$ (1.000)	$\mathbf{+0.031}_{[+0.018,+0.045]}$ (0.009)	$\mathbf{+0.021}_{[+0.010,+0.032]}$ (0.014)
All training data			
Long LOS	$-0.006_{[-0.024,+0.012]}$ (1.000)	$\mathbf{+0.079}_{[+0.058,+0.100]}$ (0.009)	$-0.018_{[-0.035,-0.001]}$ (0.840)
30-day Readmission	$-0.015_{[-0.037,+0.007]}$ (1.000)	$\mathbf{+0.045}_{[+0.025,+0.067]}$ (0.011)	$-0.002_{[-0.029,+0.026]}$ (1.000)
ICU Transfer	$-0.060_{[-0.110,-0.012]}$ (0.463)	$+0.053_{[+0.005,+0.103]}$ (0.638)	$-0.062_{[-0.115,-0.007]}$ (0.658)
Thrombocytopenia	$\mathbf{+0.045}_{[+0.035,+0.054]}$ (0.009)	$\mathbf{+0.116}_{[+0.100,+0.132]}$ (0.009)	$\mathbf{-0.040}_{[-0.049,-0.032]}$ (0.009)
Hyperkalemia	$\mathbf{+0.030}_{[+0.015,+0.045]}$ (0.009)	$\mathbf{+0.142}_{[+0.114,+0.172]}$ (0.009)	$+0.022_{[+0.006,+0.038]}$ (0.178)
Hypoglycemia	$\mathbf{-0.035}_{[-0.053,-0.019]}$ (0.009)	$\mathbf{+0.146}_{[+0.115,+0.176]}$ (0.009)	$\mathbf{+0.061}_{[+0.036,+0.086]}$ (0.009)
Hyponatremia	$\mathbf{+0.034}_{[+0.022,+0.046]}$ (0.009)	$\mathbf{+0.179}_{[+0.163,+0.195]}$ (0.009)	$\mathbf{-0.027}_{[-0.037,-0.017]}$ (0.009)
Anemia	$\mathbf{-0.021}_{[-0.023,-0.018]}$ (0.009)	$\mathbf{+0.139}_{[+0.126,+0.153]}$ (0.009)	$\mathbf{-0.009}_{[-0.012,-0.006]}$ (0.009)
Hypertension	$-0.042_{[-0.084,-0.002]}$ (0.840)	$+0.036_{[-0.009,+0.082]}$ (1.000)	$-0.033_{[-0.079,+0.011]}$ (1.000)
Hyperlipidemia	$+0.022_{[-0.017,+0.063]}$ (1.000)	$+0.017_{[-0.024,+0.057]}$ (1.000)	$-0.018_{[-0.064,+0.028]}$ (1.000)
Pancreatic Cancer	$+0.049_{[+0.002,+0.100]}$ (0.840)	$+0.052_{[-0.012,+0.110]}$ (1.000)	$-0.022_{[-0.072,+0.019]}$ (1.000)
Celiac	$+0.023_{[-0.153,+0.171]}$ (1.000)	$-0.118_{[-0.281,-0.019]}$ (0.565)	$-0.130_{[-0.322,+0.009]}$ (1.000)
Lupus	$-0.019_{[-0.134,+0.088]}$ (1.000)	$+0.059_{[-0.046,+0.174]}$ (1.000)	$-0.070_{[-0.206,+0.059]}$ (1.000)
Acute MI	$+0.014_{[-0.015,+0.042]}$ (1.000)	$-0.003_{[-0.037,+0.029]}$ (1.000)	$+0.012_{[-0.029,+0.053]}$ (1.000)
Chest X-ray Findings	$+0.009_{[-0.001,+0.018]}$ (1.000)	$\mathbf{+0.043}_{[+0.031,+0.057]}$ (0.009)	$\mathbf{+0.036}_{[+0.023,+0.048]}$ (0.009)

Table S6 Performance for All Examples on EHRSHOT Across Different Count-based Models. Mean area under the receiver operating characteristic curve (AUROC) performance with approximate 95% confidence intervals for the count-based model from [45] using ontology expansion. We tested a GBM and LR model and extensions including the encoding of string values (SV), numeric values (NV), time binning with four time bins (TB), and the extension with all three.

Model	Operational Outcomes	Anticipating Lab Test Results	Assignment of New Diagnosis	Anticipating Chest X-ray Findings	Macro Avg. Across Task Groups
GBM Model					
Counts [45]	0.774 .752-.797	0.728 .716-.741	0.719 .669-.768	0.656 .641-.671	0.719 .691-.748
Counts + SV	0.785 .764-.806	0.731 .719-.744	0.732 .685-.779	0.662 .649-.675	0.727 .700-.755
Counts + NV	0.786 .763-.809	0.789 .779-.800	0.752 .711-.792	0.656 .642-.670	0.746 .721-.771
Counts + TB	0.815 .795-.836	0.752 .741-.764	0.768 .736-.801	0.686 .674-.698	0.756 .735-.776
Counts + SV/NV/TB	0.824 .804-.844	0.841 .833-.849	0.758 .724-.793	0.686 .674-.699	0.777 .756-.799
LR Model					
Counts [45]	0.719 .692-.746	0.669 .653-.685	0.749 .711-.787	0.646 .633-.660	0.696 .670-.721
Counts + SV	0.720 .693-.747	0.669 .654-.685	0.750 .712-.788	0.647 .633-.661	0.696 .671-.722
Counts + NV	0.718 .691-.746	0.687 .671-.703	0.752 .715-.789	0.655 .641-.669	0.703 .678-.728
Counts + TB	0.763 .741-.785	0.717 .703-.730	0.741 .695-.787	0.666 .650-.683	0.722 .694-.749
Counts + SV/NV/TB	0.764 .741-.787	0.742 .729-.756	0.734 .687-.782	0.673 .656-.690	0.728 .700-.757

Table S7 Performance for All Examples on EHRSHOT for Different Serializations. Mean area under the receiver operating characteristic curve (AUROC) performance with approximate 95% confidence intervals of the list serialization used in this work and three alternatives using the first occurrences of each code and adding timestamps to each code. We also tested a handcrafted Markdown EHR serialization with three LLMs and JSON, XML, and YAML data formats with Qwen3-Emb-8B.

Model	Operational Outcomes	Anticipating Lab Test Results	Assignment of New Diagnosis	Anticipating Chest X-ray Findings	Macro Avg. Across Task Groups
EHR List Serializations for Qwen3-Emb-8B					
List codes recent (ours)	0.797 .773-.820	0.842 .835-.850	0.714 .672-.757	0.722 .711-.733	0.769 .744-.794
List codes first	0.761 .736-.785	0.715 .701-.728	0.731 .688-.773	0.676 .663-.690	0.721 .694-.747
List codes recent + time	0.795 .772-.818	0.844 .837-.851	0.692 .637-.748	0.727 .716-.738	0.765 .734-.795
List codes first + time	0.746 .720-.772	0.703 .689-.716	0.718 .674-.761	0.645 .629-.660	0.703 .675-.730
EHR Markdown Serializations					
Qwen3-Emb-8B	0.773 .749-.797	0.859 .852-.866	0.725 .683-.767	0.694 .681-.707	0.763 .737-.788
Qwen2-Emb-7B	0.756 .731-.781	0.767 .756-.778	0.717 .671-.764	0.677 .664-.690	0.729 .702-.757
Llama3.1-LLM2Vec-8B	0.769 .746-.792	0.732 .720-.744	0.705 .651-.759	0.692 .679-.705	0.724 .694-.755
EHR Alternative Serialization Formats for Qwen3-Emb-8B					
JSON	0.773 .749-.796	0.858 .851-.865	0.736 .692-.780	0.690 .677-.704	0.764 .738-.790
XML	0.771 .747-.795	0.862 .855-.868	0.726 .681-.771	0.676 .663-.690	0.759 .732-.785
YAML	0.773 .749-.796	0.863 .856-.870	0.723 .677-.769	0.684 .670-.698	0.761 .734-.787

Table S8 Code Categories Used for Ablation Study. For the content ablation study, we grouped all codes into six mutually exclusive categories based on ontology prefixes and hierarchical SNOMED parent concepts. Counts were computed across all events from all patients, excluding codes from CARE_SITE and ICDO3, as well as codes with empty descriptions.

Category	Included Codes	# Codes
Demographics	Race/, Gender/, Ethnicity/, SNOMED/3950001 (birth)	18,189 (0.0%)
Visits	Visit/, Medicare Specialty/, CMS Place of Service/	606,798 (1.5%)
Conditions	Cancer Modifier/, OMOP Extension/, Condition Type/, all remaining SNOMED codes	2,995,518 (7.3%)
Medications	RxNorm/, RxNorm Extension/, CVX/, SNOMED descendants of 373873005 (pharmaceutical product), 105590001 (substance)	2,453,197 (5.9%)
Procedures	CPT4/, ICD10PCS/, ICD9Proc/, Domain/, HCPCS/, SNOMED descendants of 71388002 (procedure)	1,840,172 (4.5%)
Lab Results	LOINC/, SNOMED descendants of 108252007 (laboratory procedure), 430925007 (measurement of substance)	33,351,150 (80.8%)
Total	*	41,265,024 (100.0%)

Table S9 Performance for All Examples on EHRSHOT for EHR Serialization Experiments. Mean area under the receiver operating characteristic curve (AUROC) performance with approximate 95% confidence intervals of the EHR list serialization used in this work (Full EHR) and different EHR serialization variants. We evaluated a generic and an empty instruction, serializations with specific components removed, and serialization consisting of an individual component.

Model	Operational Outcomes	Anticipating Lab Test Results	Assignment of New Diagnosis	Anticipating Chest X-ray Findings	Macro Avg. Across Task Groups
Original List Serialization					
Full EHR	0.797 .773-.820	0.842 .835-.850	0.714 .672-.757	0.722 .711-.733	0.769 .744-.794
Instruction Experiments					
Generic Instruction	0.788 .765-.812	0.772 .762-.782	0.706 .665-.747	0.718 .707-.730	0.746 .722-.771
Empty Instruction	0.791 .767-.815	0.756 .745-.766	0.698 .651-.745	0.715 .704-.726	0.740 .712-.767
Removing Medical Code Categories					
No Demographics	0.797 .774-.820	0.842 .834-.849	0.708 .666-.750	0.721 .710-.732	0.767 .742-.792
No Visits	0.796 .773-.819	0.842 .835-.849	0.717 .676-.758	0.723 .712-.734	0.769 .745-.794
No Conditions	0.797 .774-.820	0.847 .840-.854	0.701 .665-.737	0.716 .705-.727	0.765 .743-.788
No Medications	0.798 .775-.822	0.846 .838-.853	0.702 .657-.746	0.722 .711-.733	0.767 .741-.793
No Procedures	0.787 .764-.810	0.847 .839-.854	0.721 .678-.764	0.718 .707-.729	0.768 .743-.793
No Lab Results	0.798 .775-.821	0.752 .741-.763	0.722 .681-.762	0.711 .699-.722	0.746 .721-.770
Individual Medical Code Categories					
Only Demographics	0.549 .518-.580	0.543 .528-.559	0.606 .570-.643	0.513 .494-.531	0.553 .526-.579
Only Visits	0.591 .564-.618	0.628 .615-.642	0.560 .523-.596	0.613 .600-.625	0.598 .574-.622
Only Conditions	0.773 .750-.797	0.708 .695-.721	0.693 .649-.737	0.686 .673-.698	0.715 .688-.741
Only Medications	0.777 .756-.799	0.710 .698-.722	0.688 .641-.735	0.657 .644-.670	0.708 .681-.735
Only Procedures	0.781 .756-.807	0.718 .705-.731	0.672 .640-.704	0.697 .685-.708	0.717 .695-.739
Only Lab Results	0.777 .755-.799	0.856 .849-.862	0.665 .607-.724	0.702 .691-.713	0.750 .718-.782

Table S10 Performance for All Examples on EHRSHOT Across Context Sizes. Mean area under the receiver operating characteristic curve (AUROC) performance with approximate 95% confidence intervals for different context sizes of the LLM embedding models.

Model	Operational Outcomes	Anticipating Lab Test Results	Assignment of New Diagnosis	Anticipating Chest X-ray Findings	Macro Avg. Across Task Groups
Qwen3-Emb-8B					
8,192 context size	0.797 .773-.820	0.842 .835-.850	0.714 .672-.757	0.722 .711-.733	0.769 .744-.794
4,096 context size	0.800 .778-.823	0.850 .843-.857	0.711 .666-.757	0.727 .716-.737	0.772 .746-.798
2,048 context size	0.805 .783-.828	0.859 .852-.865	0.691 .656-.726	0.718 .706-.729	0.768 .746-.790
1,024 context size	0.799 .776-.822	0.832 .825-.839	0.707 .668-.746	0.697 .686-.709	0.759 .735-.782
512 context size	0.790 .766-.814	0.786 .778-.794	0.703 .660-.745	0.683 .672-.694	0.741 .715-.766
Qwen2-Emb-7B					
8,192 context size	0.772 .749-.796	0.746 .735-.757	0.744 .705-.784	0.685 .671-.699	0.737 .712-.761
4,096 context size	0.794 .771-.816	0.799 .790-.808	0.740 .698-.781	0.708 .696-.720	0.760 .736-.785
2,048 context size	0.806 .783-.828	0.846 .839-.853	0.718 .674-.761	0.720 .709-.731	0.772 .747-.798
1,024 context size	0.797 .776-.817	0.833 .826-.841	0.709 .665-.752	0.700 .689-.711	0.760 .735-.785
512 context size	0.784 .763-.805	0.786 .778-.794	0.741 .702-.779	0.683 .672-.694	0.748 .726-.771
Llama3.1-LLM2Vec-8B					
8,192 context size	0.763 .738-.787	0.726 .714-.738	0.727 .688-.766	0.686 .673-.699	0.725 .701-.750
4,096 context size	0.780 .756-.804	0.757 .746-.768	0.714 .664-.763	0.716 .705-.727	0.742 .713-.770
2,048 context size	0.803 .781-.825	0.826 .819-.834	0.680 .636-.725	0.721 .710-.731	0.757 .732-.783
1,024 context size	0.790 .766-.813	0.843 .836-.850	0.696 .654-.738	0.700 .689-.710	0.757 .732-.782
512 context size	0.775 .751-.800	0.789 .781-.796	0.689 .643-.735	0.686 .676-.697	0.735 .708-.762

Table S11 Performance for All Examples on EHRSHOT Across Time Windows. Mean area under the receiver operating characteristic curve (AUROC) performance with approximate 95% confidence intervals for different time windows of the LLM embedding models and the count-based baseline.

Model	Operational Outcomes	Anticipating Lab Test Results	Assignment of New Diagnosis	Anticipating Chest X-ray Findings	Macro Avg. Across Task Groups
Qwen3-Emb-8B					
Full patient history	0.797 .773-.820	0.842 .835-.850	0.714 .672-.757	0.722 .711-.733	0.769 .744-.794
3 years (1,095 days)	0.798 .775-.821	0.842 .835-.849	0.717 .674-.759	0.723 .712-.734	0.770 .745-.795
1 year (365 days)	0.802 .780-.824	0.843 .836-.850	0.720 .677-.762	0.723 .712-.734	0.772 .747-.797
1 month (30 days)	0.814 .794-.835	0.840 .832-.847	0.695 .651-.739	0.717 .707-.727	0.767 .742-.792
1 week (7 days)	0.813 .792-.834	0.832 .824-.839	0.683 .645-.722	0.702 .692-.712	0.758 .735-.780
1 day	0.812 .790-.834	0.800 .791-.808	0.697 .660-.735	0.664 .654-.675	0.743 .721-.766
1 hour	0.764 .740-.788	0.677 .668-.686	0.627 .585-.668	0.602 .591-.612	0.667 .642-.692
Qwen2-Emb-7B					
Full patient history	0.772 .749-.796	0.746 .735-.757	0.744 .705-.784	0.685 .671-.699	0.737 .712-.761
3 years (1,095 days)	0.773 .750-.796	0.754 .743-.765	0.725 .681-.770	0.688 .675-.701	0.735 .709-.761
1 year (365 days)	0.781 .758-.803	0.766 .756-.776	0.724 .685-.763	0.696 .683-.709	0.742 .718-.766
1 month (30 days)	0.810 .789-.831	0.789 .780-.798	0.715 .679-.752	0.711 .701-.722	0.756 .734-.779
1 week (7 days)	0.812 .791-.833	0.801 .792-.809	0.700 .658-.741	0.702 .692-.712	0.754 .729-.778
1 day	0.817 .797-.837	0.796 .788-.804	0.720 .669-.771	0.663 .653-.673	0.749 .721-.777
1 hour	0.771 .749-.794	0.674 .665-.682	0.599 .558-.640	0.600 .589-.610	0.661 .637-.685
Llama3.1-LLM2Vec-8B					
Full patient history	0.763 .738-.787	0.726 .714-.738	0.727 .688-.766	0.686 .673-.699	0.725 .701-.750
3 years (1,095 days)	0.763 .739-.787	0.733 .721-.744	0.696 .662-.730	0.694 .682-.705	0.721 .699-.744
1 year (365 days)	0.776 .753-.800	0.742 .731-.754	0.706 .657-.756	0.705 .694-.717	0.733 .704-.761
1 month (30 days)	0.802 .780-.824	0.770 .760-.780	0.696 .642-.751	0.718 .707-.728	0.747 .716-.777
1 week (7 days)	0.816 .795-.836	0.782 .773-.791	0.687 .634-.740	0.702 .691-.712	0.747 .718-.776
1 day	0.811 .790-.833	0.786 .777-.794	0.680 .626-.734	0.666 .656-.676	0.736 .706-.766
1 hour	0.766 .743-.790	0.673 .664-.681	0.581 .538-.625	0.595 .585-.606	0.654 .628-.680
Count-based + GBM					
Full patient history	0.824 .804-.844	0.841 .833-.849	0.758 .724-.793	0.686 .674-.699	0.777 .756-.799
3 years (1,095 days)	0.819 .799-.839	0.841 .833-.850	0.740 .691-.790	0.688 .676-.700	0.772 .745-.800
1 year (365 days)	0.824 .803-.844	0.841 .833-.849	0.749 .705-.794	0.679 .666-.692	0.773 .748-.799
1 month (30 days)	0.824 .805-.844	0.836 .828-.844	0.707 .669-.746	0.688 .677-.700	0.764 .741-.787
1 week (7 days)	0.814 .793-.835	0.842 .835-.850	0.693 .653-.734	0.686 .674-.697	0.759 .735-.782
1 day	0.820 .799-.841	0.830 .823-.837	0.702 .660-.745	0.650 .638-.662	0.751 .726-.775
1 hour	0.742 .717-.767	0.670 .662-.679	0.616 .569-.664	0.572 .559-.586	0.650 .622-.678

Table S12 Encoding Times for Models on EHRSHOT. Time required to encode EHR entries for EHRSHOT experiments on an 8-GPU H200 cluster. LLM embedding models and encoder language models use EHR list serialization with inputs of up to 8,192 tokens. Encoder language models process the input in separate 512-token chunks. Differences in multi-GPU optimization across models may affect runtime. We attempted to optimize each model for the given GPU cluster.

Model	Encoding Time	Macro Avg. Across Task Groups
Baselines [45]		
CLMBR-T-Base	6:04	0.769 $_{.746\text{-}.792}$
LLM Embedding Models		
Qwen3-Emb-8B	21:48:56	0.769 $_{.744\text{-}.794}$
Qwen3-Emb-4B	12:20:28	0.759 $_{.730\text{-}.787}$
Qwen3-Emb-0.6B	5:14:07	0.727 $_{.697\text{-}.758}$
Qwen2-Emb-7B	12:47:18	0.737 $_{.712\text{-}.761}$
Qwen2-Emb-1.5B	5:23:55	0.710 $_{.683\text{-}.738}$
Llama3.1-LLM2Vec-8B	21:39:06	0.725 $_{.701\text{-}.750}$
Encoder Language Models		
DeBERTaV3 large	7:00:21	0.692 $_{.664\text{-}.720}$
DeBERTaV3 base	2:49:35	0.685 $_{.660\text{-}.709}$
BERT large	5:31:18	0.694 $_{.667\text{-}.722}$
BERT base	2:21:35	0.701 $_{.674\text{-}.727}$

Table S13 Hyperparameter Tuning Results for Fine-Tuning Experiments. Mean validation AUROC across the tuning sweep for the operational outcomes and assignment of new diagnoses tasks at $k \in \{8, 16\}$. Rows marked with a * denote the selected configuration for each model family.

Config ID	LR	r	Dropout	$k = 8$ Val. AUROC	$k = 16$ Val. AUROC	Macro Avg.
Encoder Models						
enc_lr5e5_r8_d000	5e-5	8	0.00	0.667	0.688	0.677
enc_lr5e5_r8_d005	5e-5	8	0.05	0.641	0.696	0.668
enc_lr5e5_r8_d010*	5e-5	8	0.10	0.686	0.720	0.703
enc_lr5e5_r16_d000	5e-5	16	0.00	0.616	0.651	0.634
enc_lr5e5_r16_d005	5e-5	16	0.05	0.606	0.686	0.646
enc_lr5e5_r16_d010	5e-5	16	0.10	0.578	0.617	0.597
enc_lr5e5_r64_d000	5e-5	64	0.00	0.639	0.696	0.667
enc_lr5e5_r64_d005	5e-5	64	0.05	0.668	0.677	0.672
enc_lr5e5_r64_d010	5e-5	64	0.10	0.658	0.634	0.646
enc_lr1e4_r8_d000	1e-4	8	0.00	0.691	0.630	0.660
enc_lr1e4_r8_d005	1e-4	8	0.05	0.592	0.657	0.625
enc_lr1e4_r8_d010	1e-4	8	0.10	0.668	0.681	0.675
enc_lr1e4_r16_d000	1e-4	16	0.00	0.615	0.660	0.637
enc_lr1e4_r16_d005	1e-4	16	0.05	0.670	0.630	0.650
enc_lr1e4_r16_d010	1e-4	16	0.10	0.641	0.653	0.647
enc_lr1e4_r64_d000	1e-4	64	0.00	0.623	0.689	0.656
enc_lr1e4_r64_d005	1e-4	64	0.05	0.584	0.670	0.627
enc_lr1e4_r64_d010	1e-4	64	0.10	0.587	0.686	0.637
enc_lr2e4_r8_d000	2e-4	8	0.00	0.616	0.698	0.657
enc_lr2e4_r8_d005	2e-4	8	0.05	0.655	0.655	0.655
enc_lr2e4_r8_d010	2e-4	8	0.10	0.616	0.686	0.651
enc_lr2e4_r16_d000	2e-4	16	0.00	0.588	0.632	0.610
enc_lr2e4_r16_d005	2e-4	16	0.05	0.596	0.703	0.650
enc_lr2e4_r16_d010	2e-4	16	0.10	0.705	0.681	0.693
enc_lr2e4_r64_d000	2e-4	64	0.00	0.670	0.703	0.687
enc_lr2e4_r64_d005	2e-4	64	0.05	0.627	0.630	0.628
enc_lr2e4_r64_d010	2e-4	64	0.10	0.588	0.663	0.625
Decoder Models						
dec_lr5e5_r8_d000	5e-5	8	0.00	0.614	0.606	0.610
dec_lr5e5_r8_d005	5e-5	8	0.05	0.616	0.611	0.614
dec_lr5e5_r8_d010	5e-5	8	0.10	0.624	0.615	0.620
dec_lr5e5_r16_d000	5e-5	16	0.00	0.609	0.622	0.616
dec_lr5e5_r16_d005	5e-5	16	0.05	0.615	0.606	0.610
dec_lr5e5_r16_d010	5e-5	16	0.10	0.615	0.633	0.624
dec_lr5e5_r64_d000	5e-5	64	0.00	0.609	0.609	0.609
dec_lr5e5_r64_d005	5e-5	64	0.05	0.629	0.624	0.627
dec_lr5e5_r64_d010	5e-5	64	0.10	0.616	0.625	0.621
dec_lr1e4_r8_d000	1e-4	8	0.00	0.606	0.629	0.617
dec_lr1e4_r8_d005	1e-4	8	0.05	0.619	0.625	0.622
dec_lr1e4_r8_d010	1e-4	8	0.10	0.610	0.613	0.612
dec_lr1e4_r16_d000	1e-4	16	0.00	0.641	0.619	0.630
dec_lr1e4_r16_d005	1e-4	16	0.05	0.627	0.628	0.627
dec_lr1e4_r16_d010	1e-4	16	0.10	0.621	0.605	0.613
dec_lr1e4_r64_d000	1e-4	64	0.00	0.623	0.624	0.623
dec_lr1e4_r64_d005	1e-4	64	0.05	0.628	0.615	0.622
dec_lr1e4_r64_d010	1e-4	64	0.10	0.625	0.628	0.627
dec_lr2e4_r8_d000	2e-4	8	0.00	0.632	0.651	0.642
dec_lr2e4_r8_d005*	2e-4	8	0.05	0.706	0.637	0.671
dec_lr2e4_r8_d010	2e-4	8	0.10	0.652	0.638	0.645
dec_lr2e4_r16_d000	2e-4	16	0.00	0.657	0.645	0.651
dec_lr2e4_r16_d005	2e-4	16	0.05	0.643	0.621	0.632
dec_lr2e4_r16_d010	2e-4	16	0.10	0.668	0.632	0.650
dec_lr2e4_r64_d000	2e-4	64	0.00	0.674	0.647	0.660
dec_lr2e4_r64_d005	2e-4	64	0.05	0.651	0.619	0.635
dec_lr2e4_r64_d010	2e-4	64	0.10	0.646	0.636	0.641

1.3 Additional Performance Results on EHRSHOT

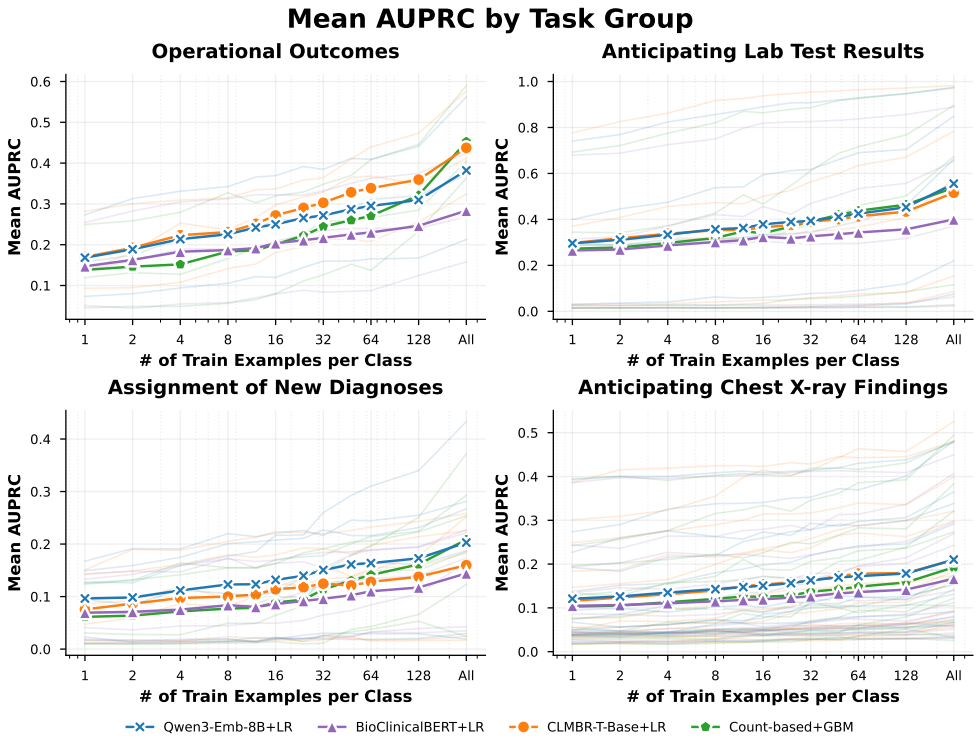

Figure S1 Few-Shot AUPRC Performance on EHRSHOT. Mean area under the precision-recall curve (AUPRC) performance across subtasks for four task groups (bold). Blurred lines show averages across five bootstrapped runs using different seeds [45].

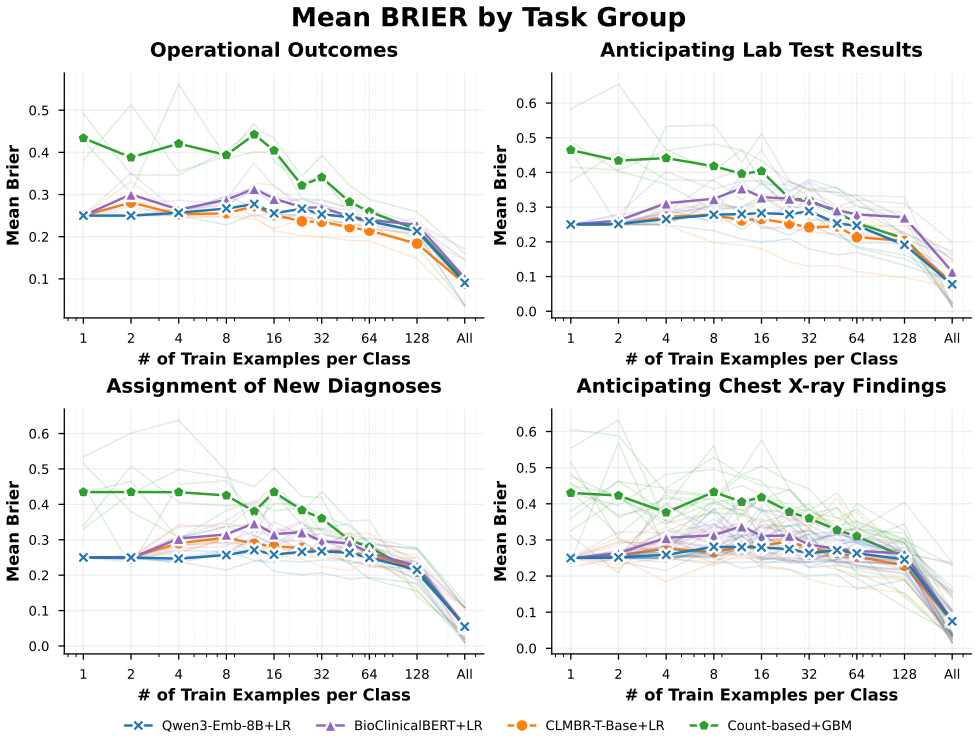

Figure S2 Few-Shot Brier Score on EHRSHOT. Mean Brier score across subtasks for four task groups (bold). Blurred lines show averages across five bootstrapped runs using different seeds [45].

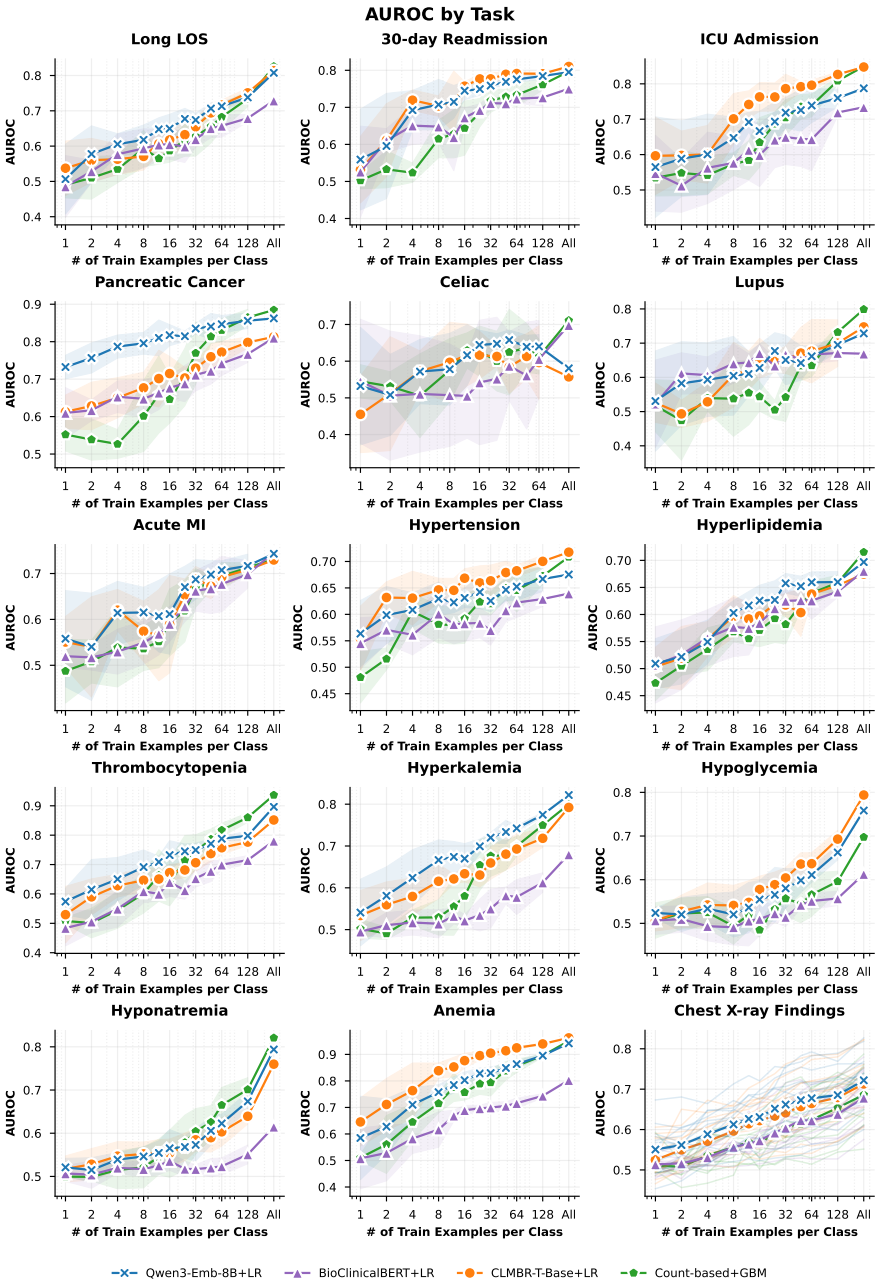

Figure S3 Task-Specific AUROC Performance on EHRSHOT. Area under the receiver operating characteristic curve (AUROC) performance with standard deviation across five few-shot replicates for all 15 prediction tasks [45].

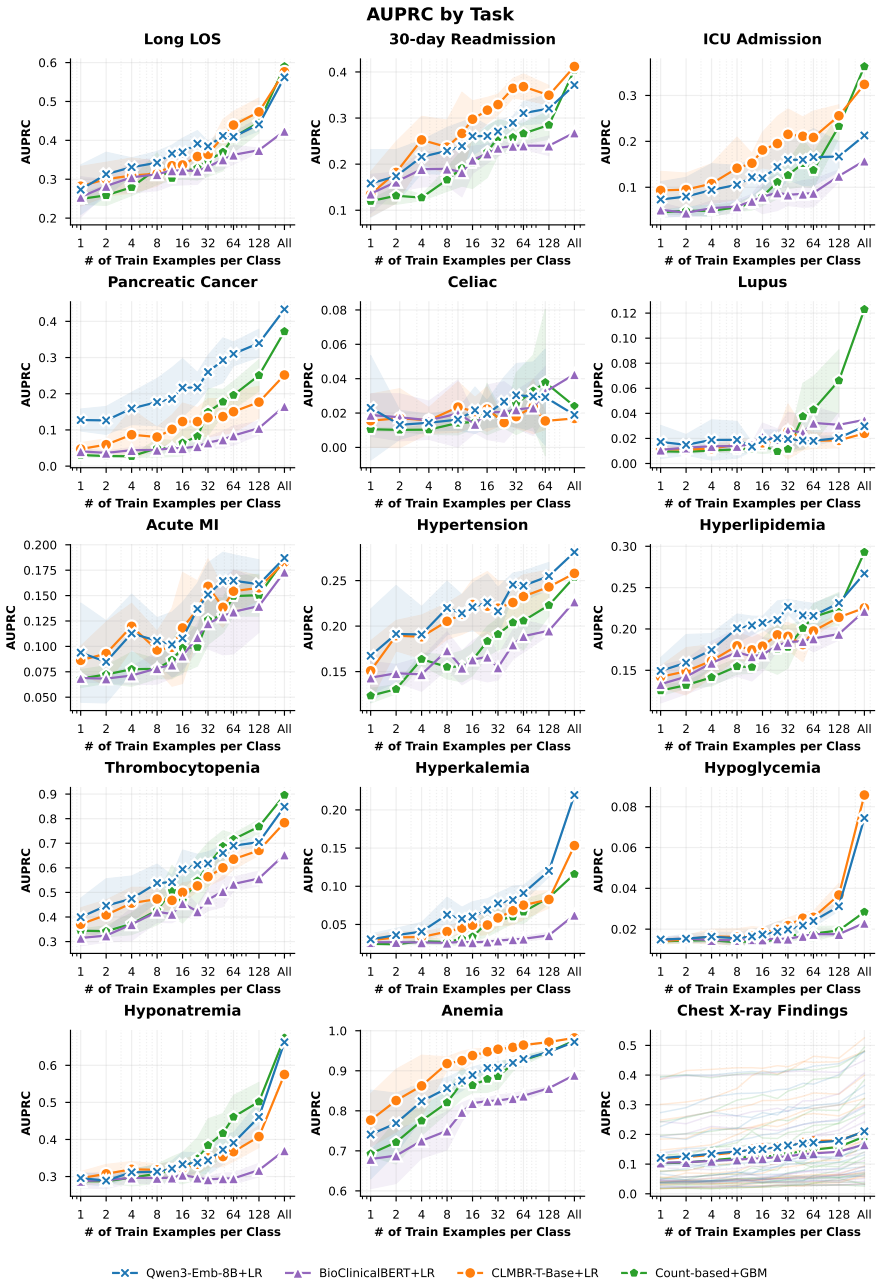

Figure S4 Task-Specific AUPRC Performance on EHRSHOT. Area under the precision-recall curve (AUPRC) performance with standard deviation across five few-shot replicates for all 15 prediction tasks [45].

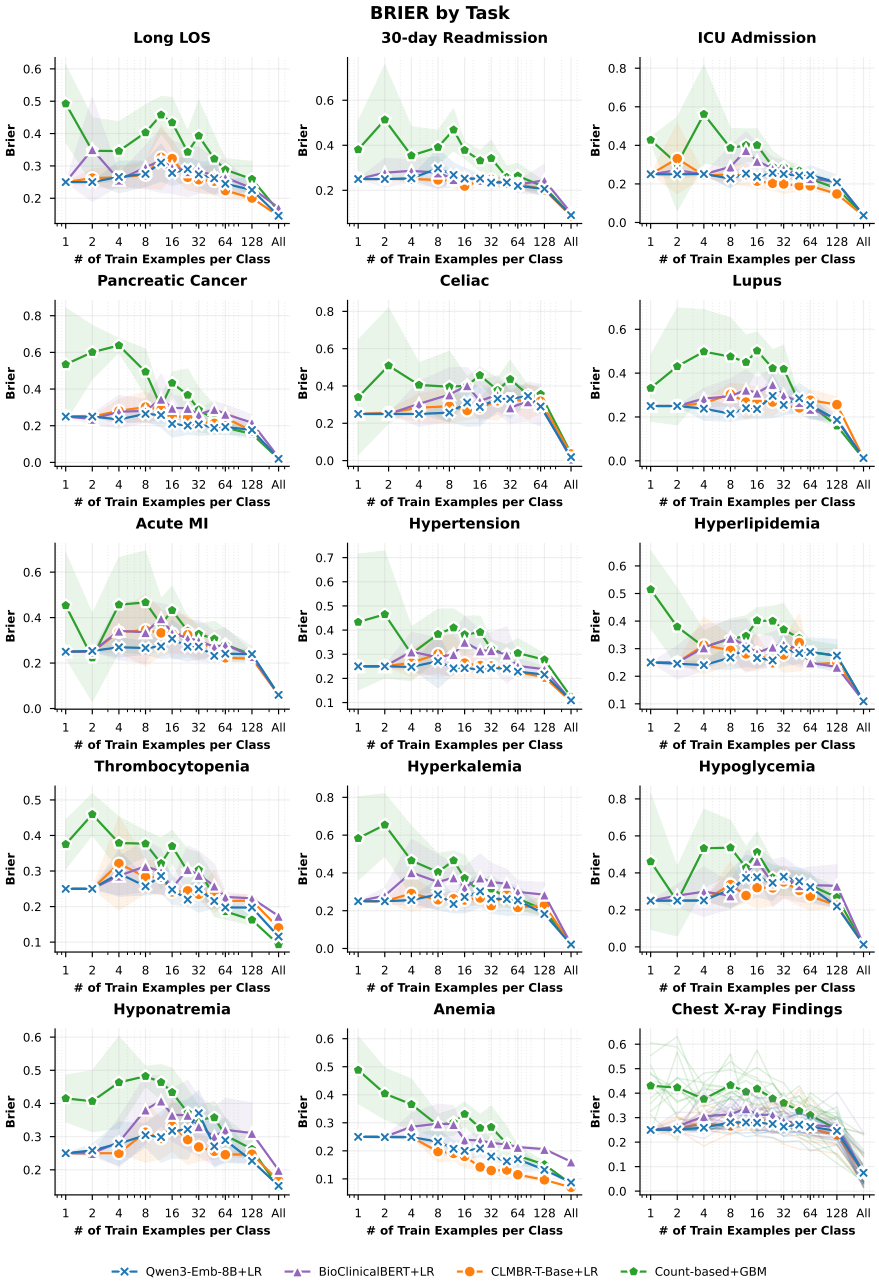

Figure S5 Task-Specific Brier Score on EHRSHOT. Brier score with standard deviation across five few-shot replicates for all 15 prediction tasks [45].

1.4 Additional Performance Results on UK Biobank

Table S14 Performance for All Examples on UKB. Mean area under the receiver operating characteristic curve (AUROC) performance with approximate 95% confidence intervals for three task groups. The assignment of new diagnoses prediction is based on the mean of all 23 provided diseases. The macro-averaged performance across all task groups is given in the right-most column. All LLM embedding models use a context size of 8,192 tokens.

Model	Mortality prediction	Operational Outcomes (Hospitalization)	Assignment of New Diagnoses	Macro Avg. Across Task Groups
Baselines [45]				
CLMBR-T-Base	0.801 .772-.830	0.689 .685-.693	0.719 .708-.731	0.736 .726-.747
Count-based + GBM	0.780 .749-.810	0.709 .705-.712	0.634 .622-.646	0.708 .697-.719
LLM Embedding Model				
Qwen3-Emb-8B	0.811 .781-.840	0.698 .694-.702	0.743 .731-.755	0.751 .740-.761
Qwen2-Emb-7B	0.804 .774-.835	0.695 .691-.699	0.747 .732-.762	0.749 .737-.760
Llama3.1-LLM2Vec-8B	0.796 .766-.827	0.690 .686-.694	0.731 .717-.746	0.739 .728-.751
Sensitivity Analysis Restricted to CLMBR Codes				
Qwen3-Emb-8B CLMBR-T-Base codes	0.806 .775-.836	0.687 .683-.691	0.736 .723-.749	0.743 .732-.754
Encoder Language Models with Chunked Inputs				
BioClinicalBERT	0.778 .746-.811	0.675 .671-.678	0.705 .693-.717	0.719 .708-.731

Table S15 Per-task ΔAUROC (Qwen3-Emb-8B minus baseline) on UKB. Cells report the AUROC difference (ΔAUROC), 95% bootstrap confidence intervals, and Holm-adjusted p-values obtained from paired patient-level bootstrap tests with 10,000 resamples. Positive values indicate better performance of Qwen3-Emb-8B. Multiple testing was controlled separately for each shot setting ($k = 8$, $k = 64$, and all training data) using Holm's procedure across all tasks and baseline comparisons (75/60 tests per setting). Bold indicates statistically significant differences ($p_{\text{adj}} < 0.05$).

Task	CLMBR-T-Base	BioClinicalBERT	Count-based Model
8-shot (8 positive / 8 negative examples)			
Hospitalization	$\mathbf{+0.044}_{[+0.039,+0.049]}$ (0.015)	$\mathbf{+0.042}_{[+0.038,+0.047]}$ (0.015)	$\mathbf{-0.032}_{[-0.036,-0.027]}$ (0.015)
Death	$+0.032_{[+0.000,+0.065]}$ (1.000)	$\mathbf{+0.083}_{[+0.046,+0.121]}$ (0.015)	$\mathbf{+0.076}_{[+0.036,+0.117]}$ (0.015)
Hypertension	$+0.010_{[-0.004,+0.024]}$ (1.000)	$\mathbf{+0.043}_{[+0.029,+0.058]}$ (0.015)	$+0.006_{[-0.008,+0.020]}$ (1.000)
Diabetes Mellitus	$+0.016_{[-0.014,+0.045]}$ (1.000)	$-0.044_{[-0.073,-0.015]}$ (0.312)	$+0.012_{[-0.019,+0.042]}$ (1.000)
Atrial Fibrillation	$-0.023_{[-0.069,+0.023]}$ (1.000)	$-0.004_{[-0.040,+0.033]}$ (1.000)	$-0.013_{[-0.048,+0.024]}$ (1.000)
Pneumonia	$-0.045_{[-0.084,-0.006]}$ (1.000)	$+0.029_{[-0.005,+0.063]}$ (1.000)	$-0.028_{[-0.069,+0.012]}$ (1.000)
COPD	$+0.021_{[-0.010,+0.052]}$ (1.000)	$\mathbf{+0.072}_{[+0.040,+0.105]}$ (0.015)	$-0.006_{[-0.038,+0.027]}$ (1.000)
Chronic Kidney Disease	$+0.046_{[+0.013,+0.078]}$ (0.399)	$-0.020_{[-0.052,+0.012]}$ (1.000)	$-0.021_{[-0.051,+0.009]}$ (1.000)
Ischemic Heart Disease	$+0.036_{[+0.011,+0.061]}$ (0.360)	$-0.007_{[-0.030,+0.016]}$ (1.000)	$-0.029_{[-0.056,-0.002]}$ (1.000)
Myocardial Infarction	$+0.052_{[-0.001,+0.104]}$ (1.000)	$\mathbf{+0.114}_{[+0.061,+0.166]}$ (0.015)	$+0.030_{[-0.019,+0.078]}$ (1.000)
Cerebral Infarction	$+0.114_{[+0.041,+0.182]}$ (0.126)	$-0.013_{[-0.070,+0.045]}$ (1.000)	$-0.050_{[-0.101,-0.002]}$ (1.000)
Heart Failure	$-0.079_{[-0.133,-0.025]}$ (0.319)	$-0.040_{[-0.100,+0.019]}$ (1.000)	$-0.031_{[-0.085,+0.023]}$ (1.000)
Cardiac Arrest	$+0.010_{[-0.105,+0.123]}$ (1.000)	$+0.022_{[-0.073,+0.112]}$ (1.000)	$+0.144_{[+0.029,+0.264]}$ (0.795)
Abdominal Aortic Aneurysm	$+0.036_{[-0.031,+0.100]}$ (1.000)	$+0.013_{[-0.034,+0.062]}$ (1.000)	$+0.033_{[-0.052,+0.118]}$ (1.000)
Pulmonary Embolism	$-0.113_{[-0.207,-0.017]}$ (1.000)	$+0.122_{[+0.039,+0.203]}$ (0.232)	$-0.059_{[-0.153,+0.031]}$ (1.000)
Aortic Stenosis	$-0.011_{[-0.082,+0.059]}$ (1.000)	$+0.033_{[-0.078,+0.148]}$ (1.000)	$-0.018_{[-0.144,+0.114]}$ (1.000)
Mitral Valve Insufficiency	$+0.072_{[-0.003,+0.143]}$ (1.000)	$-0.049_{[-0.124,+0.027]}$ (1.000)	$+0.078_{[-0.015,+0.173]}$ (1.000)
Endocarditis	$+0.042_{[-0.061,+0.142]}$ (1.000)	$-0.011_{[-0.102,+0.078]}$ (1.000)	$+0.007_{[-0.095,+0.108]}$ (1.000)
Rheumatic Fever	$+0.080_{[+0.016,+0.143]}$ (0.792)	$+0.085_{[+0.021,+0.152]}$ (0.582)	$\mathbf{+0.206}_{[+0.110,+0.302]}$ (0.015)
Anemia	$+0.021_{[-0.005,+0.047]}$ (1.000)	$+0.017_{[-0.009,+0.043]}$ (1.000)	$+0.044_{[+0.017,+0.071]}$ (0.126)
Back Pain	$\mathbf{+0.126}_{[+0.105,+0.146]}$ (0.015)	$\mathbf{+0.052}_{[+0.038,+0.066]}$ (0.015)	$-0.004_{[-0.017,+0.010]}$ (1.000)
Parkinson's Disease	$-0.075_{[-0.215,+0.069]}$ (1.000)	$+0.058_{[-0.075,+0.184]}$ (1.000)	$-0.077_{[-0.208,+0.062]}$ (1.000)
Rheumatoid Arthritis	$-0.059_{[-0.133,+0.016]}$ (1.000)	$-0.007_{[-0.082,+0.069]}$ (1.000)	$-0.006_{[-0.066,+0.055]}$ (1.000)
Psoriasis	$+0.079_{[+0.015,+0.143]}$ (0.792)	$+0.043_{[-0.004,+0.091]}$ (1.000)	$+0.027_{[-0.020,+0.073]}$ (1.000)
Suicide Ideation / Self Harm	$+0.041_{[-0.027,+0.108]}$ (1.000)	$+0.117_{[+0.047,+0.191]}$ (0.090)	$+0.072_{[-0.007,+0.154]}$ (1.000)
64-shot (64 positive / 64 negative examples)			
Hospitalization	$\mathbf{+0.023}_{[+0.018,+0.028]}$ (0.012)	$-0.002_{[-0.006,+0.002]}$ (1.000)	$+0.002_{[-0.003,+0.007]}$ (1.000)
Death	$+0.017_{[-0.008,+0.040]}$ (1.000)	$+0.029_{[+0.003,+0.055]}$ (1.000)	$+0.006_{[-0.019,+0.031]}$ (1.000)
Hypertension	$+0.007_{[-0.006,+0.020]}$ (1.000)	$\mathbf{+0.038}_{[+0.026,+0.050]}$ (0.012)	$-0.003_{[-0.016,+0.010]}$ (1.000)
Diabetes Mellitus	$\mathbf{+0.068}_{[+0.044,+0.092]}$ (0.012)	$+0.031_{[+0.012,+0.051]}$ (0.150)	$+0.008_{[-0.011,+0.027]}$ (1.000)
Atrial Fibrillation	$+0.004_{[-0.031,+0.041]}$ (1.000)	$+0.036_{[+0.007,+0.067]}$ (0.475)	$+0.007_{[-0.018,+0.032]}$ (1.000)
Pneumonia	$-0.031_{[-0.065,+0.003]}$ (1.000)	$-0.021_{[-0.056,+0.014]}$ (1.000)	$-0.063_{[-0.099,-0.027]}$ (0.071)
COPD	$+0.029_{[+0.005,+0.054]}$ (0.697)	$\mathbf{+0.079}_{[+0.052,+0.106]}$ (0.012)	$-0.016_{[-0.038,+0.006]}$ (1.000)
Chronic Kidney Disease	$+0.017_{[-0.003,+0.038]}$ (1.000)	$+0.022_{[+0.006,+0.037]}$ (0.202)	$-0.005_{[-0.021,+0.011]}$ (1.000)
Ischemic Heart Disease	$-0.018_{[-0.040,+0.003]}$ (1.000)	$+0.014_{[-0.005,+0.033]}$ (1.000)	$-0.033_{[-0.054,-0.011]}$ (0.125)
Myocardial Infarction	$-0.027_{[-0.063,+0.009]}$ (1.000)	$+0.068_{[+0.028,+0.108]}$ (0.064)	$-0.022_{[-0.057,+0.013]}$ (1.000)
Cerebral Infarction	$+0.038_{[-0.010,+0.085]}$ (1.000)	$+0.034_{[-0.001,+0.069]}$ (1.000)	$-0.040_{[-0.096,+0.015]}$ (1.000)
Heart Failure	$+0.009_{[-0.020,+0.038]}$ (1.000)	$+0.037_{[+0.008,+0.066]}$ (0.475)	$+0.005_{[-0.029,+0.041]}$ (1.000)
Cardiac Arrest	—	—	—
Abdominal Aortic Aneurysm	—	—	—
Pulmonary Embolism	$-0.047_{[-0.122,+0.029]}$ (1.000)	$+0.090_{[+0.023,+0.157]}$ (0.360)	$+0.017_{[-0.063,+0.099]}$ (1.000)
Aortic Stenosis	—	—	—
Mitral Valve Insufficiency	$+0.053_{[-0.000,+0.107]}$ (1.000)	$+0.079_{[+0.028,+0.132]}$ (0.071)	$\mathbf{+0.132}_{[+0.067,+0.200]}$ (0.012)
Endocarditis	—	—	—
Rheumatic Fever	$+0.031_{[-0.027,+0.090]}$ (1.000)	$-0.011_{[-0.074,+0.049]}$ (1.000)	$+0.004_{[-0.047,+0.054]}$ (1.000)
Anemia	$+0.002_{[-0.023,+0.027]}$ (1.000)	$+0.005_{[-0.021,+0.032]}$ (1.000)	$-0.043_{[-0.067,-0.017]}$ (0.078)
Back Pain	$\mathbf{+0.041}_{[+0.030,+0.052]}$ (0.012)	$-0.001_{[-0.011,+0.008]}$ (1.000)	$-0.003_{[-0.013,+0.006]}$ (1.000)
Parkinson's Disease	—	—	—
Rheumatoid Arthritis	$+0.009_{[-0.047,+0.068]}$ (1.000)	$+0.041_{[-0.012,+0.094]}$ (1.000)	$-0.005_{[-0.058,+0.048]}$ (1.000)
Psoriasis	$+0.042_{[+0.002,+0.082]}$ (1.000)	$+0.033_{[+0.001,+0.064]}$ (1.000)	$+0.010_{[-0.024,+0.044]}$ (1.000)
Suicide Ideation / Self Harm	$\mathbf{+0.116}_{[+0.052,+0.179]}$ (0.043)	$+0.103_{[+0.040,+0.170]}$ (0.064)	$+0.047_{[-0.005,+0.103]}$ (1.000)

Table S16 Per-task ΔAUROC (Qwen3-Emb-8B minus baseline) on UKB (continued).

Task	CLMBR-T-Base	BioClinicalBERT	Count-based Model
All training data			
Hospitalization	**+0.009**$_{[+0.007,+0.012]}$ (0.015)	**+0.023**$_{[+0.021,+0.026]}$ (0.015)	**−0.011**$_{[-0.013,-0.008]}$ (0.015)
Death	+0.009$_{[-0.009,+0.029]}$ (1.000)	+0.032$_{[+0.010,+0.056]}$ (0.263)	+0.016$_{[-0.010,+0.041]}$ (1.000)
Hypertension	**+0.019**$_{[+0.009,+0.028]}$ (0.015)	**+0.032**$_{[+0.024,+0.040]}$ (0.015)	**−0.022**$_{[-0.031,-0.012]}$ (0.015)
Diabetes Mellitus	**+0.046**$_{[+0.027,+0.065]}$ (0.015)	**+0.034**$_{[+0.017,+0.052]}$ (0.021)	−0.018$_{[-0.037,+0.001]}$ (1.000)
Atrial Fibrillation	+0.038$_{[-0.001,+0.080]}$ (1.000)	+0.030$_{[+0.001,+0.060]}$ (1.000)	**+0.358**$_{[+0.284,+0.432]}$ (0.015)
Pneumonia	−0.019$_{[-0.044,+0.005]}$ (1.000)	+0.036$_{[+0.011,+0.060]}$ (0.250)	+0.005$_{[-0.022,+0.032]}$ (1.000)
COPD	**+0.045**$_{[+0.022,+0.068]}$ (0.015)	**+0.067**$_{[+0.046,+0.089]}$ (0.015)	−0.019$_{[-0.041,+0.003]}$ (1.000)
Chronic Kidney Disease	+0.026$_{[+0.008,+0.045]}$ (0.270)	**+0.041**$_{[+0.022,+0.059]}$ (0.015)	**+0.045**$_{[+0.024,+0.067]}$ (0.015)
Ischemic Heart Disease	−0.009$_{[-0.024,+0.006]}$ (1.000)	**+0.026**$_{[+0.011,+0.040]}$ (0.041)	−0.014$_{[-0.031,+0.003]}$ (1.000)
Myocardial Infarction	−0.006$_{[-0.034,+0.021]}$ (1.000)	+0.037$_{[+0.011,+0.063]}$ (0.273)	−0.014$_{[-0.049,+0.020]}$ (1.000)
Cerebral Infarction	+0.007$_{[-0.039,+0.051]}$ (1.000)	+0.034$_{[-0.002,+0.071]}$ (1.000)	+0.073$_{[-0.013,+0.159]}$ (1.000)
Heart Failure	+0.014$_{[-0.014,+0.042]}$ (1.000)	+0.040$_{[+0.013,+0.067]}$ (0.273)	**+0.166**$_{[+0.112,+0.222]}$ (0.015)
Cardiac Arrest	+0.003$_{[-0.088,+0.094]}$ (1.000)	+0.040$_{[-0.039,+0.120]}$ (1.000)	+0.196$_{[+0.068,+0.326]}$ (0.167)
Abdominal Aortic Aneurysm	+0.067$_{[+0.005,+0.126]}$ (1.000)	+0.039$_{[-0.021,+0.100]}$ (1.000)	**+0.346**$_{[+0.236,+0.449]}$ (0.015)
Pulmonary Embolism	−0.002$_{[-0.073,+0.069]}$ (1.000)	+0.093$_{[+0.027,+0.159]}$ (0.267)	+0.109$_{[+0.031,+0.192]}$ (0.311)
Aortic Stenosis	+0.046$_{[-0.007,+0.099]}$ (1.000)	+0.001$_{[-0.070,+0.075]}$ (1.000)	+0.228$_{[+0.097,+0.353]}$ (0.080)
Mitral Valve Insufficiency	+0.042$_{[-0.009,+0.096]}$ (1.000)	+0.069$_{[+0.018,+0.123]}$ (0.435)	**+0.300**$_{[+0.232,+0.363]}$ (0.015)
Endocarditis	+0.038$_{[-0.026,+0.101]}$ (1.000)	−0.040$_{[-0.127,+0.041]}$ (1.000)	+0.155$_{[+0.016,+0.301]}$ (1.000)
Rheumatic Fever	+0.044$_{[-0.011,+0.100]}$ (1.000)	+0.010$_{[-0.044,+0.063]}$ (1.000)	**+0.318**$_{[+0.248,+0.382]}$ (0.015)
Anemia	**+0.038**$_{[+0.019,+0.058]}$ (0.015)	**+0.047**$_{[+0.028,+0.066]}$ (0.015)	+0.010$_{[-0.010,+0.029]}$ (1.000)
Back Pain	**+0.055**$_{[+0.046,+0.063]}$ (0.015)	+0.008$_{[+0.001,+0.015]}$ (1.000)	**−0.016**$_{[-0.023,-0.009]}$ (0.015)
Parkinson's Disease	−0.051$_{[-0.144,+0.039]}$ (1.000)	**+0.131**$_{[+0.060,+0.204]}$ (0.031)	+0.135$_{[-0.019,+0.277]}$ (1.000)
Rheumatoid Arthritis	+0.020$_{[-0.038,+0.081]}$ (1.000)	+0.057$_{[-0.004,+0.120]}$ (1.000)	+0.072$_{[-0.005,+0.152]}$ (1.000)
Psoriasis	+0.031$_{[+0.001,+0.061]}$ (1.000)	+0.001$_{[-0.027,+0.028]}$ (1.000)	**+0.127**$_{[+0.074,+0.179]}$ (0.015)
Suicide Ideation / Self Harm	+0.058$_{[+0.008,+0.107]}$ (1.000)	+0.048$_{[-0.013,+0.110]}$ (1.000)	**+0.300**$_{[+0.152,+0.445]}$ (0.015)

Table S17 Per-task ΔAUROC (Qwen3-Emb-8B restricted to CLMBR-T-Base codes minus CLMBR-T-Base) on UKB. Cells report the AUROC difference (ΔAUROC), 95% bootstrap confidence intervals, and Holm-adjusted p-values obtained from paired patient-level bootstrap tests with 10,000 resamples. Positive values indicate better performance of Qwen3-Emb-8B. Multiple testing was controlled separately for each shot setting ($k = 8$, $k = 64$, and all training data) using Holm's procedure across all tasks and baseline comparisons (25/20 tests per setting). Bold indicates statistically significant differences ($p_{\text{adj}} < 0.05$).

Task	8-shot	64-shot	All training data
Hospitalization	$\mathbf{+0.048}_{[+0.043,+0.053]}$ (0.005)	$-0.007_{[-0.012,-0.002]}$ (0.116)	$-0.002_{[-0.004,+0.001]}$ (1.000)
Death	$\mathbf{-0.156}_{[-0.200,-0.111]}$ (0.005)	$+0.005_{[-0.021,+0.033]}$ (1.000)	$+0.004_{[-0.015,+0.024]}$ (1.000)
Hypertension	$+0.007_{[-0.007,+0.020]}$ (1.000)	$-0.013_{[-0.026,+0.000]}$ (0.780)	$+0.003_{[-0.006,+0.012]}$ (1.000)
Diabetes Mellitus	$\mathbf{-0.060}_{[-0.094,-0.026]}$ (0.008)	$+0.031_{[+0.006,+0.057]}$ (0.266)	$\mathbf{+0.035}_{[+0.016,+0.054]}$ (0.014)
Atrial Fibrillation	$-0.008_{[-0.055,+0.041]}$ (1.000)	$-0.026_{[-0.064,+0.013]}$ (1.000)	$+0.006_{[-0.033,+0.047]}$ (1.000)
Pneumonia	$-0.065_{[-0.109,-0.020]}$ (0.094)	$+0.006_{[-0.029,+0.041]}$ (1.000)	$-0.036_{[-0.064,-0.008]}$ (0.232)
COPD	$+0.022_{[-0.009,+0.055]}$ (1.000)	$+0.003_{[-0.024,+0.028]}$ (1.000)	$+0.024_{[+0.001,+0.046]}$ (0.788)
Chronic Kidney Disease	$\mathbf{+0.067}_{[+0.040,+0.094]}$ (0.005)	$+0.006_{[-0.013,+0.026]}$ (1.000)	$+0.002_{[-0.017,+0.021]}$ (1.000)
Ischemic Heart Disease	$\mathbf{+0.102}_{[+0.077,+0.127]}$ (0.005)	$+0.018_{[-0.003,+0.038]}$ (1.000)	$+0.002_{[-0.013,+0.016]}$ (1.000)
Myocardial Infarction	$\mathbf{+0.082}_{[+0.031,+0.133]}$ (0.040)	$+0.015_{[-0.016,+0.046]}$ (1.000)	$+0.030_{[+0.004,+0.056]}$ (0.502)
Cerebral Infarction	$+0.081_{[+0.017,+0.143]}$ (0.194)	$+0.018_{[-0.030,+0.066]}$ (1.000)	$+0.013_{[-0.026,+0.049]}$ (1.000)
Heart Failure	$-0.037_{[-0.086,+0.013]}$ (1.000)	$-0.005_{[-0.036,+0.024]}$ (1.000)	$+0.001_{[-0.028,+0.029]}$ (1.000)
Cardiac Arrest	$+0.013_{[-0.105,+0.124]}$ (1.000)	—	$-0.044_{[-0.148,+0.055]}$ (1.000)
Abdominal Aortic Aneurysm	$+0.060_{[+0.010,+0.112]}$ (0.352)	—	$+0.083_{[+0.021,+0.140]}$ (0.202)
Pulmonary Embolism	$-0.112_{[-0.207,-0.015]}$ (0.402)	$-0.056_{[-0.125,+0.013]}$ (1.000)	$-0.039_{[-0.103,+0.026]}$ (1.000)
Aortic Stenosis	$+0.049_{[-0.030,+0.131]}$ (1.000)	—	$+0.065_{[-0.009,+0.137]}$ (1.000)
Mitral Valve Insufficiency	$+0.077_{[-0.005,+0.155]}$ (0.845)	$+0.031_{[-0.023,+0.085]}$ (1.000)	$+0.016_{[-0.033,+0.065]}$ (1.000)
Endocarditis	$+0.085_{[+0.003,+0.170]}$ (0.619)	—	$+0.075_{[-0.020,+0.164]}$ (1.000)
Rheumatic Fever	$-0.060_{[-0.127,+0.008]}$ (0.994)	$+0.022_{[-0.040,+0.084]}$ (1.000)	$-0.030_{[-0.091,+0.031]}$ (1.000)
Anemia	$-0.003_{[-0.032,+0.027]}$ (1.000)	$+0.014_{[-0.011,+0.039]}$ (1.000)	$+0.027_{[+0.010,+0.045]}$ (0.070)
Back Pain	$-0.010_{[-0.030,+0.010]}$ (1.000)	$\mathbf{+0.024}_{[+0.013,+0.035]}$ (0.004)	$\mathbf{+0.040}_{[+0.032,+0.048]}$ (0.005)
Parkinson's Disease	$-0.059_{[-0.176,+0.067]}$ (1.000)	—	$-0.029_{[-0.136,+0.072]}$ (1.000)
Rheumatoid Arthritis	$-0.044_{[-0.115,+0.026]}$ (1.000)	$-0.044_{[-0.104,+0.017]}$ (1.000)	$+0.034_{[-0.024,+0.096]}$ (1.000)
Psoriasis	$\mathbf{+0.092}_{[+0.029,+0.154]}$ (0.042)	$\mathbf{+0.062}_{[+0.024,+0.100]}$ (0.034)	$+0.049_{[+0.019,+0.080]}$ (0.055)
Suicide Ideation / Self Harm	$-0.046_{[-0.134,+0.042]}$ (1.000)	$\mathbf{+0.109}_{[+0.043,+0.178]}$ (0.036)	$+0.052_{[-0.001,+0.105]}$ (0.887)

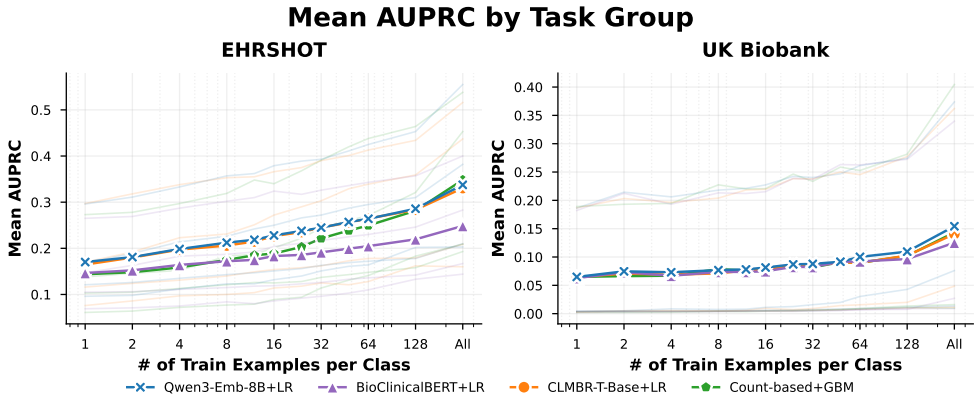

Figure S6 Few-Shot Performance on EHRSHOT and UKB. Macro-averaged area under the precision-recall curve (AUPRC) performance across all subtasks of EHRSHOT (left) and UK Biobank (right). Blurred lines show averaged AUPRC values for the different task groups.

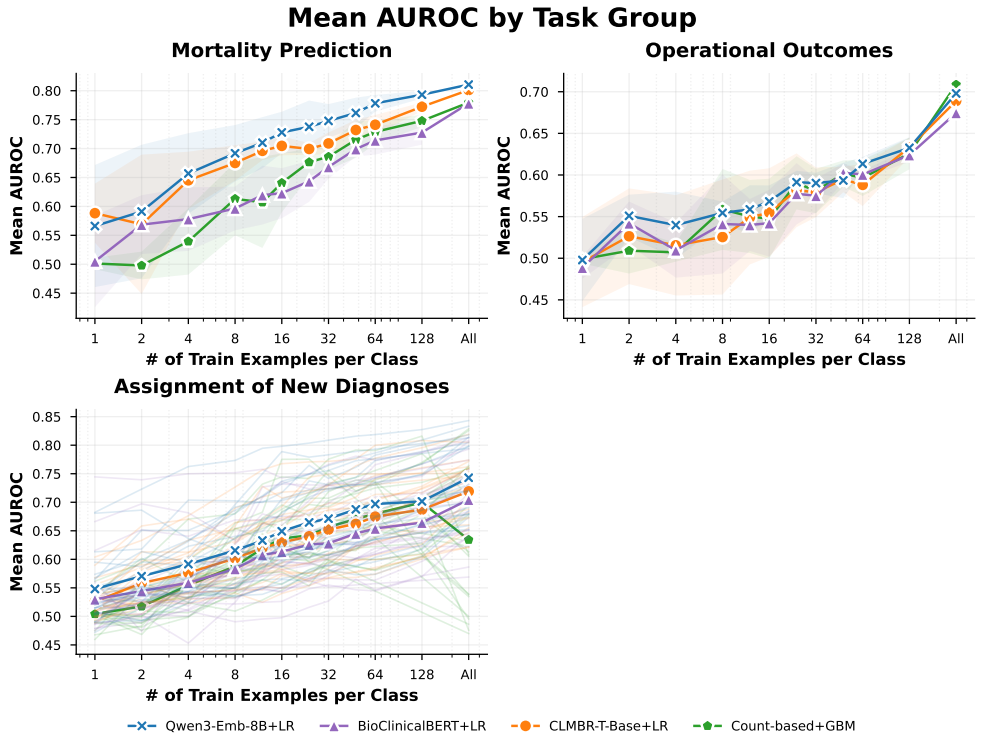

Figure S7 Few-Shot AUROC Performance on UKB. Mean area under the receiver operating characteristic curve (AUROC) performance across subtasks for three task groups (bold). Blurred lines show averages across five bootstrapped runs using different seeds. Shaded regions show standard deviation.

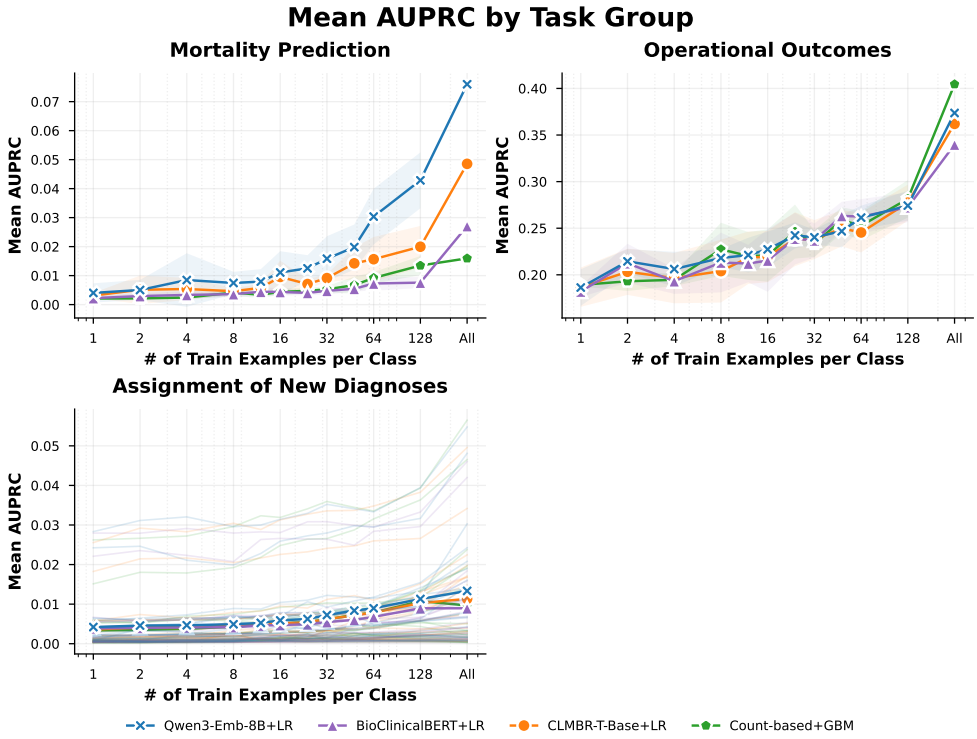

Figure S8 Few-Shot AUPRC Performance on UKB. Mean area under the precision-recall curve (AUPRC) performance across subtasks for three task groups (bold). Blurred lines show averages across five bootstrapped runs using different seeds. Shaded regions show standard deviation.

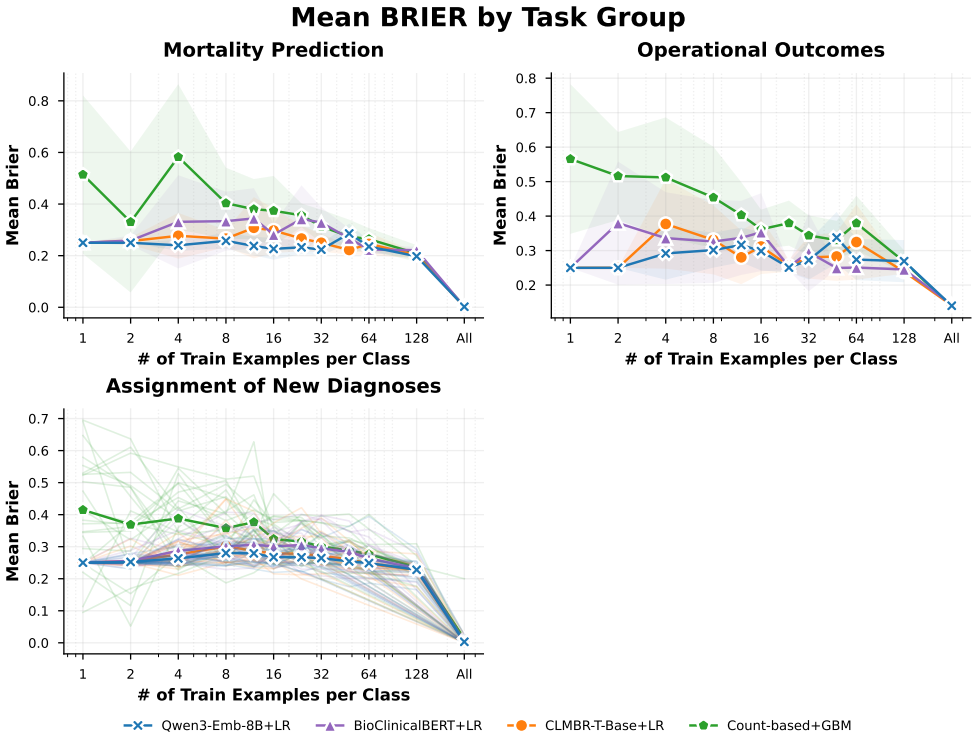

Figure S9 Few-Shot Brier Score on UKB. Mean Brier score across subtasks for three task groups (bold). Blurred lines show averages across five bootstrapped runs using different seeds [45]. Shaded regions show standard deviation.

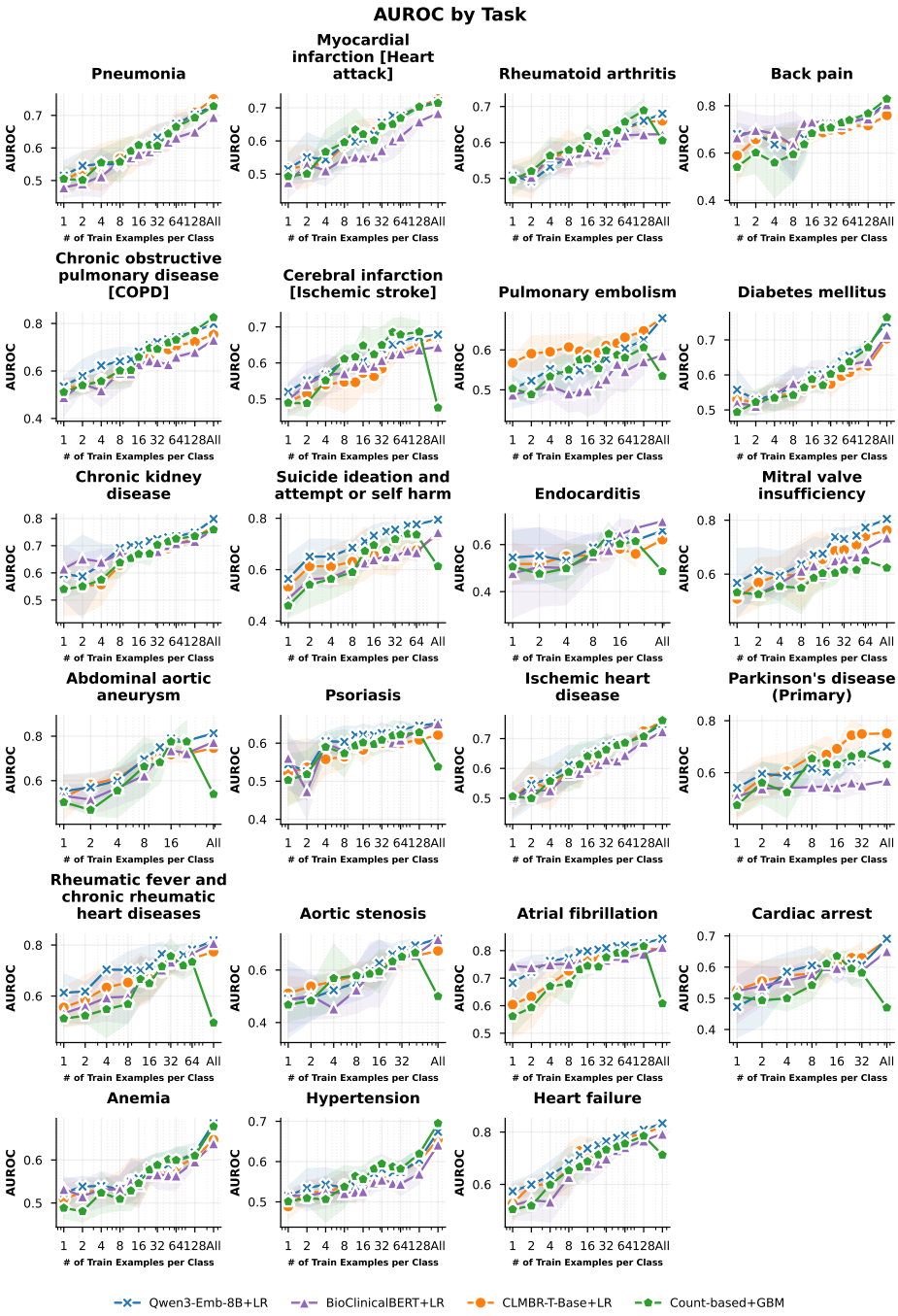

Figure S10 Disease Onset AUROC Performance on UKB. Area under the receiver operating characteristic curve (AUROC) performance with standard deviation across five few-shot replicates for all assignment-of-new-diagnosis tasks.

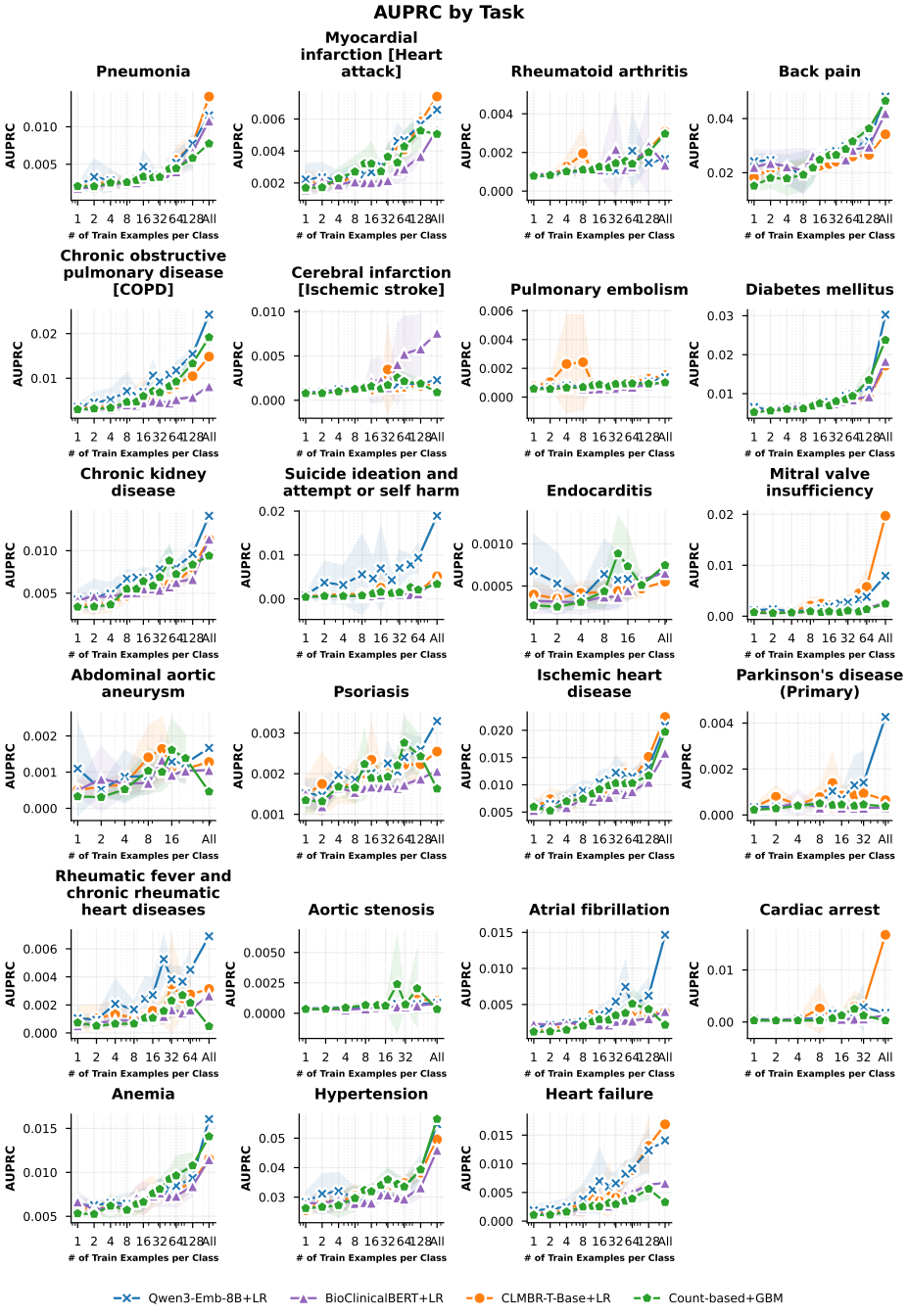

Figure S11 Disease Onset AUPRC Performance on UKB. Area under the precision-recall curve (AUPRC) performance with standard deviation across five few-shot replicates for all assignment-of-new-diagnosis tasks.

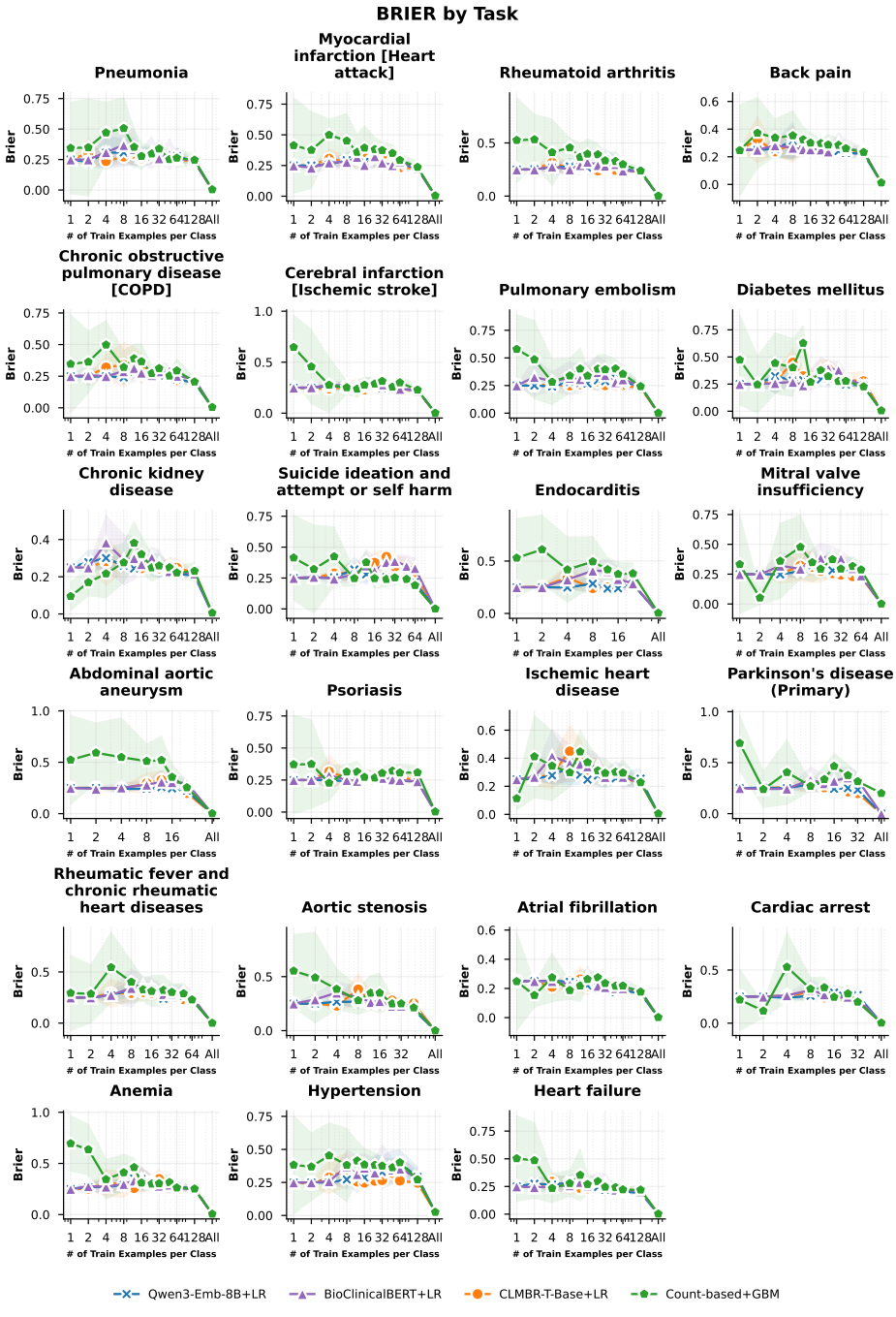

Figure S12 Disease Onset Brier Score on UKB. Brier score with standard deviation across five few-shot replicates for all assignment-of-new-diagnosis tasks.

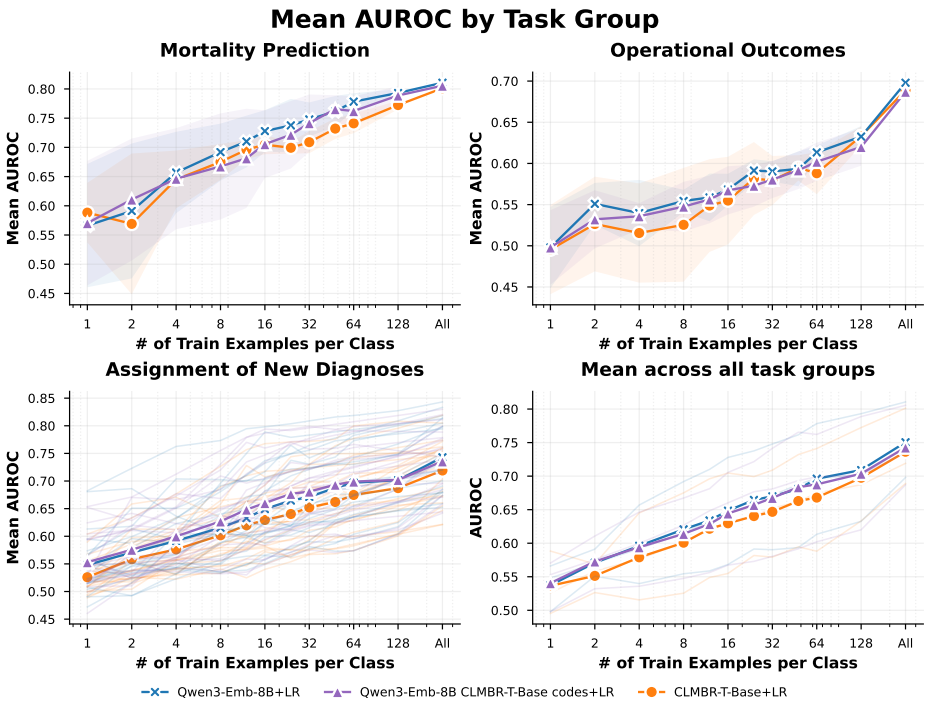

Figure S13 Few-Shot AUROC Performance for Sensitivity Analysis on UKB. Mean area under the receiver operating characteristic curve (AUROC) performance across subtasks for three task groups (bold) and macro-averaged AUROC performance across all subtasks on the UK Biobank. Results are reported for Qwen3-Emb-8B using all UKB codes, Qwen3-Emb-8B restricted to medical codes mappable to the EHR foundation model CLMBR-T-Base, and the CLMBR-T-Base model. Shaded regions indicate standard deviation. Blurred lines for assignment of new diagnoses represent averages across five bootstrapped runs using different seeds. The blurred lines for the mean across all task groups represent the averaged AUROC values of the different task groups.

1.5 Additional Performance Results for Encoder and Decoder Models

Table S18 Performance for All Examples on EHRSHOT. Macro-averaged AUROC performance and bootstrapped 95% confidence intervals for the frozen Qwen3-Emb-8B encoder baseline and the LoRA-tuned Qwen encoder and decoder variants at $k = 128$. Fine-tuning via LoRA did not improve over the frozen Qwen3-Emb-8B baseline. Among the tuned variants, the fine-tuned decoder slightly outperformed the fine-tuned encoder, but both remained below the frozen baseline and the decoder required substantially higher computational cost.

Model	Operational Outcomes	Anticipating Lab Test Results	Assignment of New Diagnoses	Anticipating Chest X-ray Findings	Macro Avg. Across Task Groups
Encoder models					
Qwen3-Emb-8B	0.767 $_{.726\text{-}.803}$	0.770 $_{.749\text{-}.789}$	0.702 $_{.614\text{-}.783}$	0.695 $_{.654\text{-}.733}$	0.733 $_{.686\text{-}.777}$
Qwen3-Emb-8B (LoRA)	0.736 $_{.693\text{-}.776}$	0.819 $_{.804\text{-}.834}$	0.667 $_{.573\text{-}.751}$	0.646 $_{.605\text{-}.686}$	0.717 $_{.669\text{-}.762}$
Decoder models					
Qwen3-8B (LoRA)	0.692 $_{.651\text{-}.732}$	0.848 $_{.835\text{-}.860}$	0.711 $_{.620\text{-}.801}$	0.626 $_{.588\text{-}.664}$	0.719 $_{.673\text{-}.764}$

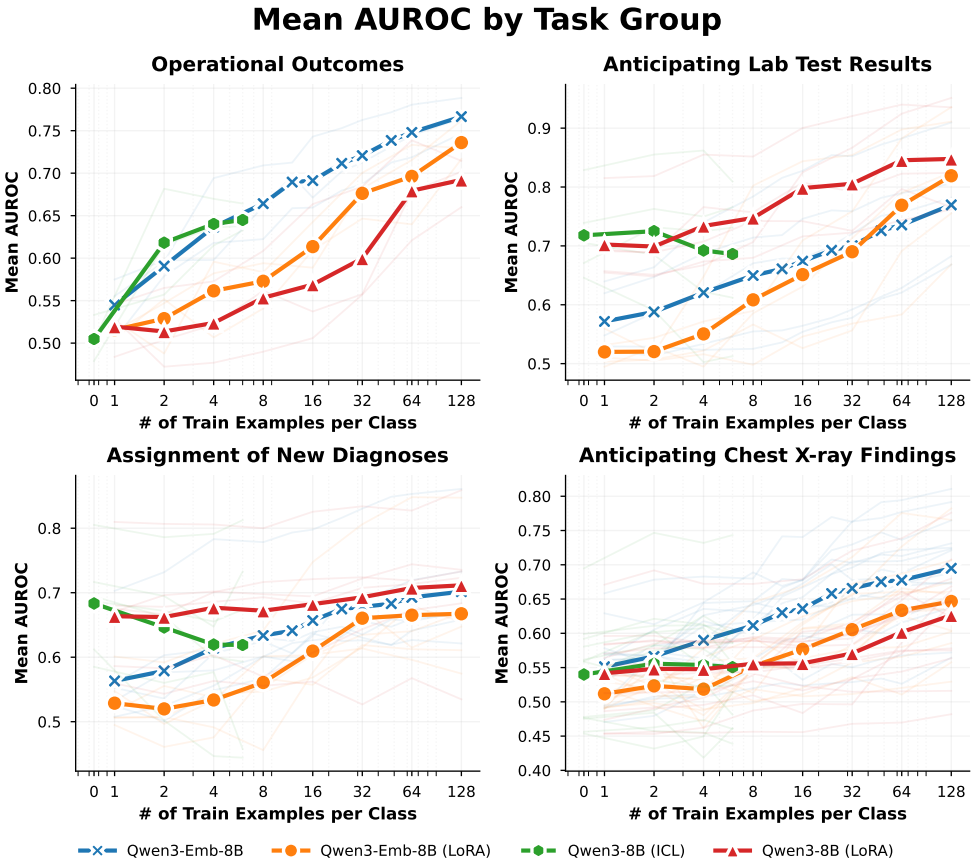

Figure S14 Few-Shot AUROC Performance of Encoder and Decoder Models on EHRSHOT by Task Group. Mean area under the receiver operating characteristic curve (AUROC) across subtasks for the four EHRSHOT task groups. Blurred lines show averages across five bootstrapped runs using different seeds. The decoder ICL curves are shown for 0, 2, 4, and 6 shots only because larger ICL settings were not computationally feasible.

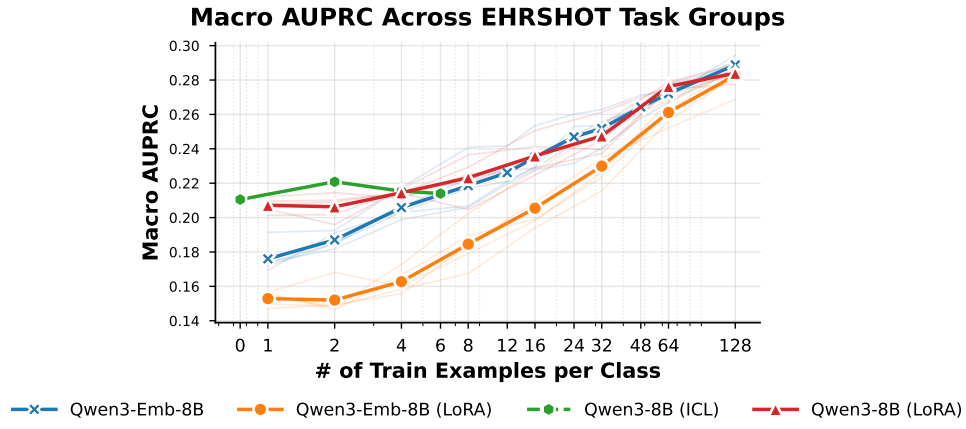

Figure S15 Few-Shot AUPRC Performance of Encoder and Decoder Models on EHRSHOT. Macro-averaged area under the precision-recall curve (AUPRC) across all EHRSHOT subtasks for zero to 128 training examples per class, comparing the frozen encoder baseline, the LoRA-tuned encoder, decoder ICL at 0, 2, 4, and 6 shots, and the LoRA-tuned decoder.

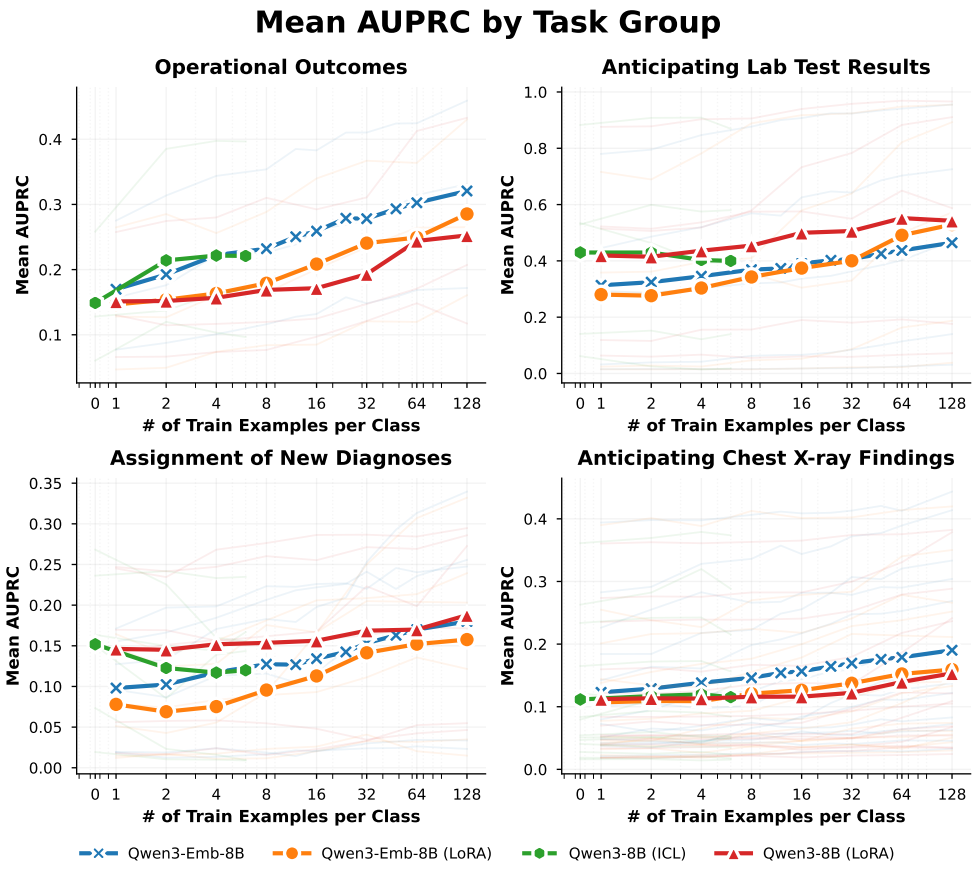

Figure S16 Few-Shot AUPRC Performance of Encoder and Decoder Models on EHRSHOT by Task Group. Mean area under the precision-recall curve (AUPRC) across subtasks for the four EHRSHOT task groups. Blurred lines show averages across five bootstrapped runs using different seeds. Decoder ICL beyond 6 shots was not computationally feasible and is therefore not shown.